Medizinische Fakultät
der
Universität Duisburg-Essen

Aus dem
Institut für Molekularbiologie

Characterization of ARC39, a new inhibitor of acid sphingomyelinase

I n a u g u r a l d i s s e r t a t i o n
zur
Erlangung des Doktorgrades der Medizin
durch die Medizinische Fakultät
der Universität Duisburg-Essen

Vorgelegt von
Eyad Naser
aus Damaskus
2020

DOI: 10.17185/duepublico/73116
URN: urn:nbn:de:hbz:464-20201209-114852-0

Dekan: Herr Univ.-Prof. Dr. med. J. Buer

1. Gutachter/in: Herr Univ.-Prof. Dr. med. E. Gulbins

2. Gutachter/in: Herr Priv.-Doz. Dr. med. J. R. Göthert

3. Gutachter/in: Frau Prof. Dr. S. Meierjohann

Tag der mündlichen Prüfung: 09. Oktober 2020

Publications

Naser, E., Kadow, S., Schumacher, F., Mohamed, Z.H., Kappe, C., Hessler, G., Pollmeier, B., Kleuser, B., Arenz, C., Becker, K.A., Gulbins, E., and Carpinteiro, A. (2020). Characterization of the small molecule ARC39, a direct and specific inhibitor of acid sphingomyelinase in vitro. J Lipid Res *61*, 896-910.

Kappe, C., Mohamed, Z.H., Naser, E., Carpinteiro, A., and Arenz, C. (2020). A Novel Visible Range FRET Probe for Monitoring Acid Sphingomyelinase Activity in Living Cells. Chemistry *26*, 5780-5783.

Table of contents

Table of contents

1. Introduction

1.1 Acid sphingomyelinase

1.1.1 Location and function in sphingolipid metabolism

Sphingolipids are important structural components of cellular membranes and an abundant class of lipids in eukaryotic cells. They are also bioactive pleiotropic molecules playing versatile roles in cellular signaling, particularly ceramide and sphingosine-1-phosphate (S1P) (Gulbins and Li, 2006; Maceyka et al., 2012). They are distinguished from other lipids by containing the eighteen-carbon amino-alcohol sphingosine which is one of the major sphingoid bases. They may contain derivatives of sphingosine like dihydrosphingosine and phytosphingosine. Their biosynthesis begins in the ER from nonsphingolipid precursors **(Fig. 1)**.

Catabolism of sphingolipids takes place, as with other major classes of lipids like glycerophospholipids, in the acidic environment of the endo-lysosomal compartment. Acid sphingomyelinase (human: ASM, *SMPD1*; murine: Asm, *Smpd1*; herein uniformly ASM. Enzyme Commission Classification number 3.1.4.12) catalyzes the hydrolysis of sphingomyelin into ceramide and phosphorylcholine with a pH optimum of ~5 **(Fig. 2)**. Sphingomyelin is particularly abundant in the outer leaflet of plasma membrane; it is also a principle phospholipid of the myelin sheath.

On one hand, the basal activity of acid sphingomyelinase is important in sphingolipid/membrane turn-over and it provides important downstream products for the salvage pathway that recycles these products. Particularly, sphingosine which is generated in the lysosomes after cleavage of ceramide into sphingosine and a free fatty acid by the enzyme acid ceramidase (human: AC, mouse Ac), is utilized for other rounds of sphingolipid biosynthesis (Le Stunff et al., 2007).

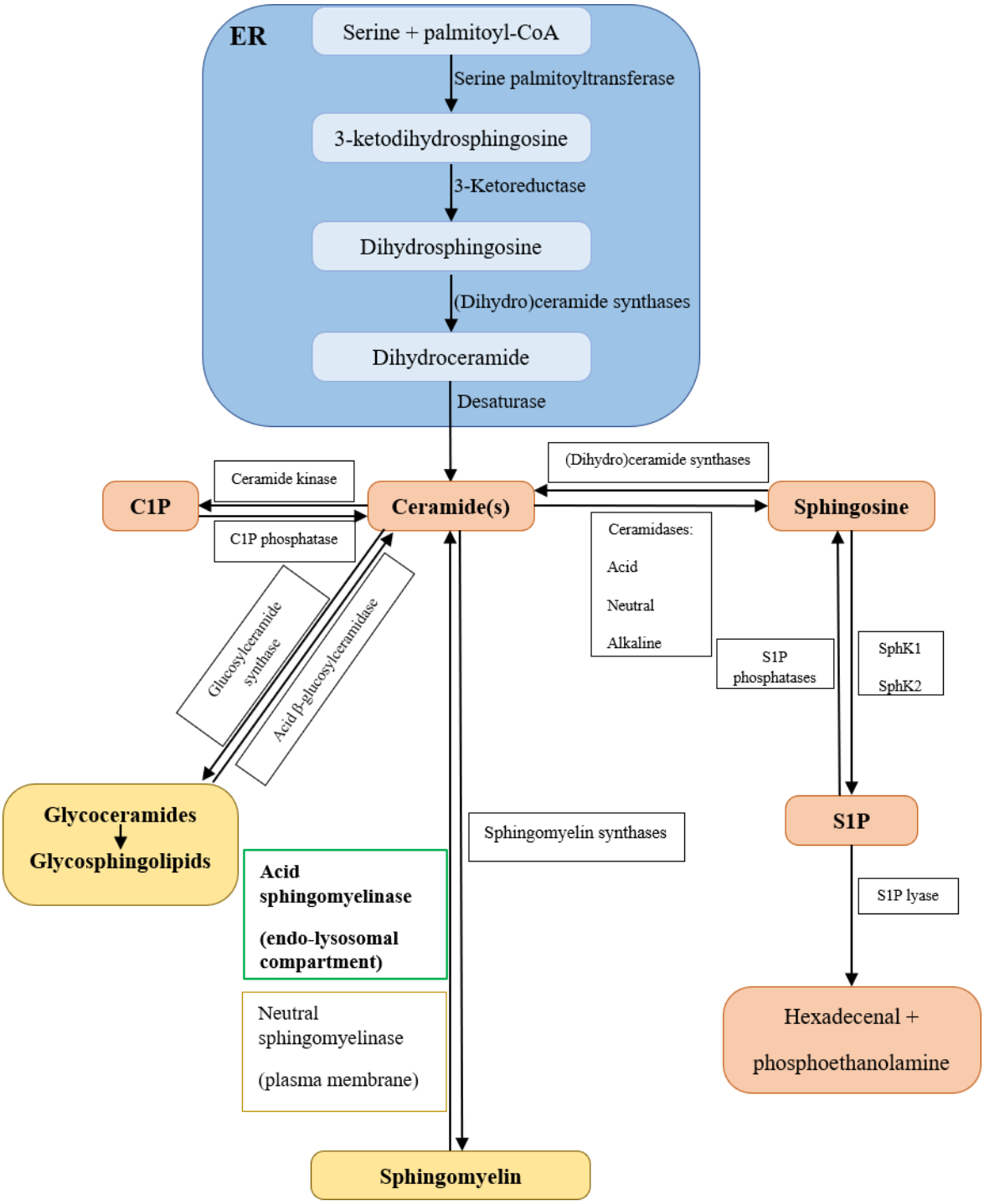

Figure 1. Basic overview of sphingolipid metabolism. ER: Endoplasmic reticulum. S1P: Sphingosine-1-phosphate. SphK: Sphingosine kinase. C1P: Ceramide-1-phosphate. The compartments in which the enzymes reside (cellular organelles) are not shown except for *de novo* synthesis.

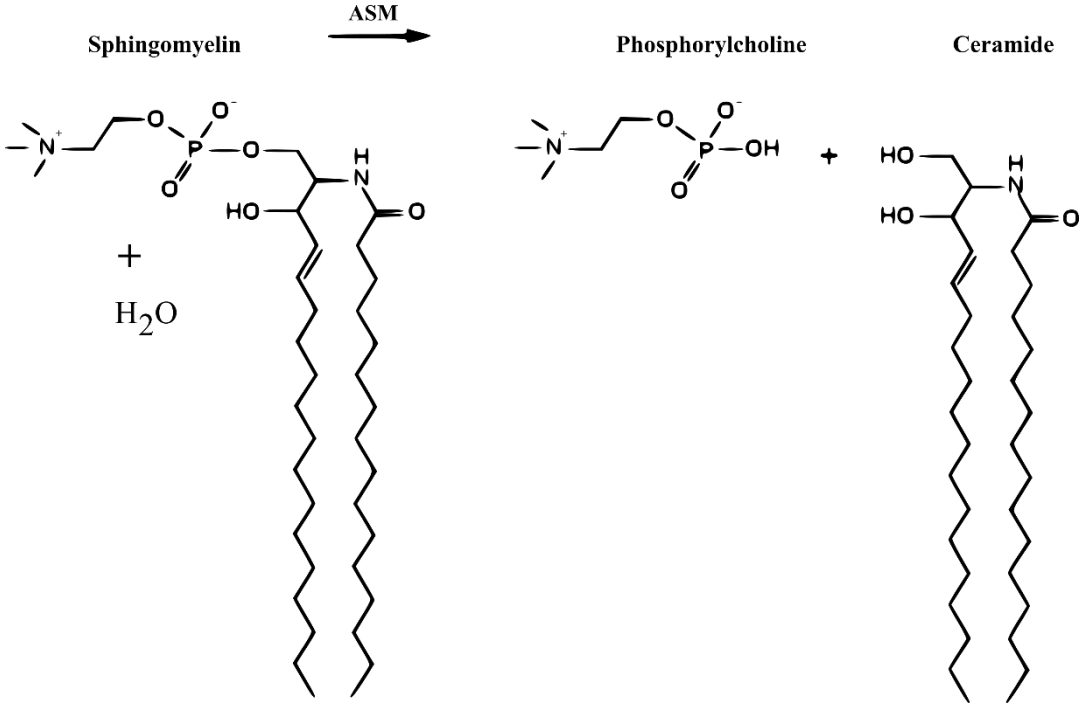

Figure 2. The reaction of sphingomyelin hydrolysis by ASM.

1.1.2 Lack of functional ASM causes Niemann-Pick disease (NPD)

Hereditary mutations of *SMPD1* (sphingomyelin phosphodiesterase 1) that lead to the production of a malfunctional enzyme cause the lysosomal storage disease Niemann-Pick type A and B (Schuchman and Desnick, 2017; Zhou et al., 2016). This etiological relationship was first described by Roscoe Brady 1966 (Brady et al., 1966). This rare genetic disorder has a birth rate of roughly 0.5-1 per 100 000. The different types of NPD represent a continuum of clinical severity (Wasserstein and Schuchman, 1993). The most common and severe type is A, the acute neuronopathic form which affects the central nervous system and is characterized by rapidly progressive neurodegeneration and hepatosplenomegaly. Most patients are diagnosed in the first 6 months of life and und most infants with type A do not survive beyond the third year of life (Brady et al., 1966; Schneider and Kennedy, 1967). In type B, there are no signs of central nervous system involvement, and patients usually present in early childhood with hepatosplenomegaly. They survive several decades of life. However, they usually suffer from liver failure, a lipid pro-atherogenic profile (Wasserstein et al., 2004) and

restrictive lung disease (McGovern et al., 2008). The standard confirmatory diagnostic procedure is measuring ASM activity in blood leukocytes or cultured skin fibroblasts. Current treatments are bone marrow transplantation for type B patients and enzyme replacement therapy with recombinant human acid sphingomyelinase (rhASM) which is currently in phase 2/3 clinical trials. However, none of these therapies seem to prevent the progressive neurological disease.

1.1.3 Maturation and structure of ASM: lysosomal and secretory ASM

ASM is a phosphoesterase enzyme, and the encoding gene (human *SMPD1*, murine *Smpd1*) is ~6 kilobases long. *SMPD1* is located on chromosome 11p15.1-11p15.4 consisting of six exons and five introns. It gives rise to 7 splice variants, among which only number 1 yields a functional enzyme (Schuchman et al., 1991). Both lysosomal ASM (L-ASM) and secretory ASM (S-ASM) originate from the same mRNA which is also translated in the same reading frame and without the involvement of alternative splicing (Schissel et al., 1998b; Schissel et al., 1996). The cDNA for transcript 1 has an open-reading frame of 1890 bp giving rise to a polypeptide of 629 amino acids (Quintern et al., 1989; Schuchman et al., 1991). Murine *Smpd1* is located on chromosome 7 and shares 82% identity with human (Newrzella and Stoffel, 1992).

The nascent polypeptide contains an N-terminal signal peptide, a saposin domain, a proline-rich linker, a catalytically active (phosphodiesterase) domain and a C-terminal domain **(Fig. 3)**. Upon entry into the endoplasmic reticulum, the N-terminal signal peptide is cleaved yielding the pre-pro-form, from which both L-ASM and S-ASM arise due to differential glycosylation processing in the Golgi (pro-form). Deletion of the signal peptide resulted in a cytosolic protein lacking the enzymatic activity in cell lysates, and is not secreted (Ferlinz et al., 1994).

In the Golgi, L-ASM has a high mannose N-glycan composition, whereas S-ASM has a complex N-glycosylation pattern (Hurwitz et al., 1994b; Schissel et al., 1998b). In the *cis*-Golgi, L-ASM acquires mannose-phosphate residues via the action of N-acetylglucosamine-1-phosphotransferase, while S-ASM is spared of this modification (Hurwitz et al., 1994b; Schissel et al., 1998b). This modification is critical for L-ASM to gain mannose-6-phosphate moieties that target the enzyme subsequently into the endo-lysosomal compartment via the mannose-6-phospate receptor pathway beginning

in the *trans*-Golgi, which is a major trafficking pathway for L-ASM and for lysosomal hydrolases in general (Hasilik et al., 1981; Takahashi et al., 2005). The S-ASM pro-form is constitutively secreted via the default Golgi secretory pathway without further processing (Jenkins et al., 2010).

In the endo-lysosomal compartment, further proteolytic processing takes place: N-terminal processing and, most importantly (unlike S-ASM), C-terminal processing which renders the enzyme catalytically highly active by promoting the coordination with lysosomal Zn^{+2} (Jenkins et al., 2011; Qiu et al., 2003).

ASM has five N-glycosylation sites and eight intramolecular disulfide bonds (Gorelik et al., 2016). Glycosylation is important for proper folding and trafficking, and for protection against the highly proteolytic environment within the lysosome (Newrzella and Stoffel, 1996), and may be important for keeping the mature enzyme in an active conformation (Bartelsen et al., 1998). The disulfide bridges in the catalytic domain are also important for the enzymatic activity.

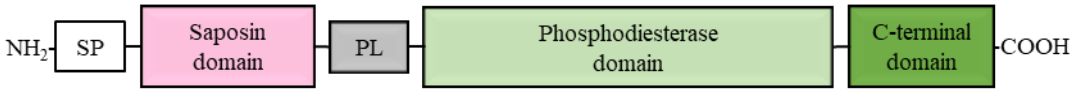

Figure 3. Schematic representation of ASM protein domains. SP: Signal peptide. PL: Proline-rich linker. N-glycosylation sites and disulfide bridges are not shown.

1.1.4 Enzymology of ASM

1.1.4.1 Mechanism of substrate hydrolysis: The catalytic domain of ASM belongs to the calcineurin-like phosphoesterase family. It assumes a spherical shape with a shallow depression on one side, at the base of which a two-zinc iron center resides (Gorelik et al., 2016). This di-metal active site possesses an octahedral coordination geometry (zinc octahedral coordination shell) composed of seven highly conserved residues, a water molecule and is completed by the phosphate group **(Fig. 4 *left*)**.

It is proposed that ASM catalyzes sphingomyelin hydrolysis via the canonical mechanism of phosphoesterases, in which a water molecule activated by zinc acts as a nucleophile attacking the phosphate group of sphingomyelin, followed by protonation of the ceramide leaving group which releases ceramide and phosphocholine **(Fig. 4 *right*)**. Among the active center residues, histidine 317 is important for the substrate binding while histidine 280 assisted by aspartate 249 is important for leaving group protonation. This became evident since mutation of histidine 317 to alanine completely abolished the catalytic activity against sphingomyelin and led to a slight reduction in the activity against the non-lipid phosphodiesterase substrate bis(*p*-nitrophenyl)phosphate (bNPP), while substitution of histidine 280 completely abolished the activity against both substrates (Gorelik et al., 2016). Other active site residues are important for interaction with zinc.

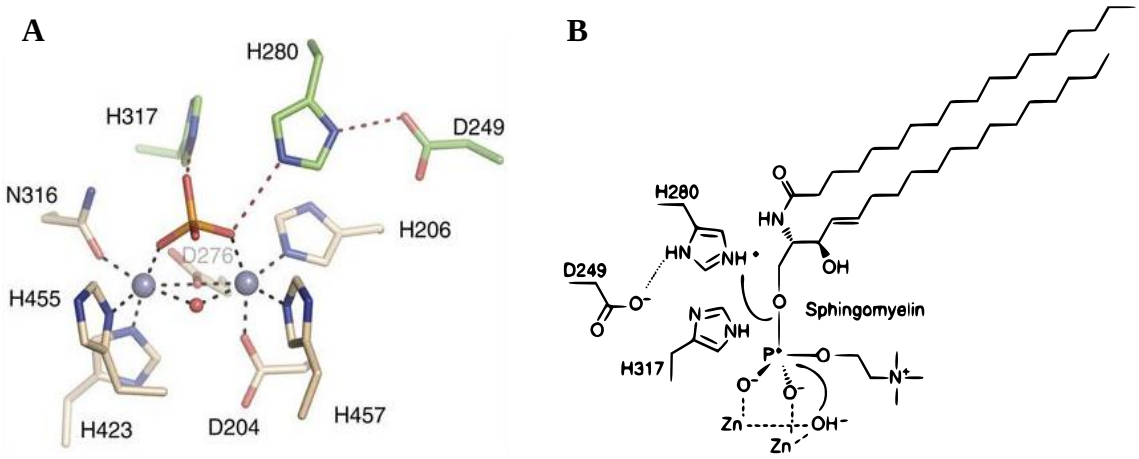

Figure 4. Catalytic mechanism of ASM (Gorelik et al., Nat Commun 2016). (A) Active site residues of ASM. Grey balls are zinc ions, red balls are water molecules, red and orange sticks is a phosphate group. Residues shown in green are important for substrate binding (H317) or leaving group protonation (H280 and D249); residues in beige are zinc-interacting. **(B)** The catalytic mechanism involves a nucleophilic attack by zinc-activated water molecule on the phosphate group of sphingomyelin followed by protonation of the ceramide leaving group by H280 assisted by D249, which releases ceramide and phosphorylcholine.

1.1.4.2 The saposin domain of ASM: ASM possesses, unlike some other sphingolipid hydrolases, its own saposin domain which is located between the N-terminal signal peptide and the proline-rich linker extending between amino acids ~85-165. This domain is analogous to the sphingolipid activator proteins (SAPs) A, B, C and D, which are non-enzymatic glycoproteins that usually function in the lysosomes in cooperation

with certain sphingolipid hydrolases and serve to extract lipid substrates from membranes exposing them to the active sites of the respective enzymes (Kolter and Sandhoff, 2005).

The saposin domain of ASM consists of 4 α-helices and adopts either a closed (inactive) globular conformation or an open V-shaped (active) conformation depending on the environment **(Fig. 5)**. The open V-shaped conformation is on one side important for membrane docking (as ASM is a soluble protein) since the surface of helix α2 is lined with positively charged residues that establish electrostatic interactions with anionic lipids in the intra-lysosomal vesicles, particularly with the abundant bis(monoacylglycero)phosphate (BMP). Importantly on the other hand, helix α3 of the open conformation forms extensive hydrophobic interface with the catalytic domain via conserved non-polar residues from both saposin and catalytic domains, which serves presumably to stabilize the open conformation of the saposin domain, allowing it to dock onto membranes and to deliver the substrate to the active site. Interestingly, several mutation in the conserved residues of the saposin domain led to decreased activity not only in liposomal but also in micellar assays, which, in contrast to the activity in liposomal membranes, could not be rescued with exogenous SAPs (Kolzer et al., 2004a). The authors suggested that the saposin domain of ASM may have other functions than lipid extraction. Resolving the crystal structure of ASM in 2016 revealed that the hydrophobic interface between the saposin domain and the catalytic domain is in contact with active site loops and analysis of the crystal temperature factors showed that interface formation reduces catalytic loop dynamics, suggesting that the interface is also important for stabilizing the catalytic domain and in activating substrate hydrolysis directly (Gorelik et al., 2016; Xiong et al., 2016). The catalytic domain alone or interface mutants in the complete enzyme exhibited no activity or diminished activity, respectively not only against sphingomyelin but also against bNPP. Addition of several non-ionic detergents at concentrations below or above the critical micellar concentration increased the activity of wild-type ASM against bNPP. Lastly, Triton X-100 could partially restore the activity against bNPP in several interface mutants by presumably stabilizing the open conformation and the hydrophobic interface, bypassing the need for the substituted residues (Gorelik et al., 2016; Xiong et al., 2016).

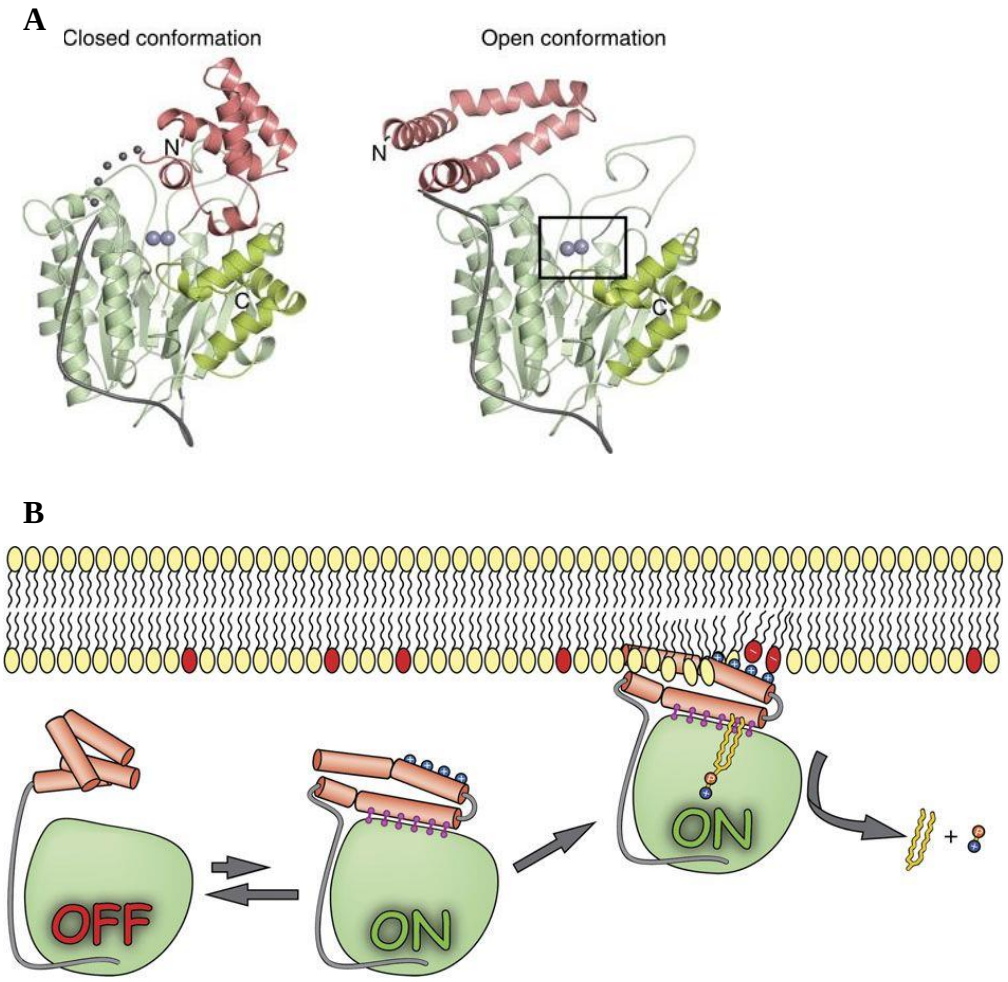

Figure 5. Saposin domain and activation of ASM (Gorelik et al., Nat Commun 2016). (A) Ribbon diagram of ASM proteins showing the open and closed conformation of saposin domain (pink), the catalytic domain (light green) and the C-terminal domain (dark green). Grey balls are zinc ions. Consecutive dotted spheres are the disordered region in the proline-rich linker; the rest is a rigid L-shaped region. **(B)** Proposed model where ASM exists in equilibrium between an open (on) and a closed (off) forms of saposin domain: presence of anionic lipids (red) shifts the balance towards the open form exposing the positively charged residues (blue), interacting with anionic lipids and stabilizing the open conformation, thus allowing the saposin domain concomitantly to establish hydrophobic interface with the catalytic domain (purple), which activates sphingomyelin hydrolysis.

1.1.4.3 Effect of pH: Michaelis-Menten kinetic analysis revealed that lysosomal ASM requires acidic pH for substrate binding (K_m) but not for the catalytic velocity (V_{max}) (Callahan et al., 1983).

L-ASM is presumably not active at neutral pH. Whether S-ASM could function in neutral pH is unclear. There is some discrepancy in this regard depending on the source and purification of secretory ASM, with several studies reporting no residual zinc-

dependent activity at pH 7 in serum, plasma, cerebrospinal fluid, saliva and urine (Kornhuber et al., 2015). Recombinant human ASM from Chinese hamster ovary (CHO) cells exhibits no detectable activity at pH 7 either (He et al., 1999).

There is evidence of markedly increased S-ASM activity against sphingomyelin at neutral pH in LDL from patient-derived atherosclerotic lesions (Schissel et al., 1998a).

Moreover, the presence of acidic microdomains in the vicinity of cell surface in various cell types could offer an explanation how S-ASM may function. Translocation of L-ASM onto the outer leaflet of the plasma membrane was accompanied by a concomitant translocation of the lysosomal V1 H^+-ATPase upon FasL stimulation in coronary artery endothelial cells, which was necessary for ASM-mediated formation of ceramide-enriched membrane platforms (Xu et al., 2012).

1.1.4.4 Zinc requirement: Both lysosomal and secretory ASM are zinc metalloenzymes and require zinc for their activity. L-ASM encounters and tightly binds Zn^{+2} during its maturation, making it possible to detect its activity in cell lysates without further addition of exogenous Zn^{+2}. Secretory ASM in body fluids, cellular supernatants and rhASM from CHO cell-supernatants typically requires the addition of exogenous Zn^{+2} to be activated, usually around 100 µM, which is similar to the concentration in the extracellular fluid and serum. S-ASM activity is inhibited by the zinc-specific chelator 1, 10-phenanthroline (He et al., 1999). This Zn^{+2} requirement of S-ASM may be of physiological and pathophysiological relevance for regulation since the availability and accessibility of extracellular and perhaps intracellular Zn^{+2} could be regulated by zinc-binding factors and since Zn^{+2} levels are reported to be elevated in atherosclerotic (Mendis, 1989) and inflammatory lesions (Milanino et al., 1988).

Endothelial secretory ASM seems to be partially active in the absence of exogenously added Zn^{+2}. This is in contrast to secretory ASM from macrophages, fibroblasts or CHO cells (Marathe et al., 1998). Although the precise mechanism is not clear, it is proposed that secretory ASM in the secretory pathway of endothelial cells has, unlike other cell types, access to cellular pools of Zn^{+2}.

1.1.4.5 C-terminal cysteine and copper: Unlike the lysosomal form, S-ASM is not proteolytically processed at its carboxyterminal end. The C-terminal 629 cysteine in secretory ASM is free and is not engaged in a disulfide bridge.

Deletion, mutation, oxidation or copper-promoted dimerization via this cysteine causes ~5-fold increase in the catalytic velocity (V_{max}) but not substrate binding (K_m) of rhASM from CHO cell-supernatants (Qiu et al., 2003). The suggested mechanism is that the free cysteine competes with H_2O and coordinates better with Zn^{+2} giving rise to an atypical coordination shell and a low activity form. However, once this cysteine is removed or bound with copper to form rhASM dimers, Zn^{+2} becomes available for coordination with H_2O making the typical coordination shell and the high activity form. This could also serve as a regulatory mechanism.

Importantly, in Wilson disease, a copper storage disease, Cu^{+2} accumulation was linked to the activation of both lysosomal and secretory ASM, which contributed significantly to the pathophysiology of liver cirrhosis and anemia although no copper-induced dimerization of ASM was detectable (Lang et al., 2007).

1.1.4.6 Lipid activators and inhibitors: Lipid components of membranes could regulate the activity of ASM, which itself changes the composition of these membranes by catalyzing sphingomyelin and producing ceramide. Bis(monoacylglycero)phosphate (BMP) is a potent activator of rhASM in liposomal assays (Linke et al., 2001). It is proposed that BMP interacts electrostatically with the saposin domain of ASM and this favors and stabilizes the open V-shaped active conformation (Gorelik et al., 2016).

Other activators include also phosphatidylinositol (PI), phosphatidic acid and phosphatidylglycerol (Linke et al., 2001). Both BMP and PI are more abundant in the endo-lysosomal compartment.

Importantly, other than interacting directly with ASM, glycerophospholipids like phosphatidylcholine and phosphatidylethanolamine are important in liposomal membranes to increase ASM activity against sphingomyelin by increasing the proportion of sphingomyelin that is in the fluid state at 37°C, i.e. accessible for hydrolysis by ASM since otherwise most molecular species of sphingomyelin are in gel state in the physiological range of temperatures (Ruiz-Arguello et al., 2002).

Conversely, phosphorylated derivatives of PI (PI-3,5-biphosphate and PI-3,4,5-triphosphate) which are more abundant at the plasma membrane are inhibitors of ASM (Kolzer et al., 2003; Testai et al., 2004).

Normally, cholesterol is gradually depleted from the membranes of the endo-lysosomal compartment during maturation via the action of NPC1 and NPC2 proteins that mediate its trafficking from the cells to lipoproteins, keeping its levels low. Mutations in NPC1 and NPC2 lead to Niemann-Pick disease type C, which is characterized by accumulation of unesterified cholesterol in the lysosomes with secondary inhibition of ASM and accumulation of sphingomyelin. Membrane cholesterol exhibits an inhibitory effect on ASM activity (Reagan et al., 2000). While the precise mechanism in not clear, some sterol cholesterol derivatives like 7-ketocholesterol inhibit ASM directly (Maor et al., 1995).

1.2 ASM in disease

As mentioned earlier, lack of functional ASM is the cause of Niemann-Pick disease type A and B.

ASM and ASM-generated ceramide play significant roles in a vast number of physiological and pathophysiological processes, and ceramide is a key pleiotropic signaling molecule with versatile roles in many signaling events, particularly in stress response (Gulbins and Li, 2006). Many stimuli can induce rapid translocation of lysosomal ASM onto the outer leaflet of the plasma membrane and generation of ceramide, which dramatically influences membrane dynamics and biophysical properties and also has the ability to self-associate forming large ceramide-enriched platforms (Grassme et al., 2007). These platforms serve as sites for reorganizing and clustering cell-surface receptors, amplifying their signaling cascades and achieving the biological effects (Grassme et al., 2007; Zhang et al., 2009). This has been shown for many receptors, stress stimuli and in infectious biology (Grassme et al., 2007; Gulbins and Li, 2006; Zhang et al., 2009). Ceramide is implied in different types of apoptosis including receptor-mediated apoptosis, nonreceptor stress stimuli-mediated apoptosis and growth factor-deprivation-mediated apoptosis (Gulbins and Li, 2006).

Table 1, taken from Beckmann, Nadine: Identification of novel clinical applications for acid sphingomyelinase inhibitors. 2017. Universität Duisburg Essen (DuEPublico 2,

Duisburg-Essen Publications online) provides a thorough overview of diseases which have been linked to ASM/ceramide signaling.

Autoimmunity	**Inflammatory diseases**
Kawasaki disease	Graft-versus-host-disease
Multiple sclerosis	Hemophagocytic lymphohistocytosis
Systemic sclerosis	Hepatic fibrosis
Cancer	Inflammatory bowel disease
Chemotherapeutics	**Metabolic diseases**
Irradiation and radiotherapy	Diabetes
Metastasis	Diabetic retinopathy
Cardiovascular disease	Obesity-induced kidney damage
Atherosclerosis	Steatohepatitis
Cardiomyocyte apoptosis (cardioplegia/reperfusion)	**Neurological disorders**
Thrombus formation	Alzheimer disease
Genetic disorders	Major depression
Sickle-cell disease	Parkinson ’s diseases
Niemann-Pick disease type A and B	**Skin conditions**
Wilson disease/liver cirrhosis	Atopic dermatitis
Infectious diseases	Scleroderma
Bacterial infections	**Respiratory diseases**
L. monocytogenes	Acute lung injury
M. avium	Aspiration pneumonia
N. gonorrhea	Cystic fibrosis
P. aeruginosa	Hypoxemic respiratory failure
S. aureus	Lung fibrosis
S. typhimurium	Tuberculosis
Endotoxic shock syndrome	
Malaria/plasmodia	
Virus infections	
Measles virus	
Rhinovirus	
Sindbis virus9	

Table 1. ASM in disease (N. Beckmann 2017). Overview of diseases which have been linked to ASM/ceramide signaling.

In the past years, both genetic deficiency as well as pharmacological inhibition of ASM have been utilized in preclinical studies to ameliorate disease progression in numerous

disease models, owing to the significance of ASM, ceramide and also sphingomyelin in the pathophysiology of these diseases.

1.2.1 Cystic fibrosis

Cystic fibrosis (CF) is the most common autosomal recessive disorder in Europe and in the United States. It is caused by mutations in the CF transmembrane conductance regulator gene (*CFTR*). Chronic pulmonary infection with bacterial pathogens, in particular *Pseudomonas aeruginosa* is the main cause of morbidity and mortality in CF patients. CFTR deficiency leads to a shift in lysosomal pH and an imbalance between the activity of ASM and acid ceramidase (AC) with the net result of ceramide accumulation in the respiratory epithelium in mouse models and in humans (Nahrlich et al., 2013; Teichgraber et al., 2008). Ceramide accumulation plays a central role in the pathophysiological vicious circuit in CF as it increases the susceptibility for infection with *P. aeruginosa*, respiratory inflammation and cell death (Teichgraber et al., 2008). Moreover, it leads to an ectopic luminal accumulation of β1-integrins on the epithelium of the upper respiratory tract in mice and humans further downregulating AC, accumulating ceramide and reducing downstream sphingosine which has antibacterial properties (Grassme et al., 2017). Genetic deficiency, heterozygosity and pharmacological inhibition of ASM with amitriptyline (a tricyclic antidepressant and a functional inhibitor that leads to the proteolytic degradation of ASM, discussed later) reduce ceramide levels in the respiratory epithelium ameliorating all pathological and clinical manifestations (Becker et al., 2010; Teichgraber et al., 2008). Phase II clinical studies showed that long-term treatment with amitriptyline significantly increased forced expiratory volume in 1 sec (FEV1) and weight of CF patients (Adams et al., 2016).

1.2.2 Major depression

Fluoxetine and amitriptyline are clinically approved antidepressants. They are also functional inhibitors of ASM (FIASMAs). Studies revealed that inhibition of ASM is essential for their antidepressant action *in vivo*, and that they, as well as genetic deficiency of ASM, lead to reduction of ceramide in the hippocampus, increased neuronal proliferation, maturation, and survival and improved behavior in mouse models of stress-induced depression (Gulbins et al., 2013). More recently, it was

revealed that the induction of autophagy in the hippocampal neurons downstream of ceramide accumulation in the endoplasmic reticulum is essential for the therapeutic effects of tricyclic antidepressants and that inhibiting sphingomyelin synthase, thus accumulating ceramide in the endoplasmic reticulum, has a much more rapid onset of action in models of stress-induced depression (Gulbins et al., 2018).

1.2.3 Hematogenous cancer metastasis

In a mouse model of hematogenous cancer metastasis, genetic deficiency, heterozygosity, and pharmacological inhibition of ASM with amitriptyline significantly reduced the metastasis of B16F10 murine melanoma cells injected intravenously as well as the spontaneous hematogenous metastasis of MT/*ret* melanoma cells injected subcutaneously (Carpinteiro et al., 2015). Tumor cells interact with and activate platelets in blood stream, which in turn secrete ASM rapidly onto the surface of interacting tumor cells generating ceramide that clusters and activates α5β1 integrins leading to the adhesion of the tumor cells and augmenting their metastasis (Carpinteiro et al., 2015).

1.2.4 Specific toxicity to transformed cancers

Although ceramide is generally considered pro-apoptotic, inhibiting ASM in this context has different consequences. Resistance to therapy in transformed tumors is usually acquired early when genetic changes lead to defects in caspase-dependent pathways. Furthermore, chemotherapy may lead to the expression of multidrug resistance proteins that are able to efflux drugs. However, this transformation is associated with important changes in sphingolipid metabolism, and these tumors exhibit reduced ASM expression and activity accompanied by reduced sphingomyelin in their lysosomal membranes (Petersen et al., 2013). Their lysosomes are vulnerable and are particularly susceptible to ASM inhibition with FIASMAs (especially siramesine) that lead to dose-dependent specific toxicity both *in vitro* and *in vivo* and reduction in tumor size, owing to the leakage of lysosomes and eventually lysosomal cell death, which could represent a novel therapeutic option in otherwise resistant cancers (Petersen et al., 2013).

1.2.5 Farber Disease

Farber disease is a rare lysosomal storage disease resulting from acid ceramidase deficiency and accumulation of ceramide with subsequent organ failure. No treatments are clinically available and affected patients have severely shortened lifespan. A novel Ac-mutant mouse model was successfully established to understand the pathogenesis and investigate new therapies (Beckmann et al., 2018). Crossbreeding Ac-deficient mice with Asm-deficient mice reduced ceramide levels and disease manifestations and led to prolonged survival (Beckmann et al., 2019). In contrast to the previous diseases however, pharmacological inhibition of ASM with amitriptyline not only could not phenocopy the genetic deficiency but also worsened disease progression and led to toxicity and rapid death. One possible explanation is that most FIASMAs lack specificity and inhibit AC at least *in vitro,* which could be relevant in Farber mice, albeit the unaltered ceramide levels in liver upon treatment with amitriptyline (Beckmann et al., 2019).

1.3 Pharmacological inhibition of ASM

1.3.1 Functional inhibitors of ASM (FIASMAs)

FIASMAs are currently widely used as ASM inhibitors both *in vitro* and *in vivo*. There is no evidence that they could inhibit ASM directly, e.g. they do not inhibit the recombinant enzyme. Instead, they inhibit ASM via an alternative mechanism (Hurwitz et al., 1994a; Kolzer et al., 2004b; Kornhuber et al., 2008). Most of them can be classified as cationic amphiphilic drugs (Kornhuber et al., 2011), i.e. they have a lipophilic part that enables them to passively pass through the plasma membrane and the lysosomal membrane and a cationic part which in this case is a weak organic base, so that they are only slightly protonated at physiological pH. In contrast, in the acidic pH of the lysosomes, they are heavily protonated (positively charged) and thus trapped and highly accumulated within the lysosomes (usually referred to as lysosomotropic). They interfere with the electrostatic interactions that attach the saposin domain of L-ASM (positively charged) to the lysosomal anionic lipids, in particular BMP, which stabilize the saposin open V-shaped conformation rendering the enzyme highly active (Gorelik et al., 2016; Xiong et al., 2016) and also protect it against proteolytic digestion by lysosomal proteases. This interference leads to detachment of L-ASM from the surface

of the intra-lysosomal vesicles, inactivating it and, importantly, culminating in its proteolytic degradation **(Fig. 6)** (Hurwitz et al., 1994a; Kolzer et al., 2004b). According to this definition, FIASMAs are also capable of inhibiting ASM in liposomal assays (Gorelik et al., 2016; Kolzer et al., 2004b) albeit the considerably higher doses (in the low millimolar range compared to the low micromolar range in cells) which could be attributed to the lack of sufficient protonation and thus entrapment, and the lack of proteolytic degradation in liposomal assays.

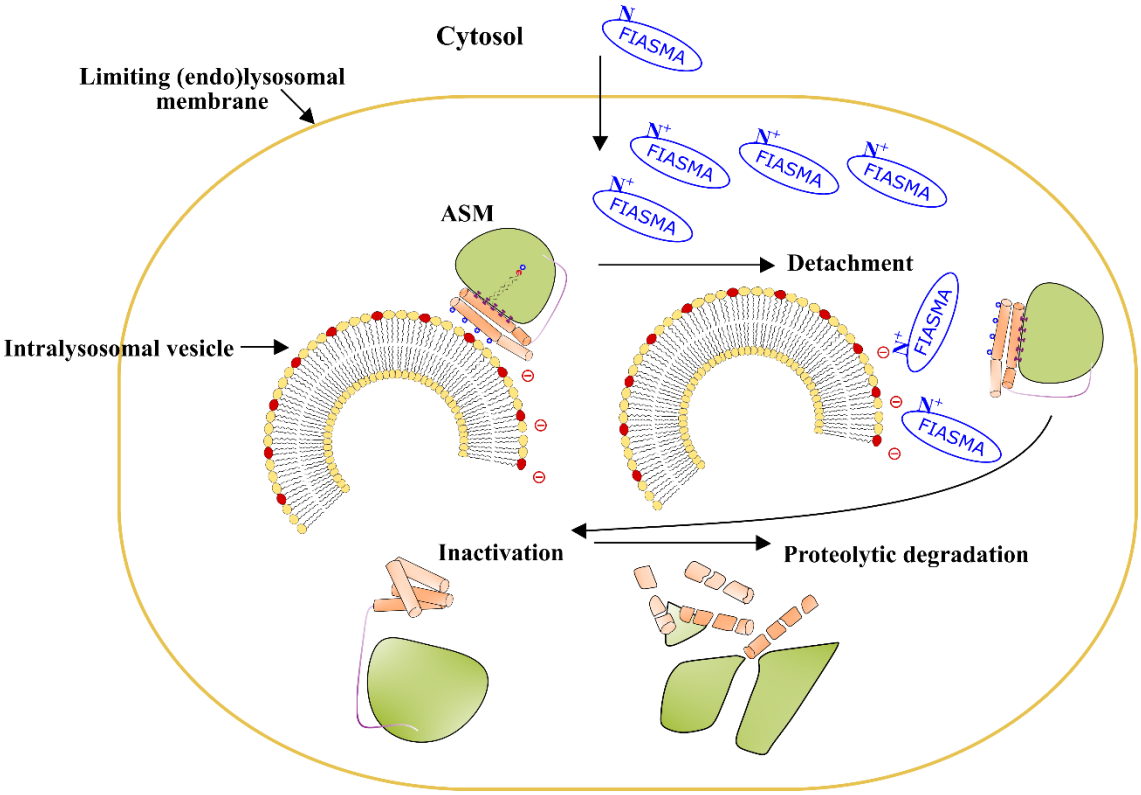

Figure 6. Schematic representation of the proposed mechanism of action for ASM inhibition by FIASMAs. FIASMAs reach the lumen of the endo-lysosomal compartment by passive diffusion. They are structurally diverse but all have a basic nitrogen atom. In the acidic milieu of the (endo)lysosomes, they are protonated and, thus, trapped and accumulated. They interfere with the electrostatic interactions between the saposin domain of ASM and the intra-lysosomal anionic lipids, leading to detachment, inactivation and subsequent proteolytic degradation of the enzyme.

Extensive screening led to identification and experimental validation of 72 FIASMAs, defined by ≤50% reduction in ASM activity at 10 µM (Kornhuber et al., 2011; Kornhuber et al., 2008). They represent a wide spectrum of heterogenous compounds, most of which are clinically approved for treatment of diverse entities of diseases, e.g.

tricyclic antidepressants or psychoanaleptics like amitriptyline, desipramine and fluoxetine, psycholeptics like fluphenazine, calcium channel blockers like amlodipine, antihistamines like loratadine.

Structurally, these compounds are diverse, but they share critical physiochemical properties important for lysosomotropism and ASM inhibition, particularly the log *P* value (5.35 ± 1.13) and the pK_a value (9.04 ± 1.18) (Kornhuber et al., 2011), which show that FIASMAs cluster around a preferred range of log *P* and pK_a higher than that for a cationic amphiphilic drug in general (log $P \geq 3$, p$K_a \geq 7.4$), meaning that most of them are cationic amphiphilic drugs but the opposite is not true.

Pharmacodynamically and pharmacokinetically they do not lead to complete ASM inhibition, do not induce habituation, they have a reversible mode of action, do not induce rebound effects, they have other molecular targets (no compound acts exclusively as FIASMA), they have favorable ADME (Absorption, Distribution, Metabolism and Excretion) properties, they bypass the blood-brain barrier (Kornhuber et al., 2005; Kornhuber et al., 2011; Kornhuber et al., 2010).

Concerning specificity, their inhibitory effects seem to be restricted to the lysosomes (Kornhuber et al., 2010), thus sparing for example neutral sphingomyelinase and other sphingolipid-metabolizing enzymes outside the endo-lysosomal compartment. They do not seem to primarily inhibit S-ASM either. Regarding lysosomal hydrolases, however, there is evidence *in vitro* that FIASMAs lack specificity due to their mechanism of action and could potentially inhibit other important hydrolases in a similar mechanism and dose-range for ASM inhibition like acid ceramidase (Elojeimy et al., 2006; Zeidan et al., 2006), acid lipase (Albouz et al., 1981), phospholipase A and C (Matsuzawa and Hostetler, 1980). *In vitro*, they are also linked to upregulation of Cathepsin L (Elojeimy et al., 2006), induction of a lysosomal stress response (Lu et al., 2017), and induction of phospholipidosis (Muehlbacher et al., 2012). However, it is difficult to generalize: inhibition of AC was essentially identified with desipramine, while siramesine was shown not to inhibit AC at the dose-range relevant for its ASM inhibitory effect (Petersen et al., 2013). Induction of phospholipidosis also differs significantly among FIASMAs: for instance, amitriptyline and desipramine induce phospholipidosis to a

lesser extent at the dose-range relevant for ASM inhibition compared with amiodarone which induces significant phospholipidosis *in vitro* (Muehlbacher et al., 2012).

Lastly, it should be noted that some of these *in vitro* studies used high concentration that are above those required for ASM inhibition and that there is no evidence for inducing such effects *in vivo.* In fact, particularly tricyclic antidepressants have successfully reproduced the phenotype observed in ASM knock-out or heterozygous mice used in various disease models *in vivo* like cystic fibrosis and major depression, leading to a reduction in ceramide levels (Gulbins et al., 2013; Teichgraber et al., 2008).

1.3.2 Development of direct inhibitors: phosphate-containing inhibitors and ARC39

1.3.2.1 Phosphoinositide and carbohydrate-derived inhibitors: Early work characterized, among others, adenosin-3,5-diphosphate and PI-4,5-bisphosphate as moderate inhibitors of ASM (IC_{50}=1-5 µM) (Quintern et al., 1987). Later, phosphoinositides were identified as inhibitors of ASM with PI-3,5-bisphosphate **(Fig. 7)** being the most potent (K_i=0.53 µM) and selective sparing neutral sphingomyelinase and acid ceramidase (Kolzer et al., 2003). However, phosphoinositides are chemically instable and also biologically labile since they are substrates for phospholipases A_1, A_2, C and D, as well as other inositol-specific or unspecific phosphatases. As structural components of biological membranes, they also have poor off-rates from membranes, meaning that spontaneous flip-flip transmembrane movements are unlikely since they are charged molecules, which reduces their intracellular distribution. There are no reports about their successful use as ASM inhibitors in cell culture or in animals (Arenz, 2010).

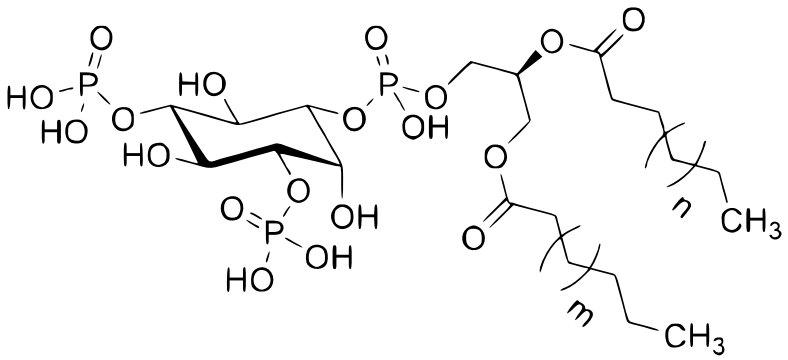

Figure 7. Chemical structure of PI-3,5-bisphosphate.

The observation that lysolipids (one-tailed) like sphingosine and S1P migrate, in contrast to two-tailed lipids, readily between liposomal membranes in lipid-transfer assays (Babalola et al., 2007) indicating better off-rates and intracellular distribution led to the development of one-tailed PI-3,5-bisphosphate analogues, where structure-activity-relationship studies revealed that not only the inositol hydroxyl groups are important for inhibition, but also the lipophilic residue, which in the case of PI-3,5-bisphosphate is the two-tailed diacylglycerol (DAG) (Roth et al., 2009b). Replacement of the latter by one-tailed alkyl dodecyl sulfone ester yielded an analogue **(Fig. 8A)** that is equally potent but inert against phospholipases and active in cell culture as indicated by inhibition of dexamethasone-induced apoptosis in HEK 293 cells at 2 µM (Roth et al., 2009b).

Replacing the inositol moiety with a carbohydrate derivative **(Fig. 8B)** yielded even a slightly more active compound versus ASM than the inositol-based one (Roth et al., 2010).

A

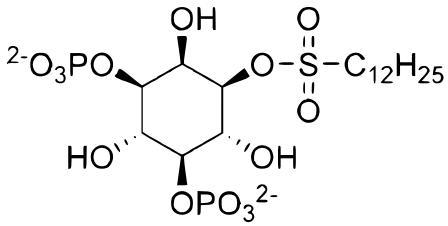

B

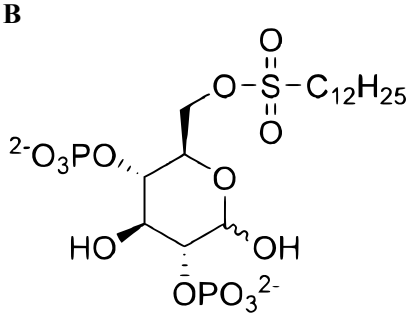

Figure 8. Chemical structures of one-tailed phosphate-containing ASM inhibitors. (A) Roth et al., 2009. **(B)** Roth et al., 2010.

1.3.2.2 Bisphosphonates: In efforts to replace the biologically labile phosphate groups by uncleavable phosphonates, attempts were undertaken to synthesize phosphonate analogues of PI-3,5-bisphosphate, which yielded only moderate inhibitors.

Scanning a collection of bisphosphonates that had been synthesized in the GDR Academy of Science and are structurally related to phosphoinositides led to the observation that the geminal bisphosphonate with an α-amino group **(Fig. 9 compound 1b) (Table 2)** is one order of magnitude more potent than PI-3,5-bisphosphate. Interestingly containing two additional methylene groups than **compound 1a** increased the inhibitory effect 100-fold **(Table 2)** (Roth et al., 2009a).

To gain deeper insight into the structure-activity-relationship, additional bisphosphonates harboring different functional groups (H, -OH or -NH_2) at the α position and displaying lipid tails of different length were synthesized. The inhibition correlated to the length of the lipid tail (holds true as long as the compound is readily soluble), and functional groups at the α position with lone electron pairs increases the inhibitory effect on ASM (-NH_2>-OH>H) **(Fig. 9) (Table 2)**.

Among the newly synthesized compounds, the most active was 1-aminodecylidene bis-phosphonic acid IC_{50}=20 nM **(Fig. 9 compound 1c)**, herein called ARC39: Anke Roth project C39.

Bisphosphonates have the propensity to form stable bidentate complexes with divalent metal ions like Zn^{+2}, Ca^{+2} and Mg^{+2}. The presence of an amino group leads to the formation of even more stable tridentate complexes. This could be necessary as ASM inhibitors in order to bind Zn^{+2} at the active site. However, this complex-forming propensity was not enough to explain the inhibitory effect on ASM because of two observations: 1) adding millimolar concentrations of Zn^{+2} did not significantly diminish the inhibitory effect, and 2) adding an amino group to the lipid tail led to a significant drop in the inhibitory effect (30-100 fold), albeit the ability to form tridentate complexes (Roth et al., 2009a).

In fact, zoledronate, a nitrogen-containing bisphosphonate that is used in the clinic, is an inhibitor of ASM **(Fig. 9) (Table 2)** (Roth et al., 2009a).

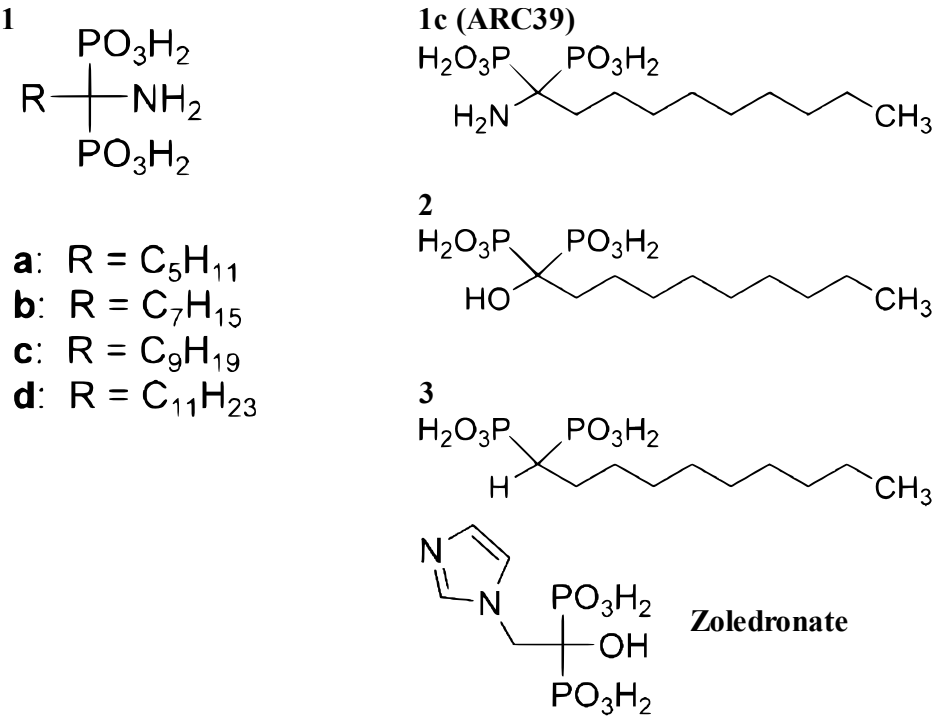

Figure 9. Bisphosphonate inhibitors of ASM (Roth et al., 2009).

Compound	IC_{50} (µM)	Compound	IC_{50} (µM)
1a	4.66 ±1.07	**2**	0.08 ±0.01
1b	0.04 ±0.01	**3**	0.31 ±0.12
1c (ARC39)	0.02 ±0.00	**Zoledronate**	5.08 ±0.74
1d	0.29 ±0.09		

Table 2. Bisphosphonate inhibitors of ASM (Roth et al., 2009).

All compounds were not active towards NSM with IC_{50}>100 µM, and ARC39 did not inhibit the remote ASM analogue serine/threonine phosphatase 1, suggesting selectivity (Roth et al., 2009a).

The same work also addressed some biological effects and showed:

- Treating HepG2 cells with 0.1 µM ARC39 inhibited dexamethasone-induced apoptosis.
- Adding ARC39 to the perfusate led to a dose-dependent (0.1-1 µM) reduction in edema formation in a model of platelet-activating factor-induced pulmonary

edema of isolated ventilated and perfused rat lungs, consistent with the previously reported role of ASM (Goggel et al., 2004).

It should be noted that these biological effects are mainly attributed to S-ASM and/or cell surface activity of L-ASM on the outer leaflet of plasma membrane upon translocation.

1.3.2.3 Mechanism of ASM inhibition by ARC39: Co-crystallizing ARC39 with ASM provided valuable insight about how ARC39 works and helped directing the future rational design of new ASM inhibitors by exploiting the shape of the active site **(Fig. 10)** (Gorelik et al., 2016).

This work suggested that the phosphate group of ARC39 not only competes with the substrate and blocks the substrate binding site, but also completes the octahedral zinc coordination shell by excluding the nucleophilic water molecule. This phosphate group is positioned in a different direction than the scissile phosphate and appears as a product, as if its configuration has been inverted after the nucleophilic attack by the zinc-activated water molecule **(Fig. 10B)**. Interestingly, the nine-carbon lipid tail of ARC39 sits in a relatively featureless groove distinct from that of sphingomyelin and coincides only with the choline head group of sphingomyelin **(Fig. 10A)**.

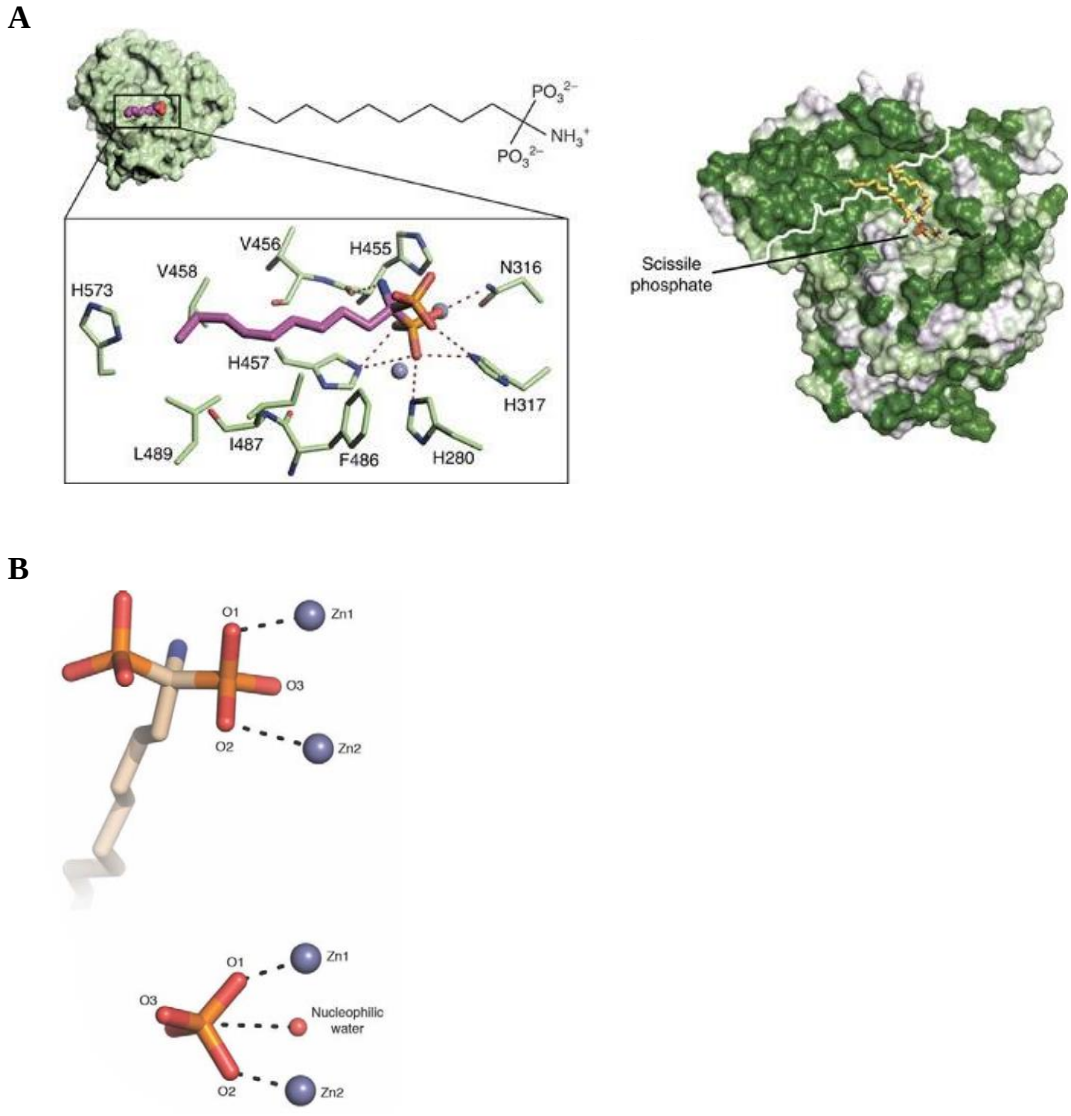

Figure 10. Proposed model of ARC39 binding at the active site of ASM (Gorelik et al, Nat Commun 2016). (A) *Left*: ARC39 bound to ASM. Shown in the magnified box are the active site residues and the zinc ions. *Right:* Both sphingomyelin (yellow sticks) and ARC39 (black sticks) are bound to ASM. The white line represents the boundary between the saposin domain and the catalytic domain. **(B)** Comparison between the phosphate-bound active site (below) and that of ARC39-bound (above). In the phosphate-bound structure, the phosphate group is positioned as a substrate with O3 pointed at a direction opposite to that of ARC39, which appears to be positioned as a product. The phosphate group of ARC39, thus, not only blocks the substrate binding site, but also completes the octahedral zinc coordination shell by excluding nucleophilic water molecule.

1.4 Aim of the study

To this date, no direct and selective inhibitors of ASM are sufficiently characterized or widely used. Since the discovery of ARC39 as the hitherto most potent high-affinity direct inhibitor of ASM, it was applied individually in sparse studies without actually understanding the characteristics of its inhibitory action in a biological context.

The purpose of this study is to characterize ARC39 systematically both *in vitro* and *in vivo* in order to provide useful input about its potential application as a new ASM inhibitor. The diagram summarizes the main points to be addressed.

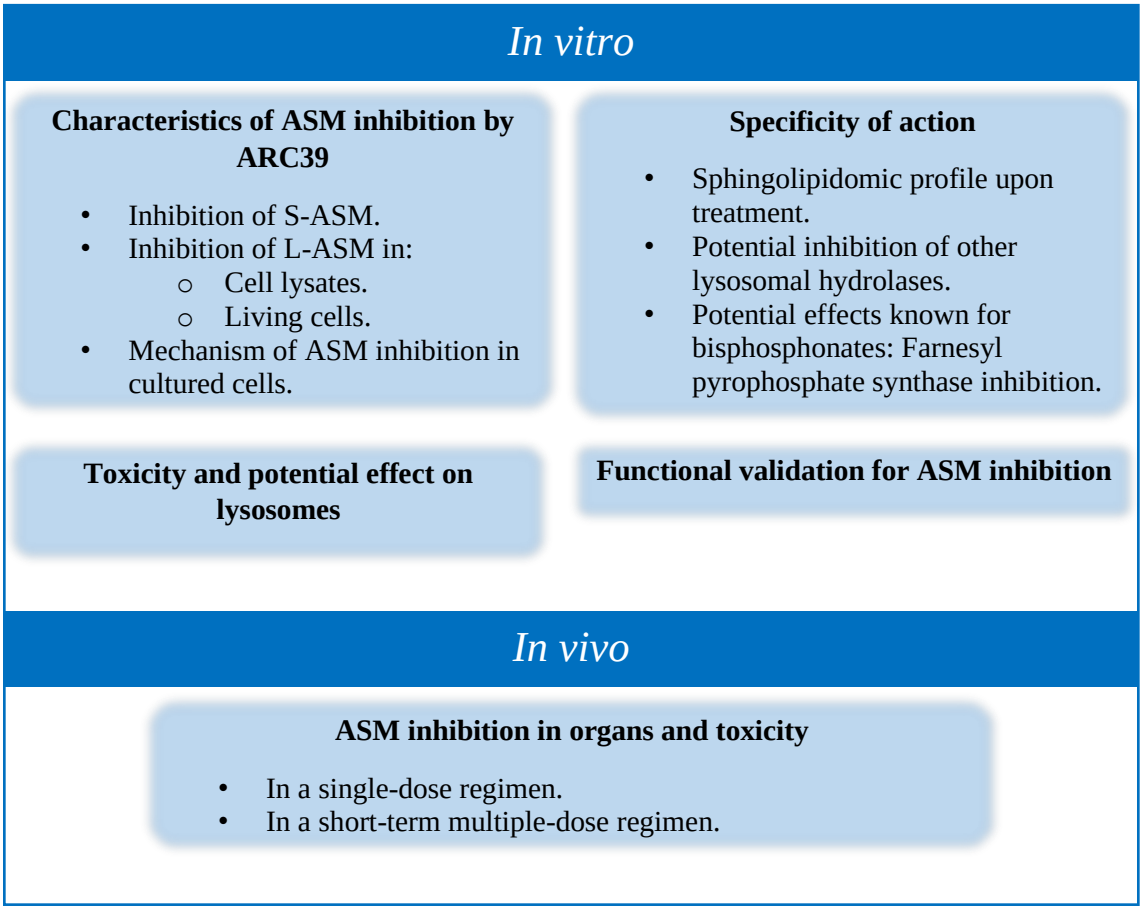

2. Materials and methods

2.1 Materials

2.1.1 Chemicals

Acetic acid (100 %)	Merck KGaA, Darmstadt, Germany
Acrylamide	Carl-Roth GmbH & Co, Karlsruhe, Germany
Ammonium chloride (99.5%)	Carl-Roth GmbH & Co, Karlsruhe, Germany
Ammonium persulfate (APS)	Carl-Roth GmbH & Co, Karlsruhe, Germany
Aprotinin	Carl-Roth GmbH & Co, Karlsruhe, Germany
ATP (99%)	Sigma-Aldrich Chemie GmbH, Steinheim, Germany
Bovine serum albumin (BSA), fatty acid free	Sigma-Aldrich Chemie GmbH, Steinheim, Germany
Bradford Protein assay	Biorad Laboratories GmbH, München, Germany
Calcium chloride (≥ 99 %)	Carl-Roth GmbH & Co, Karlsruhe, Germany
Chloroform	VWR International, Radnor, PA, USA
Complete protease inhibitor cocktail	Roche Deutschland Holding GmbH, Freiburg, Germany
DAPI	Sigma-Aldrich Chemie GmbH, Steinheim, Germany
Di-potassium hydrogen phosphate	Carl-Roth GmbH & Co, Karlsruhe, Germany
Di-sodium hydrogen phosphate	Merck KGaA, Darmstadt, Germany
DMSO (sterile)	Sigma-Aldrich Chemie GmbH, Steinheim, Germany
EDTA	Sigma-Aldrich Chemie GmbH, Steinheim, Germany
Ethanol (absolute, anhydrous)	Diagonal GmbH & Co. KG, Münster, Germany
Ethyl acetate	Diagonal GmbH & Co. KG, Münster, Germany
Glycerol (≥ 99.5 %)	Carl-Roth GmbH & Co, Karlsruhe, Germany
Glycine (≥99%)	Carl-Roth GmbH & Co, Karlsruhe, Germany
HEPES	Carl-Roth GmbH & Co, Karlsruhe, Germany
Hydrochloric acid (fuming, 37 %)	Sigma-Aldrich Chemie GmbH, Steinheim, Germany

Isoflurane (Isothesia)	Henry Schein Vet GmbH, Hamburg, Germany
Leupeptin	Carl-Roth GmbH & Co, Karlsruhe, Germany
Liquid Nitrogen	AIR LIQUIDE Medical GmbH, Düsseldorf, Germany
Magnesium chloride hexyhydrate (≥ 99 % p.a.)	Carl-Roth GmbH & Co, Karlsruhe, Germany
Magnesium sulfate heptahydrate (≥ 99 %)	Sigma-Aldrich Chemie GmbH, Steinheim, Germany
Methanol (BAKER ANALYZED)	VWR International, Radnor, PA, USA
NP-40 (Igepal)	Sigma-Aldrich Chemie GmbH, Steinheim, Germany
Paraformaldehyde (powder, 95 %)	Sigma-Aldrich Chemie GmbH, Steinheim, Germany
Potassium chloride (≥ 99 %)	Carl-Roth GmbH & Co KG, Karlsruhe, Germany
Propidium iodide (95-98 %)	Sigma-Aldrich Chemie GmbH, Steinheim, Germany
Sodium acetate	Sigma-Aldrich Chemie GmbH, Steinheim, Germany
Sodium chloride (≥ 99.5 %)	Carl-Roth GmbH & Co KG, Karlsruhe, Germany
Sodium citrate (tribasic, dehydrate)	Sigma-Aldrich Chemie GmbH, Steinheim, Germany
Sodium fluoride (≥99%)	Carl-Roth GmbH & Co KG, Karlsruhe, Germany
Sodium hydroxide	Carl-Roth GmbH & Co KG, Karlsruhe, Germany
Sodium Orthovanadate (≥90%)	Sigma-Aldrich Chemie GmbH, Steinheim, Germany
Sodium periodate (≥99%)	Sigma-Aldrich Chemie GmbH, Steinheim, Germany
ß-glycero-phosphate disodium salt hydrate (≤1.0 mol % L-α-isomer)	Sigma-Aldrich Chemie GmbH, Steinheim, Germany
ß-Mercaptoethanol	Sigma-Aldrich Chemie GmbH, Steinheim, Germany
Starting Block TBS Blocking Solution	Thermo Fisher Scientific, Waltham, MA, USA
Sucrose	Sigma-Aldrich Chemie GmbH, Steinheim, Germany
Tris (≥99%)	Carl-Roth GmbH & Co KG, Karlsruhe, Germany
Tris-HCl (≥99%)	Carl-Roth GmbH & Co KG, Karlsruhe, Germany
TWEEN 20	Carl-Roth GmbH & Co KG, Karlsruhe, Germany

Umbelliferone (99%)	Sigma-Aldrich Chemie GmbH, Steinheim, Germany
Zinc chloride (97%)	Sigma-Aldrich Chemie GmbH, Steinheim, Germany

2.1.2 Cell culture

	Producer	Product number
Cell lines		
B16F10	ATCC	CRL-6475
HepG2	ATCC	HB-8065
Jurkat	ATCC	TIB-152
Media and additives		
Cell Dissociation Buffer Enzyme-free PBS-based	ThermoFisher Gibco™	13151014
FCS	PAA	A15-151
L-glutamine	ThermoFisher Gibco™	25030081
MEM medium	ThermoFisher Gibco™	11090081
Non-essential amino acids	ThermoFisher Gibco™	11140035
Penicillin/streptomycin	ThermoFisher Gibco™	15140122
RPMI 1640 medium	ThermoFisher Gibco™	21875034
Sodium pyruvate	ThermoFisher Gibco™	11360070
Trypsin 0.25% 1× EDTA	ThermoFisher Gibco™	25200072
Consumables		
24-well plates	Sarstedt	83.1836
96-well plates	Sarstedt	83.1835
Cell culture T75 flasks	Sarstedt	83.3911
Other		
Fibronectin (pure)	Roche	11051407001

2.1.3 ASM inhibitors

	Producer	Product number
Amitriptyline hydrochloride	Merck	A8404
ARC39	Provided kindly by Zainelabdeen Mohamed and Prof. Christoph Arenz	
Desipramine hydrochloride	Merck	D3900

2.1.4 Conventional ASM, Neutral sphingomyelinase (NSM), neutral ceramidase (NC), acid ceramidase (AC) assays, Sphingosine kinase 1 (SphK1) and 2 (SphK2) assays, and *In-situ* ASM assay

	Producer	Product number
Probes		
BODIPY FL C_{12}-sphingomyelin	ThermoFisher Invitrogen™	D7711
NBD-C_{12}-ceramide	Cayman Chemical	10007958
RBM14C12	A kind gift from Dr. Gemma Fabrias and Dr. Antonio Delgado	
NBD-C_{18}-sphingosine	Avanti Polar Lipids	810205P
Sphingomyelinase FAM/BODIPY TR FRET probe	Provided kindly by Christian Kappe and Prof. Christoph Arenz	
Consumables		
5mm stainless steel beads	Qiagen	69989
96-well plates black non-binding	Corning™	07-200-590
96-well plates polypropylene	Corning™	3355
Pre-coated TLC sheets ALUGRAM™ Xtra SIL G	MACHEREY-NAGEL	818232

2.1.5 Recombinant enzymes and antibodies

Recombinant enzymes	Producer	Product number
rhASM	R&D Systems	5348-PD-010
rhSphK1	R&D Systems	5536-SK-010
rhSphK2	R&D Systems	5298-SK-010
Primary antibodies		
Anti-AC Polyclonal IgG Host: Rabbit Reactivity: Human, mouse, rat	ProSci	4741
Anti-ASM Polyclonal IgG Host: Goat Reactivity: Human	R&D Systems	AF5348
Anti-RAP1A Monoclonal (E-6) IgG_1 Host: Mouse Reactivity: Human, mouse, rat	Santa Cruz	398755
Anti-β-actin, HRP-coupled	Santa Cruz	4778

Monoclonal (C4) IgG_1 Host: Mouse Reactivity: Multispecies		
Secondary antibodies		
Goat-anti-mouse AP-coupled	Cell Signaling Technology	7056
Goat-anti-rabbit HRP-coupled	Cell Signaling Technology	7074
Rabbit-anti-goat HRP-coupled	Abcam	Ab6741

2.1.6 Kits and probes

	Producer	**Product number**
Annexin V Binding Buffer 10×	BD Bioscience	556454
APC Annexin V	Biolegend	640941
GoScript™ Reverse Transcription System	Promega	A5001
HCS LipidTOX™ Green Phospholipidosis Detection Reagent	ThermoFisher Invitrogen™	H34350
LysoSensor™ Blue DND-167	ThermoFisher Invitrogen™	L7533
LysoTracker™ Red DND-99	ThermoFisher Invitrogen™	L7528
PowerUp™ SYBR™ Green Master Mix	Applied Biosystems	A25742
RNeasy Mini Kit	Qiagen	74104
XTT Cell Viability Assay Kit	Biotium	30007

2.2 Methods

2.2.1 Cell culture

L929, HepG2 and B16F10 cells were cultured in Minimum Essential Medium (MEM); Jurkat cells in RPMI 1640 supplemented with 10% FCS, 100 U/mL penicillin, 100 µg/mL streptomycin, 2mM L-glutamine, 1 mM sodium pyruvate and 100 µM non-essential amino acids. Cells were maintained at 37°C and 5% CO_2 in a humidified incubator and were used until passage 20. Cells were grown to subconfluency before experiments.

2.2.2 Bone marrow-derived macrophage (BMDM) differentiation and culture

Culture of bone marrow derived macrophages (BMDMs) was performed as previously described (Zhang et al., 2008). Briefly, wild-type C57BL/6 mice 8-12 weeks old were euthanized and their femurs and tibiae were aseptically removed and left on ice-cold PBS with 2% FCS until use. The bones were flushed with 21-23G needles and a single cell suspension was made by passing the flushed material three times through 22G needle followed by filtering with a 70 µm filter. The bone marrow was cultured in MEM with 10% FCS and supplements as above at 37°C and 5% CO_2. The next day (day 1), the medium containing non-adherent cells was removed and pelleted, and the cells were resuspended at 7.5×10^4/mL in MEM containing 10% FCS and 15% L929-derived supernatant medium (L-sup) and then cultured for an additional three days. On day 4, medium was partially replaced with an equal volume of MEM + 20% L-sup. On day 8, medium was replaced with a fresh MEM without L-sup (for ASM assay) and the cells were used for experiments. For apoptosis and cell viability assays, the medium was replaced with fresh MEM plus 10% L-sup.

2.2.3 Mice

All mice were C57BL/6 Harlan wild-type female mice 8-12 weeks old. All mice were bred and housed in the vivarium of the University of Duisburg-Essen, Germany. All mice were pathogen-free according to the 2002 recommendations of the Federation of European Laboratory Animal Science Associations (FELASA). All procedures performed on mice were approved by the Animal Care and Use Committee of the Bezirksregierung Düsseldorf, Düsseldorf, Germany.

2.2.4 ASM inhibitors

ARC39 was dissolved at 1 mM in PBS and sonicated in a water bath for 2h with alternating vortexing. The solution was stored in dark at RT. Amitriptyline hydrochloride and desipramine hydrochloride were prepared always as fresh solutions at 1 mM in PBS.

2.2.5 Conventional ASM, NSM and NC enzyme assays

Cells were seeded in 24-well plates and left to rest overnight before treatment was started. Cells were washed twice with ice-cold PBS. For ASM assay, cells were lysed on ice in ASM lysis buffer (250 mM sodium acetate, 1% NP-40, pH 5.0) for 10 min.

For mouse experiments, peritoneal lavage was collected by washing the abdominal cavity with a total of 10 mL cold PBS followed by centrifugation at 300 ×*g*, 4°C for 5 min. The pellet was then lysed in ASM lysis buffer on ice for 10 min. Peripheral blood was collected from the lateral tail vain and left 1.5-2h at RT to coagulate followed by centrifugation 2 500 ×*g* at RT for 20 min. Serum was collected and centrifuged again 2500 ×*g* for 5 min and diluted with ASM assay buffer. Organs were harvested in cold ASM lysis buffer in a volume 500-1200 µL and homogenized in a TissueLyser (Qiagen) for 5 min at 50 Hz using 5 mm stainless steel beads. Tissue homogenates were briefly centrifuged at 200 ×*g*, 4°C for 2 min and the supernatant was collected and kept on ice. For ASM assay, homogenates were diluted averagely 1:10.

For NSM and NC assays, cells were collected in a neutral buffer (200 mM HEPES, 0.1% NP-40, pH 7.0).

Protein concentration in all cases was determined using the Bradford Protein Reagent according to the manufacturer's instructions. Tissue samples were diluted 1:10-1:40 to be in the linear range. Serum was diluted 1:40. 3 µL sample was subsequently used with the reagent. A Standard of BSA (0.078-5 mg/mL) was used to determine protein concentration after measuring the absorbance at 595 nm. The corresponding lysis buffers were used to obtain blank values.

BODIPY FL C_{12}-sphingomyelin and NBD-C_{12}-ceramide were dissolved at a final concentration of 0.5 µM corresponding to 100 pmol/sample in the corresponding assay buffer: ASM assay buffer (250 mM sodium acetate, 0.1% NP-40, 100 µM $ZnCl_2$ (only for secretory ASM), pH 5.0), NSM assay buffer as previously described (Muhle and Kornhuber, 2017) (200 mM HEPES, 200 mM $MgCl_2$, 0.05% NP-40, pH 7.0), NC assay buffer (Muhle and Kornhuber, 2017) (200 mM HEPES, 100 mM NaCl, 0.03% NP-40, pH 7.0). Substrate solutions and samples were sonicated in a water bath for 10 min. The reaction mixtures consisted of 20 µL lysate and 180 µL assay buffer and were incubated for 0.5-3h at 37°C with 300 rpm. The reaction was terminated by adding chloroform:methanol (2:1, *v/v*). Phases were separated by centrifugation at 20 000 ×*g* for 5 min and the organic phase was collected and dried in a SpeedVac (ThermoFisher). Dried lipids were resuspended in chloroform:methanol (2:1, *v/v*) and spotted onto a thin layer chromatography plate ALUGRAM^{TM} Xtra SIL G. Chromatography was

conducted with chloroform:methanol (80:20, *v/v*) in sphingomyelinase assays, and with ethyl acetate:acetic acid (100:1, *v/v*) in neutral ceramidase assays. The plates were scanned using a Typhoon FLA 9500 (GE Healthcare) and spots were quantified with ImageQuant software (GE Healthcare).

2.2.6 AC assay with RBM14C12

The fluorogenic AC probe RBM14C12 was obtained from Dr. Antonio Delgado (Faculty of Pharmacy, University of Barcelona). The assay was done as previously described (Bedia et al., 2010): L929 cells were harvested in 100 µL 0.2 M sucrose on ice provided with 1× complete protease inhibitor cocktail and then were sonicated with a probe for 3 rounds, 10W each for 10 s on ice. Cell homogenates were centrifuged at 15 000 ×*g* for 3 min. The supernatant was collected, and protein quantification was performed. The enzymatic assay was carried out in black non-binding 96-well plates. Briefly, each well contained a mixture of 74.5 µL of 25 mM sodium acetate buffer, pH 4.5 (assay buffer), 0.5 µL of a 4 mM RBM14C12 substrate solution in ethanol (substrate final concentration 20 µM; ethanol final concentration 0.5%), and a fixed amount of protein (cell lysates: 20-40 µg, serum: 100 µg) in a volume of 25 µL of a 0.2 M sucrose solution (for cell lysates) or 25 µL assay buffer for serum. Negative controls consisted of 25 µL sucrose or 25 µL assay buffer. After incubation at 37°C for 6h (serum 1h) without agitation, the enzymatic reaction was stopped by adding 50 µL methanol and 100 µL 2.5 mg/ml $NaIO_4$ fresh solution in 100 mM glycine/NaOH buffer, pH 10.6 in each well. After 2h incubation in dark, the released fluorescence was quantified using a FLUOstar Omega microplate reader (BMG Labtech) (λ_{Ex} 355 nm, λ_{Em} 460 nm). The amount of umbelliferone released was calculated using calibration curves with umbelliferone standard.

2.2.7 *In-situ* ASM assay with sphingomyelinase FAM/BODIPY TR FRET probe

L929 and HepG2 cells were seeded in 96-well plates and left to rest overnight before the experiment was started. Cells were treated with ARC39 or with amitriptyline as indicated, with PBS as a control. For comparison between the *in-situ* assay and the conventional assay, cells were seeded simultaneously and treatment with amitriptyline (same batch and same solution) was done in parallel. The conventional ASM assay was done as mentioned above. At the end of the treatment for the *in-situ* assay, cells were

incubated with the sphingomyelinase FAM/BODIPY TR FRET probe (thereafter FRET probe) for an additional 30 min (L929) or 1h (HepG2). The final concentration of the FRET probe in the culture medium was 1 µM (from 1mM stock in DMSO). After incubation, the medium was removed, and cells were washed once with fresh medium followed by brief trypsinization. Cold fresh medium was added (3:1, *v/v*) to trypsin, and the plate was kept in dark on ice. The mean fluorescence intensity (MFI) on the green channel (520 nm), which correlated to the cleavage of the substrate and MFI on the red channel (700 nm), and thereby the uptake of the substrate was detected with an Attune NxT flow cytometer (ThermoFisher). A minimum of 10 000 events per sample was acquired. Each experiment included unstained controls. To calculate ASM activity, the background fluorescence was first subtracted from all samples then the ratio of green:red fluorescence was taken to correct for differences in substrate uptake. Ratios were then normalized to the average ratio of untreated cells and expressed as % residual ASM activity.

2.2.8 SDS-PAGE and immunoblotting

Cells were lysed in RIPA buffer (25 mM Tris-HCl, pH 7.3, 0.1% sodium dodecyl sulfate, 0.5% sodium deoxycholate, 1% NP-40, 125 mM NaCl, 10 mM NaF, 10 mM $Na_2P_2O_7$, 1 mM Na_3VO_4, 10 mM EDTA, 10 µg/mL aprotinin, 10 µg/mL leupeptin) supplemented with 1× complete protease inhibitor cocktail for 10 min on ice. Cells were then scraped, transferred into 1.5 mL tubes and vortexed thoroughly. Lysates were centrifuged at 20 000 ×*g*, 4°C for 5 min. Supernatants were collected and incubated at 96°C for 5 min with 1:5 of 5× SDS sample buffer (250 mM Tris, pH 6.8, 20% glycine, 4% SDS, 8% β-mercaptoethanol, 0.2% bromophenol blue).

SDS-PAGE was performed using 10-30 µg total protein in 10% gel for ASM and AC, or 12.5% gel for RAP1A. Proteins were transferred to nitrocellulose membranes blocked 1h with StartingBlock Blocking Buffer and then incubated with the appropriate primary antibody overnight at 4°C: anti-AC (1:1000), anti-ASM (1:50), anti-RAP1A (1:200). Membranes were washed 5 times each for 10 min with Tris-buffered saline-TWEEN (TBS-T) (20 mM Tris, 150 mM NaCl, 0.1% TWEEN) and subsequently incubated with secondary HRP- or AP-conjugated anti-rabbit, anti-goat or anti-mouse antibodies (1:100 000 in StartingBlock diluted 1:10 in TBS-T) for 1h at RT, and then washed again 5 times each for 10 min with TBS-T then with AP Washing Buffer when

applicable then were developed, washed 3 times for 8 min each with TBS-T and subsequently incubated for 1h with anti-β-actin (1:100 000 in TBS-T) then washed 3 times each 8 min with TBS-T and eventually developed.

2.2.9 RT-PCR analysis

Total RNA was isolated with RNeasy Mini Kit according the manufacturer's instructions and cDNA synthesis was performed with GoScript Reverse Transcription Kit according to the manufacturer's instructions using a Biometra TRIO Thermocycler (analyticjena). RT-PCR was conducted using PowerUp SYBR Green Master Mix according to the manufacturer's instructions in StepOnePlus System (Applied Biosystems) for a total of 40 cycles each 15 s at 95°C and 1 min at 60°C. *Hprt1/HPRT1* was used as an endogenous control to calculate $\Delta\Delta C_t$.

Primers used: *Hprt1*_fwd, 5´-ACAGGCCAGACTTTGTTGGAT-3´; *Hprt1*_rev, 5´-ACTTGCGCTCATCTTAGGCT-3´; *Smpd1*_fwd, 5´-TAACCCTGGCTACCGAGTTT-3´; *Smpd1*_rev, 5´-TTGGCCTGGGTCAGATTCAA-3´; *HPRT1*_fwd, 5´-CCCTGGCTGCTCAGTTCTTT-3´; *HPRT1*_rev, 5´-TGGTACACACGGTAACCAGG-3´ (all from Eurofins). *SMPD1* primers were from RT² qPCR Primer Assay for Human *SMPD1* (330001, Qiagen).

2.2.10 BODIPY sphingomyelin staining

Cells were treated as indicated together with 1 µM BODIPY FL C_{12}-sphingomyelin for 24h. For confocal microscopy, LysoTracker Red DND-99 was added at 25 nM for additional 30 min, the medium was subsequently changed, and cells were observed under a Leica TCS SP5 confocal microscope (Leica Mikrosysteme Vertrieb). For flow cytometric analysis, cells were trypsinized (without adding LysoTracker) and MFI was analyzed with an Attune NxT flow cytometer (ThermoFisher). A minimum of 10 000 events per sample was acquired.

2.2.11 Preparation of mouse plasma and tissues for mass spectrometric analysis

Peripheral blood was collected from the retro orbital plexus into EDTA tubes (Greiner Bio-One) on ice. The tubes were centrifuged at 1 700 ×*g*, 4°C for 10 min. Plasma was collected and centrifuged again at 3 000 ×*g*, 4°C for 5 min and stored at -80°C until use. Peritoneal lavage was collected by washing the abdominal cavity with a total of 10 mL cold PBS followed by centrifugation at 300 ×*g*, 4°C for 5 min. The pellet was

resuspended in PBS and an aliquot was taken to determine protein concentration, then the lavage was pelleted again followed by adding 500 µL methanol and stored at -80°C until use. Indicated organs were harvested and snap-frozen in liquid nitrogen followed by preparing organ powder in liquid nitrogen with a pestle and mortar. The powder was stored at -80°C until use.

2.2.12 Sphingolipid quantification by HPLC-MS/MS

Cell, tissue and plasma samples were subjected to lipid extraction using 1.5 mL methanol/chloroform (2:1, *v:v*) as described (Gulbins et al., 2018). The extraction solvent contained C17-dihydrosphingosine (C17 dhSph), d_7-sphingosine (d_7-Sph), d_7-sphingosine 1-phosphate (d_7-S1P), C17-ceramide (Cer17) and C16-d_{31}-sphingomyelin (d_{31}-SM16) (all Avanti Polar Lipids, Alabaster, USA) as internal standards. Chromatographic separations were achieved on a 1260 Infinity HPLC (Agilent Technologies, Waldbronn, Germany) equipped with a Poroshell 120 EC-C8 column (3.0 × 150 mm, 2.7 µm; Agilent Technologies). A mobile phase system consisting of water (solvent A) and acetonitrile/methanol (1:1, *v:v*; solvent B), both acidified with 0.1% formic acid, was used for gradient elution at an initial composition of 40:60 (A:B, *v:v*) and a flow rate of 0.5 mL/min. MS/MS analyses were carried out using a 6490 triple-quadrupole mass spectrometer (Agilent Technologies) operating in the positive electrospray ionization mode (ESI+). The following ion source parameters were set: sheath gas temperature, 375 °C; sheath gas flow, 12 L/min of nitrogen; nebulizer pressure, 30 psi; drying gas temperature, 200 °C; drying gas flow, 15 L/min of nitrogen; capillary voltage, 4000 V; nozzle voltage, 1500 V; iFunnel high pressure RF voltage, 150 V and iFunnel low pressure RF voltage, 60 V. The following mass transitions were recorded (collision energies (CE) in parentheses): *long-chain bases*: *m/z* 288.5 → 270.5 for C17 dhSph (12 eV), *m/z* 300.3 → 282.3 for Sph (8 eV), *m/z* 302.3 → 284.3 for dhSph (6 eV), *m/z* 307.3 → 289.3 for d_7-Sph (8 eV), *m/z* 380.3 → 264.3 for S1P (16 eV) and *m/z* 387.3 → 271.3 for d_7-S1P (16 eV); *ceramides* (CE = 25 eV for all transitions): *m/z* 520.5 → 264.3 for Cer16, *m/z* 534.5 → 264.3 for Cer17, *m/z* 548.5 → 264.3 for Cer18, *m/z* 576.6 → 264.3 for Cer20, *m/z* 604.6 → 264.3 for Cer22, *m/z* 630.6 → 264.3 for Cer24:1 and *m/z* 632.6 → 264.3 for Cer24; *sphingomyelins* (CE = 25 eV for all transitions): *m/z* 703.6 → 184.1 for SM16, *m/z* 731.6 → 184.1 for SM18, *m/z* 734.8 → 184.1 for d_{31}-SM16, *m/z* 759.6 → 184.1 for SM20, *m/z* 787.7 → 184.1 for

SM22, *m/z* 813.7 → 184.1 for SM24:1 and *m/z* 815.7 → 184.1 for SM24. The dwell time for all mass transitions recorded was 75 ms. Quantification was performed with MassHunter Software (Agilent Technologies). Depending on the sample type analyzed sphingolipid contents were normalized to cell count or protein (as determined by Bradford assay).

2.2.13 Sphingosine kinase 1 (SphK1) and sphingosine kinase 2 (SphK2) assay

NBD-C_{18}-shingosine was prepared and dissolved in 5% Triton X-100 at 3.5 mM by sonication in a water bath ~4h with alternative vigorous vortexing, and SphK1 and SphK2 assays were performed in real-time as previously described (Lima et al., 2014) with slight changes. Briefly, 96-well polypropylene plates were used. Fluorescence emission was measured with a FLUOstar Omega (BMG Labtech). Excitation wavelength was 544 nm, and emission wavelength was 590 nm. Assays were initiated with 20× ATP (20 mM ATP, 200 mM $MgCl_2$, 900 mM Tris-HCl, pH 7.4) followed by shaking and mixing for 15 s. Assays were prepared as master mixes immediately before use in either SphK1 or SphK2 reaction buffer containing 30 µM NBD-Sphingosine, 150 nM rhSphK1, or 6.9 nM rhSphK2. ARC39 was added as indicated. SphK1 reaction buffer contained 30 mM Tris-HCl, pH 7.4, 0.05% Triton X-100, 150 mM NaCl, 10% glycerol, 1 mM Na_3VO_4, 10 mM NaF, and 10 mM β-glycero-phosphate. SphK2 reaction buffer contained 30 mM Tris-HCl, pH 7.4, 0.05% Triton X-100, 200 mM KCl, and 10% glycerol.

2.2.14 Mouse platelet isolation

As previously described (Carpinteiro et al., 2015), blood was collected by tail vein puncture and anti-coagulated with 0.38% sodium citrate, and 9 ml PBS, pH 7.2 supplemented with 3.5% BSA, fatty acid free were added, and this mixture was incubated for 15 min at 37°C. Samples were centrifuged at 120 ×*g* without brake for 20 min at room temperature, and the platelet-containing supernatant was collected. Platelets were pelleted by centrifugation with 1 340 ×*g* for 10 min and were resuspended in Tyrode 's buffer (134 mM NaCl, 0.34 mM Na_2HPO_4, 2.9 mM KCl, 12 mM $NaHCO_3$, 20 mM HEPES, 5 mM glucose). After preparation, platelets were used immediately for the respective experiments in the indicated concentrations.

2.2.15 Preparation of tumor cells

Cells were brought into suspension by treatment with cell dissociation solution, enzyme-free PBS-based, washed extensively, and resuspended in HEPES/saline (H/S; 132 mM NaCl, 20 mM HEPES, pH 7.4, 5 mM KCl, 1 mM $CaCl_2$, 0.7 mM $MgCl_2$, and 0.8 mM $MgSO_4$) in the indicated concentration.

2.2.16 Adhesion assays

As previously described (Carpinteiro et al., 2015), B16F10 melanoma cells and platelets were prepared simultaneously as described above. 4×10^4 B16F10 tumor cells were then incubated with 2×10^7 wild-type or Asm-deficient platelets or 0.125 µg rhASM for 5 min in a total volume of 100 µL at 37°C. After the addition of 300 µL complete culture medium, tumor cells were transferred to fibronectin-coated glass cover slips in 24-well plates and incubated for 3 min at 37°C. Unbound tumor cells were washed away with H/S buffer for 4 times, and cells were fixed with 2% PBS-buffered PFA for 15 min. After being washed 3 times with PBS, cells were stained with 1 µg/mL DAPI in PBS for 15 min at RT and washed three times with PBS. Adherent cells per coverslip (diameter 12 mm) were counted with an EVOS FL Imaging System (ThermoFisher).

2.2.17 Cell death and viability

To assess cell death, cells were harvested, washed once with Annexin V Binding Buffer (10 mM HEPES, pH 7.4, 140 mM NaCl, 2.5 mM $CaCl_2$) after the indicated treatment and incubated for 15 min at RT with APC Annexin V (1:20) / propidium iodide at 1 µg/mL, in Annexin V Binding Buffer. Data acquisition and analysis was performed with an Attune NxT flow cytometer (ThermoFisher). A minimum of 10 000 events per sample was acquired.

Cell viability was determined with XTT Cell Viability Assay Kit according to the manufacturer's instructions. Briefly, cells were cultured and treated as indicated in 96-well plates in a volume of 100 µL then 50 µL of the activated XTT solution (after diluting the activation reagent with XTT solution 1:200) was added and incubated for 2-4h in the incubator. Subsequently absorbance at 475 nm and background absorbance at 650 nm was measured and subtracted with a FLUOstar Omega (BMG Labtech) microplate reader.

2.2.18 Lysosomal staining

After indicated treatments, either LysoTracker Red DND-99 final concentration 25 nM or LysoSensor Blue DND-167 final concentration 10 µM was added and incubated at 37°C for 30 min. For confocal microscopy, the medium was replaced with fresh medium and cells were observed under a Leica TCS SP5 confocal microscope (Leica Mikrosysteme Vertrieb). For flow cytometric analysis, cells were trypsinized and MFI was analyzed with an Attune NxT (ThermoFisher). A minimum of 10 000 events per sample was acquired.

2.2.19 Detection of phospholipidosis

HCS LipidTOX Green Phospholipidosis Detection Reagent was diluted 1:1000 with the complete culture medium, and then the medium was added to the cells. This reagent characterizes potentially toxic side effects of compounds on lipid metabolism in mammalian cells, and the fluorescently labeled phospholipids accumulate if the test compound induces phospholipidosis. Cells were then treated as indicated and incubated for 24h. For confocal microscopy, the medium was replaced with fresh medium and cells were observed under a Leica TCS SP5 confocal microscope (Leica Mikrosysteme Vertrieb). For flow cytometric analysis, cells were trypsinized and MFI was analyzed with an Attune NxT (ThermoFisher). A minimum of 10 000 events per sample was acquired.

2.2.20 Mouse blood chemistry analysis

Peripheral blood was collected from the lateral tail vain and left 1.5-2h at RT to coagulate followed by centrifugation 2 500 ×*g* at RT for 20 min. Serum was collected and centrifuged again 2 500 ×*g* for 5 min.

Serum was analyzed by using SpotChem EZ chemistry analyzer with the corresponding parameter strips (Scil, Viernheim, Germany). Parameters determined are: Blood urea nitrogen (BUN) (single stripes), aspartate transaminase (GOT) (Liver-1 stripes), alanine transaminase (GPT) (Liver-1 stripes), lactate dehydrogenase (LDH) (Liver-1 stripes), creatine phosphokinase (CPK) (single stripes), and amylase (single stripes).

2.2.21 Statistical analyses

Statistical analysis was performed using Prism GraphPad 8.3.0 (GraphPad Software, La Jolla, CA, USA). Data are expressed as arithmetic means ± standard deviation. 2-tailed

unpaired Student's *t*-test was used for two-group comparisons, and one-way or two-way analysis of the variance ANOVA with Tukey's or Bonferroni post hoc test for multiple comparisons. Values of $P<0.05$ were considered significant. All data were obtained from independent measurement.

3. Results

3.1 ARC39 inhibits both L-ASM and S-ASM directly and specifically in micellar assays

To confirm the direct interaction between ARC39 and ASM, L929 whole-cell lysates (L-ASM), L929-derived supernatant medium (S-ASM), and mouse serum (S-ASM) were treated directly with ARC39. No zinc was added to the assay buffer of L-ASM, while the activity of S-ASM from L929 medium and FCS was not detectable without further addition of zinc **(Fig. 11C)**. ARC39 led to an efficient dose-dependent inhibition of L-ASM activity in cell lysates **(Fig. 11A)** and S-ASM activity in mouse serum and L929 medium **(Fig. 11B, C)**, respectively.

In contrast, amitriptyline, a tricyclic antidepressant and a FIASMA, as already known due to its indirect mode of action, does not inhibit ASM in this setting neither in cell lysates nor in serum even when applied at up to 80 µM **(Fig. 11D, E)**, which is a high dose that is far above the dose used to treat cells.

To confirm the enzyme-specificity of ARC39, its direct effect on AC, NC and NSM in this same setting was investigated in L929 cell lysate and in mouse serum. No reduction in the activities of these enzymes was detected **(Fig. 11A, B)**. Amitriptyline did not inhibit any of these enzymes in this setting either **(Fig. 11D, E)**.

3.2 ARC39 inhibits L-ASM directly and specifically in cultured cells

Next, ARC39 was tested under cell culture conditions. L929 murine fibroblasts, with an abundant ASM activity compared to e.g. HepG2 (own observations, data not shown), were treated with increasing doses of ARC39 and the activities of ASM, NSM, AC, and NC were determined. ARC39 inhibited ASM efficiently in a dose-dependent manner while having no inhibitory effect on the other enzymes **(Fig. 12A, B)**.

The commonly used ASM inhibitors desipramine and amitriptyline efficiently inhibited ASM under these conditions as well **(Fig. 12G)** but also, and in contrast to ARC39, reduced AC activity **(Fig. 12B)** subsequent to the degradation of AC protein **(Fig. 12C)**.

Using the conventional ASM assay, a dose-response was obtainable with ARC39 after incubation for 2h in HepG2, Jurkat and in BMDMs. 20-40 µM ARC39 according to the

results with this assay led to <10% residual activity within 2h. Incubation time had a positive effect on ASM inhibition by ARC39, as demonstrated in L929 and HepG2 **(Fig. 12E, F *right*)**.

To investigate or exclude other potential mechanisms of ASM inhibition in cells such as down-regulating mRNA or ASM protein, *SMPD1*/*Smpd1* mRNA and ASM protein expression levels were determined 2h and 24h after treatment with ARC39 in L929 and HepG2 cells **(Fig. 12E, F)**, respectively. *SMPD1*/*Smpd1* mRNA was not down regulated. In contrast, in L929 cells, a transient up-regulation 2h after treatment with ARC39 was observed **(Fig. 12E *left*)**. ASM protein level was not significantly changed although the enzyme activity was not detectable **(Fig. 12E, F *middle* and *right*)**, respectively.

Desipramine was reported to induce the proteolytic degradation of ASM, and this effect was prevented by pretreatment with the serine/cysteine protease inhibitor leupeptin (Hurwitz et al., 1994a). Pre-incubating cells with leupeptin abrogated ASM inhibition induced by amitriptyline and desipramine but not by ARC39 **(Fig. 12G)**.

Taken together, these data suggest that direct inhibition of ASM catalytic activity is also the mechanism by which ARC39 inhibits ASM in cultured cells. Of note, ARC39 has the following values: log P = 3.35, pK_a (non-ionized) = 2.179 (calculated with ChemDraw 8.0, CambridgeSoft Corporation). These values differ clearly from those reported for FIASMAs (log P = 5.35 ± 1.13, pK_a = 9.04 ± 1.18) (Kornhuber et al., 2011).

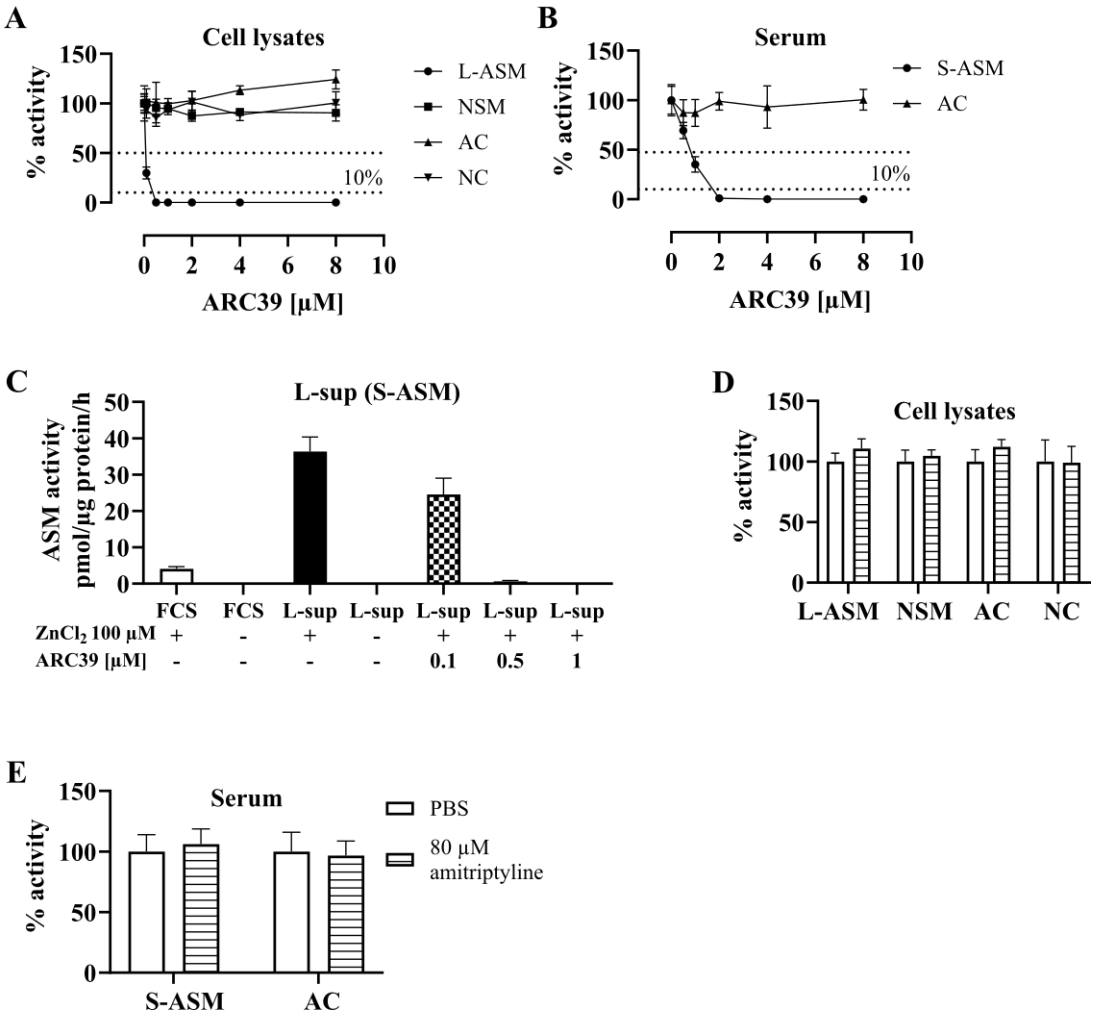

Figure 11. Direct and selective inhibition of L-ASM and S-ASM by ARC39 in micellar assays. (A) L929 whole-cell lysates were treated with ARC39 as indicated and the activity of L-ASM (No $ZnCl_2$ was added to the assay buffer), NSM, AC and NC was determined. **(B)** Mouse serum was treated with ARC39 as indicated and the activity of S-ASM (+ 100 µM $ZnCl_2$ in the assay buffer) and AC was determined. **(C)** L929-derived supernatant medium (L-sup) and FCS were treated as indicated with or without addition of $ZnCl_2$ to the assay buffer and the activity of S-ASM was determined. **(D, E)** L929 cell lysates or mouse serum, respectively were treated with PBS control or 80 µM amitriptyline and the activity of ASM (L-ASM in cell lysates and S-ASM in serum), NSM, AC and NC was determined. Enzyme activity is normalized to the protein concentration and control values are normalized to their mean except in (C) where they are expressed as absolute values. Data represented as mean ± SD, n=3 experiments.

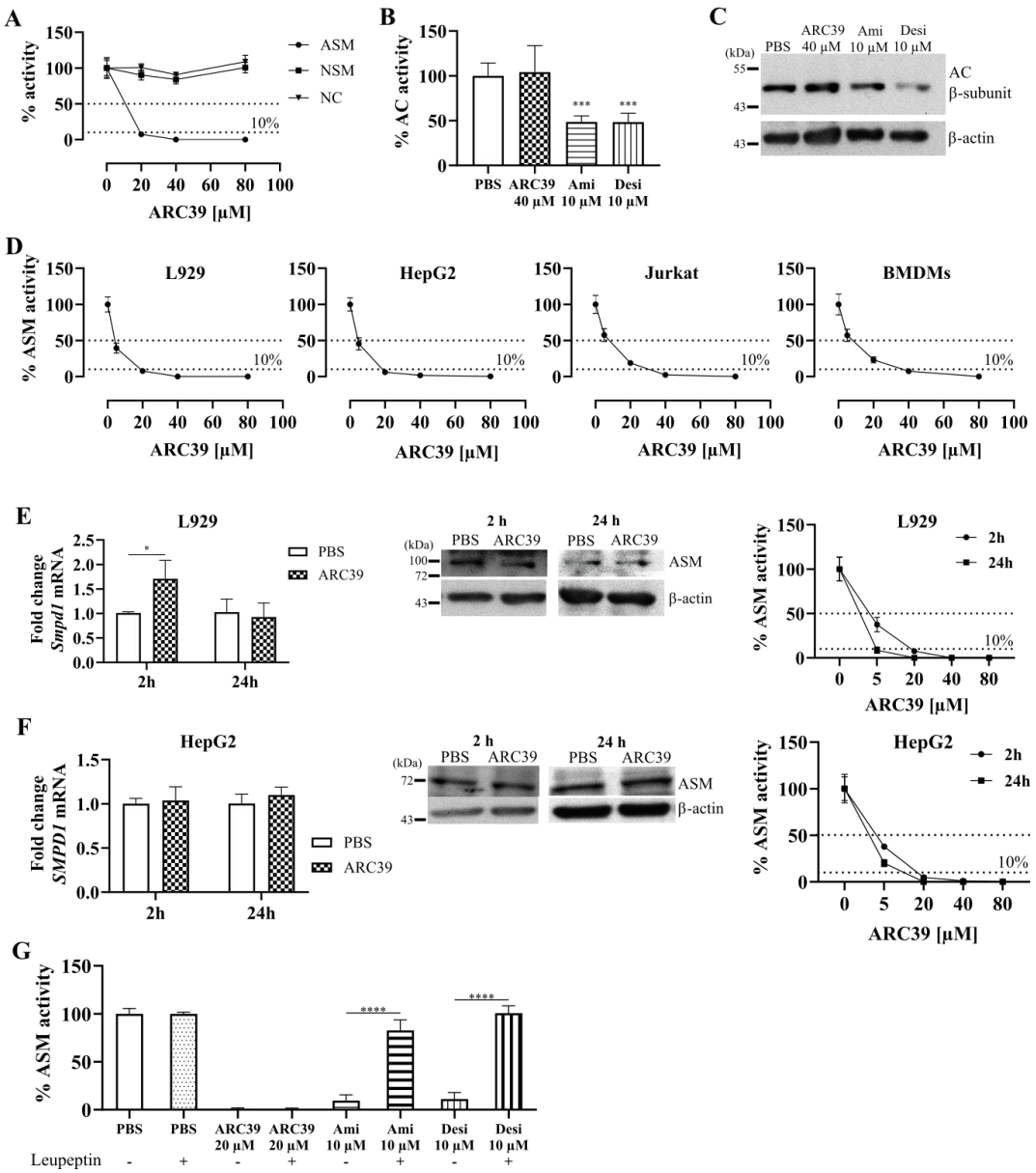

Figure 12. Direct and specific inhibition of L-ASM by ARC39 under cell culture conditions. (A) L929 cells were treated for 2h with ARC39 as indicated and the activity of ASM, NSM and NC was determined. L929 cells were treated for 2h with ARC39, amitriptyline (Ami) or desipramine (Desi) as indicated and AC activity was subsequently determined in **(B)**, and AC protein was analyzed by western blotting in **(C)**. **(D)** ASM activity after 2h treatment with ARC39 as indicated in L929, HepG2, Jurkat cells and in primary murine bone marrow-derived macrophages (BMDMs). **(E)** *Left:* Fold change of *Smpd1* mRNA relative to *Hprt1* (treated with 20 µM), *middle:* ASM protein level (treated with 20 µM) and a representative western blot, *right:* ASM activity after treatment with ARC39. All in L929 cells. $P<0.01$ for time as a source of variation in ASM activity. **(F)** *Left:* Fold change of *SMPD1* mRNA relative to *HPRT1* (treated with 20 µM), *middle:* ASM protein level (treated with 20 µM) and a representative western blot, *right:* ASM activity after treatment with ARC39. All in HepG2 cells. $P<0.05$ for time as a source of variation in ASM activity. **(G)** L929 were preincubated for 24h with 25 µM leupeptin or vehicle, then were treated for 4h as indicated and ASM activity was subsequently determined. Enzyme activity is normalized to the protein concentration and control values are normalized to their mean. ASM activity shown in this figure is determined with the conventional assay. Data represented as mean ± SD, n=3-5 experiments. One-way ANOVA was used in (B, G) and two-way ANOVA in (E, F), both followed by Bonferroni correction (except the effect of time on ASM activity). *$P<0.05$ ***$P<0.001$ ****$P<0.0001$.

3.3 Development of a new FRET probe-based *in-situ* ASM assay in intact living cells

While the conventional ASM assay used here is quite useful and reliable when investigating changes in activity subsequent to alterations in ASM protein itself, e.g. up- and downregulation, certain mutations, genetic knock-out models in mice, diagnosis of most Niemann Pick mutations (Schuchman and Desnick, 2017), and proteolytic degradation upon treatment with FIASMAs, both in cell and tissue lysates (Muhle and Kornhuber, 2017), they may not be as reliable when investigating inhibitors with a direct mode of action because of the many processing and dilution steps after initial treatment, which may affect the interaction between the enzyme and the inhibitor. Thus, depending on the binding affinity of the inhibitor to the enzyme and on other conditions, values obtained in such an assay may not reflect the actual inhibition.

Very recently, a new FRET probe-based *in-situ* ASM assay was developed and validated (Kappe et al., 2020). The FRET probe is a dual-labelled sphingomyelin in which FAM acts as FRET donor and BODIPY as FRET acceptor. Cleavage of the probe results in a slight decrease in BODIPY fluorescence and a marked increase in FAM fluorescence (Kappe et al., 2020). This dual emission was exploited here to establish an *in-situ* ASM assay utilizing flow cytometry. A dose-response was reproducibly and consistently obtainable in living cells: the FRET probe emits green (520 nm) only upon cleavage, while the red fluorescence (700 nm) corresponds to the uptake and can be used to correct for differences in the uptake of the probe by cells. Since amitriptyline is an indirect inhibitor, it was used to validate and compare this assay with the conventional one **(Fig. 13A)** (Kappe et al., 2020). Notably, there is an inherent difference between this assay and the conventional assay: the *in-situ* assay with the FRET probe tends to give higher residual activity values, and there is inevitably 5-10% residual activity **(Fig. 13A)** (Kappe et al., 2020). The incubation time with the FRET probe (L929: 30 min, HepG2: 1h) was determined experimentally as the time point after which no increase in green:red fluorescence intensity ratio was obtained. Using 1 µM as final concentration of the substrate yielded consistent and reproducible results. Of note, increasing the concentration increased both uptake (red fluorescence) and cleavage (green fluorescence) and yielded close ratios to 1 µM (not shown).

3.4 ARC39 inhibits L-ASM in intact living cells in a dose- and time-dependent manner

Using the new *in-situ* assay with the FRET probe, ARC39 led to an efficient dose- and time-dependent inhibition of ASM activity in intact L929 cells **(Fig. 13B-D)**. The inhibitory effect started within 30 min and reached its maximum at ~6h after treatment in L929 cells **(Fig. 13E)**.

Moreover, ARC39 led after 24h to a dose-dependent increase in the ratio of total sphingomyelins/ceramides in L929 whole-cell lysates beginning from 5 µM (and significant from 10 µM) as determined by mass spectrometric analysis **(Fig. 13F)**, further corroborating the results obtained with the FRET probe.

A dose-response was also obtained after 2h and 24h in HepG2 cells using the FRET probe **(Fig. 13G)**.

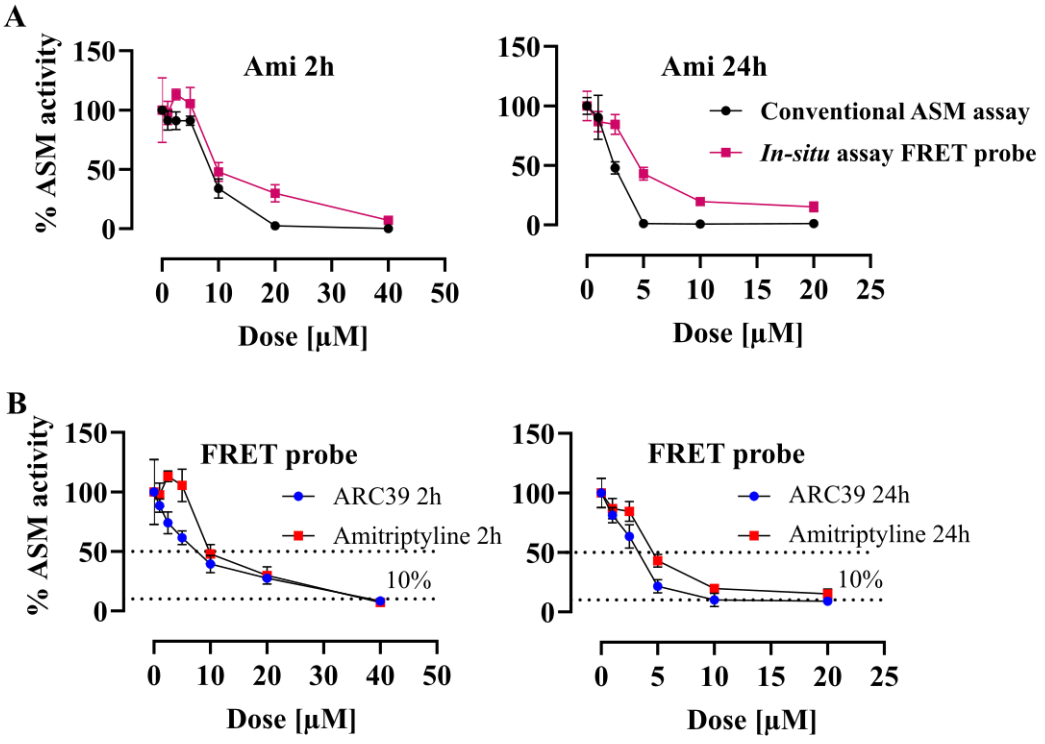

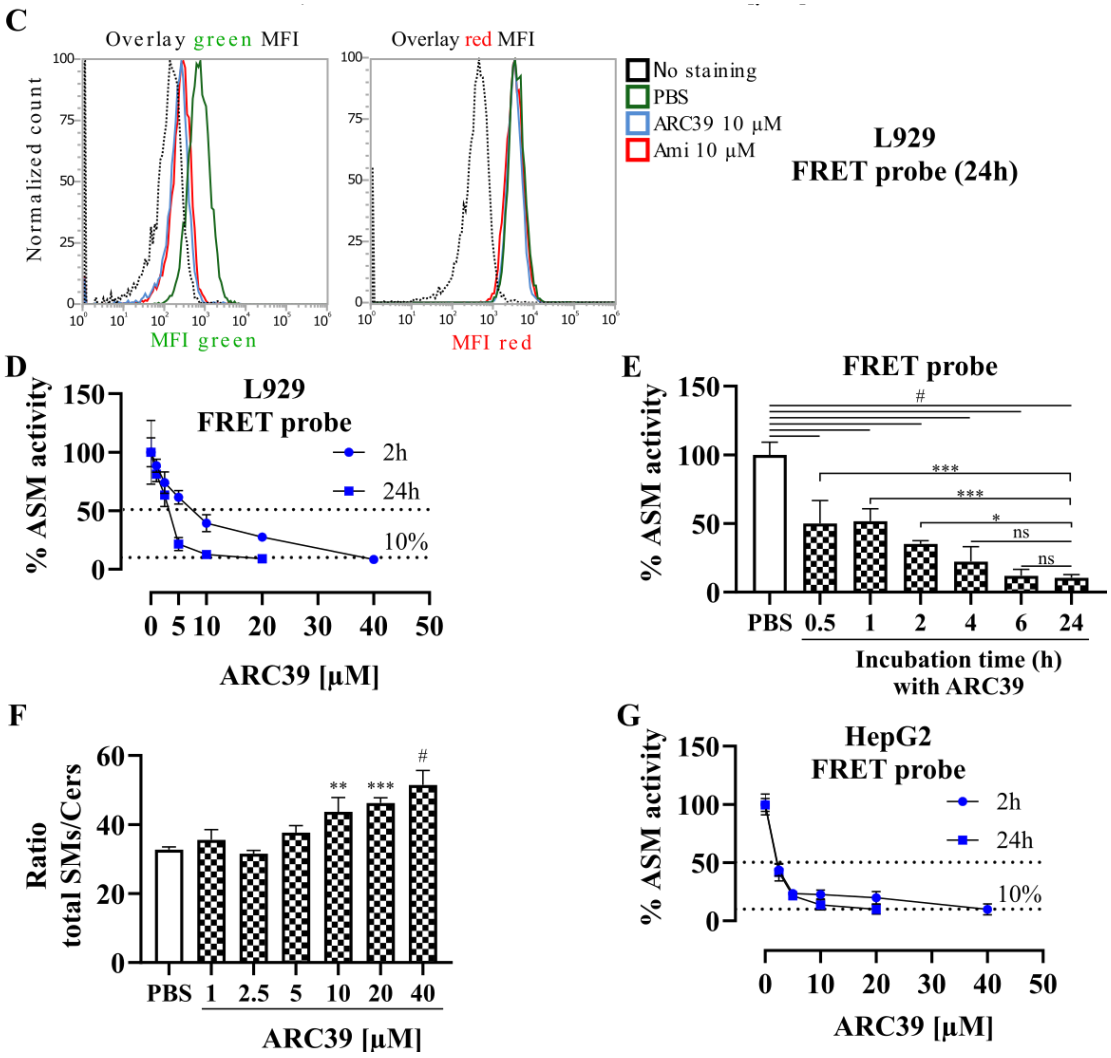

Figure 13. A new FRET probe-based *in-situ* ASM assay in intact cells and inhibition of L-ASM in living cells by ARC39. After indicated treatments for the indicated durations, cells were incubated with the FRET probe at a final concentration of 1 µM for 30 min (L929) or 1h (HepG2), then were washed, briefly trypsinized and analyzed by flow cytometry. **(A)** Validation of the *in-situ* assay with the FRET probe and comparison between the *in-situ* ASM assay and the conventional ASM assay in a dose-response for ASM activity in L929 cells treated with amitriptyline (Ami) for 2h (left) and 24h (right). **(B)** Dose-response obtained with the FRET probe in L929 cells treated with amitriptyline or ARC39 for 2h (left) and 24h (right). **(C)** Representative histogram overlay for the mean fluorescence intensities (MFI) of the FRET probe in both green (520 nm) and red (700 nm) channels from L929 treated as indicated for 24h. **(D)** Comparison of the dose-response in L929 cells treated with ARC39 for 2h or 24h. $P<0.0001$ for time as a source of variation in ASM activity. **(E)** Effect of the treatment duration on ASM inhibition by ARC39: L929 were treated with 20 µM ARC39 for the indicated times, then ASM activity was determined with the FRET probe. **(F)** Mass spectrometric analysis of the ratio of total sphingomyelins (SMs)/total ceramides (Cers) in whole-cell lysates from L929 cells that had been treated for 24h with ARC39 as indicated. **(G)** Comparison of the dose-response in HepG2 cells treated with ARC39 for 2h or 24h. $P<0.05$ for time as a source of variation in ASM activity. Control values are normalized to their mean. Data represented as mean ± SD, n=3 experiments. One-way ANOVA was used in (E, F) followed by Bonferroni correction, and two-way ANOVA in (D, G). *$P<0.05$ **$P<0.01$ ***$P<0.001$ #$P<0.0001$.

3.5 ARC39 leads to lysosomal accumulation of exogenous sphingomyelin in living cells.

Next, the lysosomal accumulation of sphingomyelin upon treatment with ARC39 was further validated by using exogenous fluorescently labeled sphingomyelin. L929 cells were incubated with BODIPY FL C_{12}-sphingomyelin together with 10 µM ARC39 or 10 µM amitriptyline as a positive control for 24h. In cells treated with either ARC39 or amitriptyline, intracellular accumulation of the exogenous sphingomyelin within aggregates was detected after 24h, which co-localized with LysoTracker Red, as assessed with confocal microscopy **(Fig. 14A)**. LysoTracker is a lysosomotropic compound that fluoresces only in an acidic environment and is commonly used as a lysosomal marker in intact cells. An increase in the MFI of BODIPY FL was also evident by flow cytometric analysis **(Fig. 14C, D)**.

Similar lysosomal accumulation of exogenous sphingomyelin was observed in HepG2 cells **(Fig. 15)**.

Together, this indicates that treatment with ARC39 leads to accumulation of sphingomyelin in the lysosomal compartment.

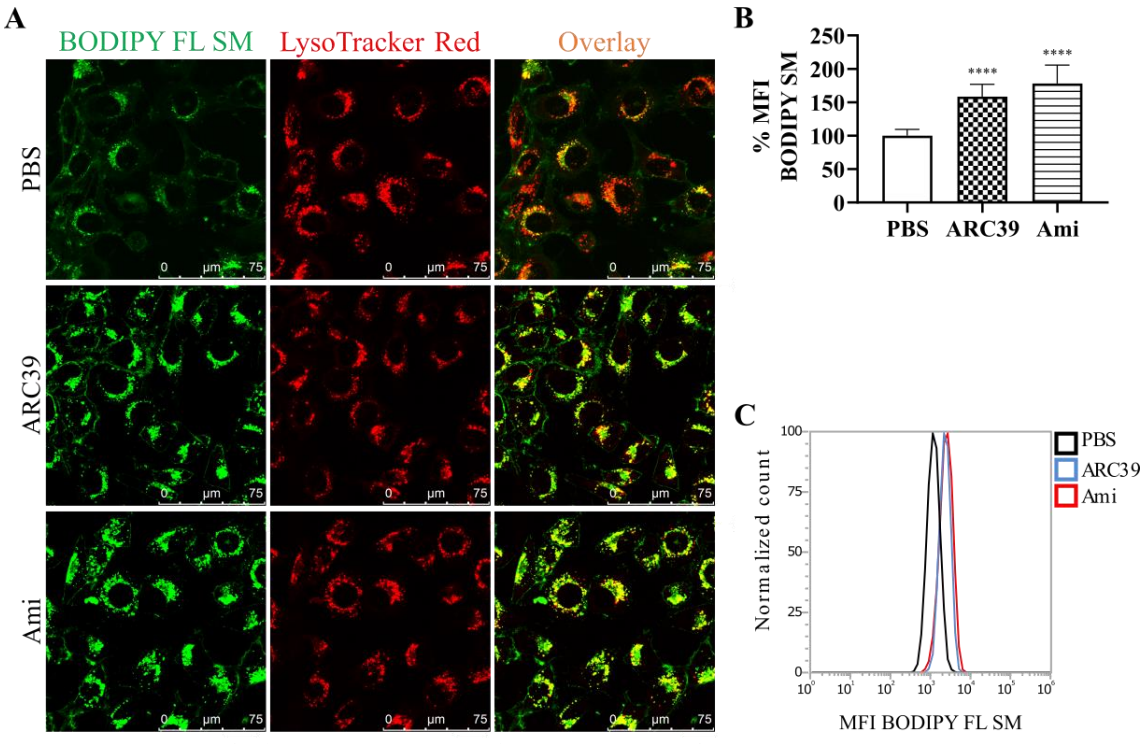

Figure 14. ARC39 leads to lysosomal accumulation of exogenous sphingomyelin. (A, B) L929 cells were incubated for 24h with 1 µM BODIPY FL sphingomyelin (SM) together with PBS as control, 10 µM ARC39 or 10 µM amitriptyline (Ami) as a positive control. Then, they were incubated 30 min at 37°C with 25 nM LysoTracker Red DND-99. Fresh medium was added then the cells were analyzed by confocal microscopy in **(A)**, magnification 100×. **(B)** MFI of BODIPY FL SM was analyzed by flow cytometry. **(C)** Representative histograms of MFI from (B). Control values are normalized to their mean. Data represented as mean ± SD, n=3-4 experiments. One-way ANOVA was used in (B) followed by Bonferroni correction. ****P<0.0001.

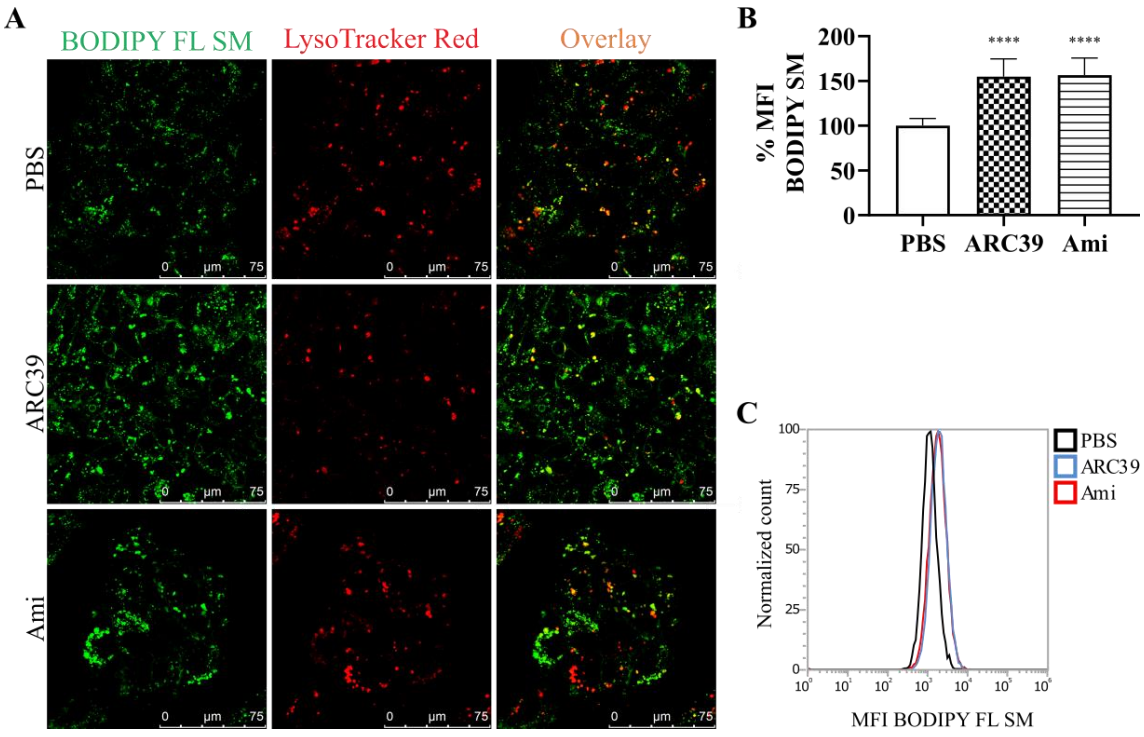

Figure 15. ARC39 leads to lysosomal accumulation of exogenous sphingomyelin. (A, B) HepG2 cells were incubated for 24h with 1 µM BODIPY FL sphingomyelin (SM) together with PBS as control, 10 µM ARC39 or 10 µM amitriptyline (Ami) as a positive control. Then, they were incubated 30 min at 37°C with 25 nM LysoTracker Red DND-99. Fresh medium was added then the cells were analyzed by confocal microscopy in **(A)**, magnification 100×. **(B)** MFI of BODIPY FL SM was analyzed by flow cytometry. **(C)** Representative histograms of MFI from (B). Control values are normalized to their mean. Data represented as mean ± SD, n=3-4 experiments. One-way ANOVA was used in (B) followed by Bonferroni correction. ****P<0.0001.

3.6 Changes in sphingolipids upon treatment with ARC39

To address the effect of ARC39 on the sphingolipidomic profile, mass spectrometric analysis was undertaken to determine potential changes in endogenous sphingolipids in whole-cell lysates from cells that had been treated with 20 µM ARC39 for 1h, 2h, 4h, and 24h.

In L929 cells, an increase in total sphingomyelins and in all tested sphingomyelin species (C_{16}-C_{24}) was observed after 24h **(Fig. 16A)**. Among the abundant species, the increase in $C_{24:1}$-sphingomyelin was more pronounced than the increase in C_{16}-sphingomyelin.

A faster reduction in total ceramides and in individual C_{16}-C_{24} ceramide species was detected within 2h after treatment **(Fig. 16B)**, where a more pronounced and time-dependent decrease in C_{16}-ceramide than $C_{24:1}$- and C_{24}-ceramide was observed.

Overall, there were no significant changes in dihydrosphingosine **(Fig. 16C)** or dihydroceramides (not shown). This would suggest the *de novo* synthesis is not affected.

Sphingosine, however, was reduced downstream of ceramide reduction except at 24h **(Fig. 16C)**.

Interestingly, the intracellular levels of S1P were, albeit in the relatively low pmol range, significantly and time-dependently reduced **(Fig. 16C)**.

Mass spectrometric analysis in HepG2 cells yielded similar results regarding sphingomyelins **(Fig. 17A)**, ceramides **(Fig. 17B)**, dihydrosphingosine except at 4h where it was reduced **(Fig. 17C).**

The reduction in sphingosine in HepG2 persisted after 24h, and a significant reduction in S1P was also observed **(Fig. 17C)**.

3.7 Effect of ARC39 on sphingosine kinases

The pronounced changes in intracellular S1P necessitated investigating whether ARC39 could potentially inhibit sphingosine kinases SphK1 or SphK2.

ARC39 was directly incubated with rhSphK1 or rhSphK2 and enzyme activities were subsequently determined in real-time as previously described (Lima et al., 2014). This assay exploits a phenomenon called red edge excitation shift that is specifically observed in NBD-C_{18}-sphingosine, which implies a shift in both λ_{Ex} (from 474 nm to 550 nm) and λ_{Em} (from 539 nm to 584 nm) of NBD upon conversion of NBD-sphingosine to NBD-S1P.

0.5-10 µM ARC39 was tested and up to 10 µM ARC39 did not exhibit an inhibitory effect on SphK1 neither on SphK2 **(Fig. 18)** (for convenience, shown only 5 and 10 µM).

This suggests that the observed decrease in intracellular S1P is not due to concomitant inhibition of sphingosine kinases but rather takes place downstream of ASM inhibition and the subsequent decrease in ceramides and sphingosine upon treatment with ARC39.

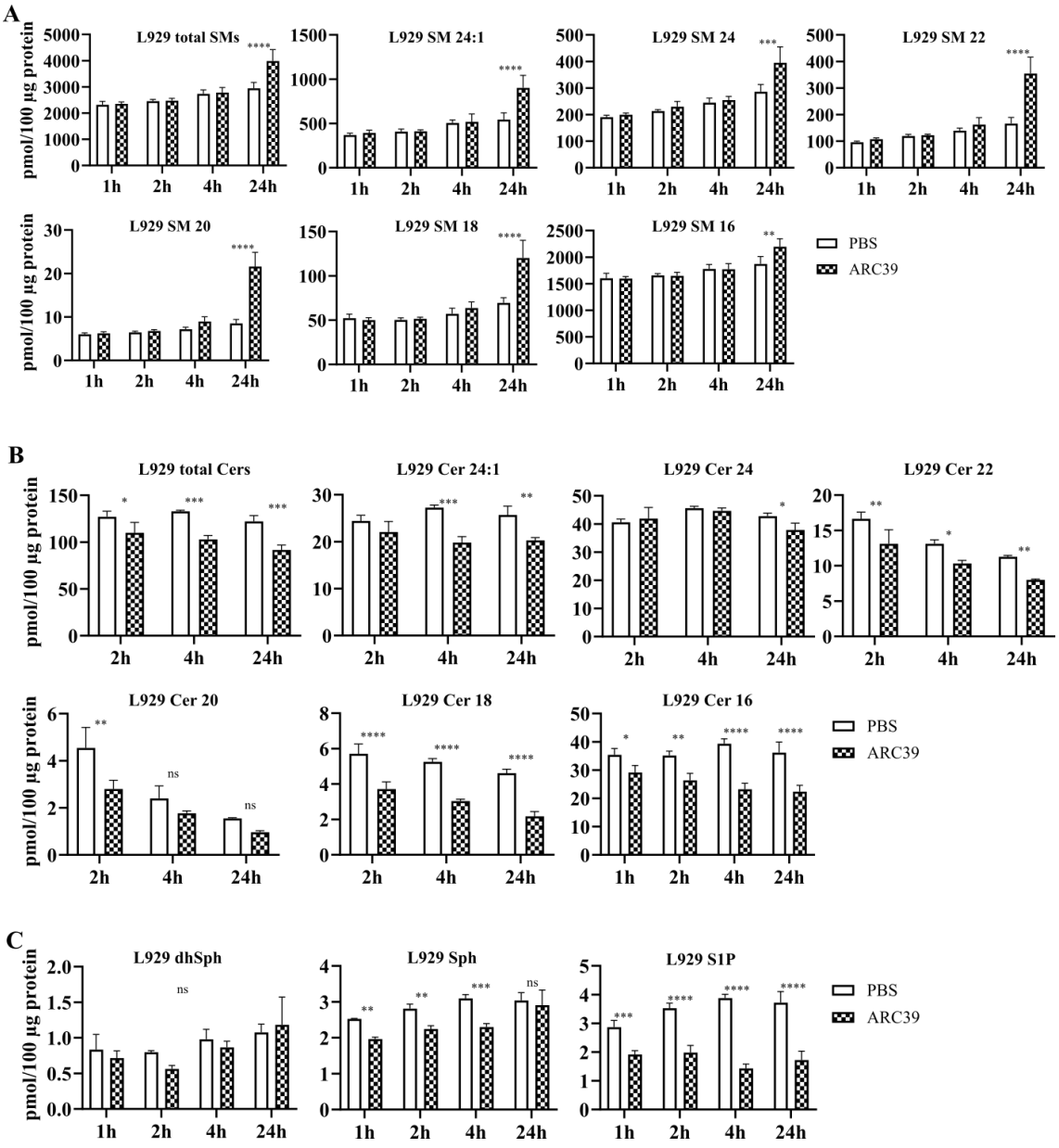

Figure 16. Sphingolipidomic analysis after treatment with ARC39 in L929 cells. Cells were treated with 20 µM ARC39 and at the indicated time points the endogenous levels of the following sphingolipids were determined by mass spectrometry in whole-cell lysates. **(A)** Sphingomyelins (SMs). **(B)** Ceramides (Cers). Numbers indicate the chain length and saturation of the fatty acyl chain. **(C)** Dihydrosphingosine (dhSph), Sphingosine (Sph) and sphingosine-1-phosphate (S1P), respectively. Data represented as mean ± SD, n=3 experiments. Two-way ANOVA was used followed by Bonferroni correction. **P*<0.05 ***P*<0.01 ****P*<0.001 *****P*<0.0001.

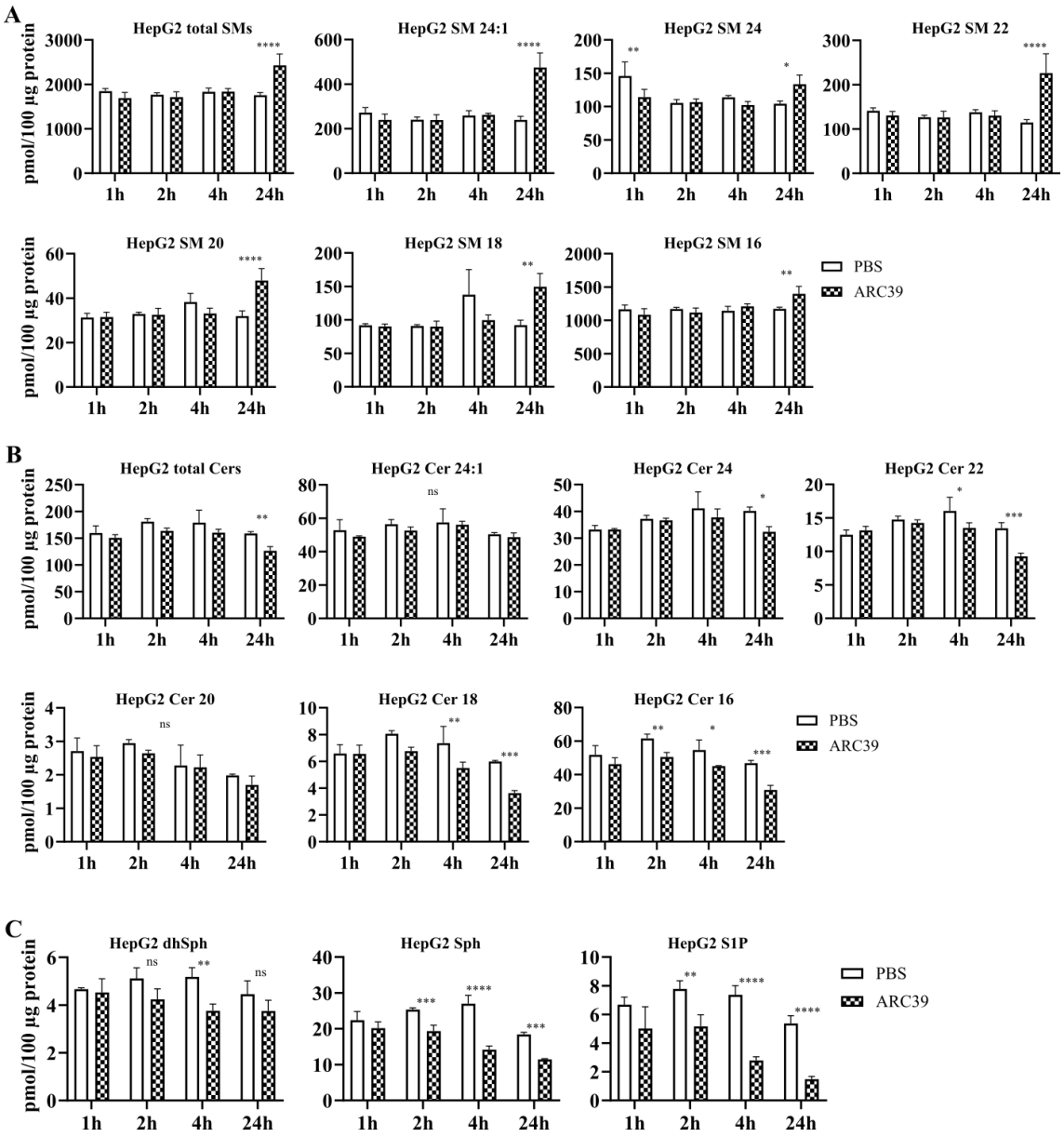

Figure 17. Sphingolipidomic analysis after treatment with ARC39 in HepG2 cells. Cells were treated with 20 µM ARC39 and at the indicated time points the endogenous levels of the following sphingolipids were determined by mass spectrometry in whole-cell lysates. **(A)** Sphingomyelins (SMs). **(B)** Ceramides (Cers). Numbers indicate the chain length and saturation of the fatty acyl chain. **(C)** Dihydrosphingosine (dhSph), Sphingosine (Sph) and sphingosine-1-phosphate (S1P), respectively. Data represented as mean ± SD, n=3 experiments. Two-way ANOVA was used followed by Bonferroni correction. **P*<0.05 ***P*<0.01 ****P*<0.001 *****P*<0.0001.

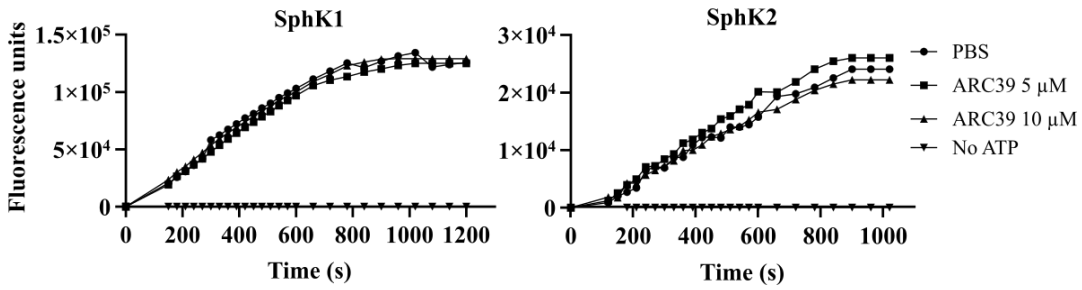

Figure 18. Effect of ARC39 on sphingosine kinases. Shown is Time-resolved fluorescence emission at 590 nm. Activity of rhSphK1 (left) and rhSphK2 (right) was determined in real-time after pretreatment with ARC39 as indicated. The reaction mixture contained 30 µM NBD-C_{18}-sphingosine, 150 nM SphK1 or 6.9 nM SphK2 with or without 1mM ATP. Additionally, SphK1 reaction buffer contained 30 mM Tris-HCl, pH 7.4, 0.05% Triton X-100, 150 mM NaCl, 10% glycerol, 1 mM Na_3VO_4, 10 mM NaF and 10 mM β-glycero-phosphate. SphK2 reaction buffer contained 30 mM Tris-HCl, pH 7.4, 0.05% Triton X-100, 200 mM KCl and 10% glycerol. Data represented as mean of 3 experiments.

3.8 ARC39 inhibits platelet- and ASM-promoted adhesion of tumor cells

ARC39 has been used in numerous studies to yield functional results related to the inhibition of ASM activity (Chung et al., 2016; Martinez et al., 2012; McVey et al., 2017; Roth et al., 2009a; Sosna et al., 2016; Voigt et al., 2014).

Carpinteiro et al. previously showed that adhesion and metastasis of murine B16F10 melanoma is highly promoted by a secreted zinc-dependent form of ASM that is rapidly released from wild-type (WT) platelets upon interaction with tumor cells due to clustering and activation of α5β1 integrins on the surface of tumor cells in ceramide-enriched platforms (Carpinteiro et al., 2015). Tumor cells are not the source of ASM in this case, and their promoted adhesion *in vitro* and metastasis *in vivo* is abrogated upon interaction with $Asm^{-/-}$ platelets (Carpinteiro et al., 2015).

To obtain a functional validation in the current study, B16F10 melanoma cells were incubated with WT platelets with or without 1 µM ARC39, platelets from $Asm^{-/-}$ mice, or rhASM with or without 1 µM ARC39, and the adhesion of melanoma cells to fibronectin-coated cover slips was determined. Both WT platelets and rhASM rapidly promoted the adhesion of melanoma cells. $Asm^{-/-}$ platelets did not promote B16F10 cell adhesion, which was phenocopied by adding 1 µM ARC39 just before incubating WT platelets with melanoma cells. The same was observed with rhASM **(Fig. 19)**.

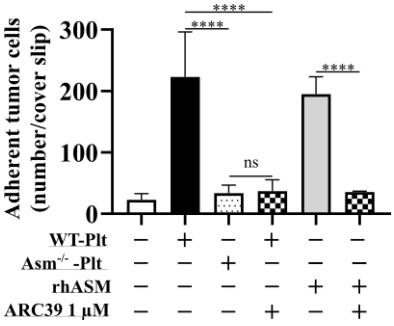

Figure 19. Functional validation of ASM inhibition by ARC39: ARC39 inhibits platelet- and ASM-promoted adhesion of tumor cells. 4×10^4 B16F10 melanoma cells were incubated for 5 min at 37°C in 100 µL total volume with 2×10^7 wild-type (WT), Asm-deficient ($Asm^{-/-}$) platelets (Plts) or rhASM (0.125 µg in 50 µL) in the presence or absence of 1 µM ARC39, which was added directly upon co-incubation without previous pre-treatment. After addition of 300 µL of B16F10 MEM complete culture medium (also containing 1 µM ARC39 where indicated), tumor cells were incubated for 3 min on fibronectin-coated cover slips, washed, fixed and stained with DAPI. Adherent tumor cells were then counted. Data represented as mean ± SD, n=3-4 experiments. One-way ANOVA was used in followed by Tukey 's correction. ****P<0.0001.

3.9 Toxicity of ARC39 *in vitro*

In the cells tested (L929, HepG2, Jurkat and BMDMs), no induction of cell death was detected 24h after incubation with ARC39 even with doses as high as 160 µM, except for L929 that showed a slight increase of the Annexin V^+ population **(Fig. 20A)**.

The overall cell viability was not significantly reduced after 24h with higher doses except BMDMs with 80 µM as determined with XTT reduction assay **(Fig. 20B)**. Toxicity after 48h appeared in L929, HepG2 and Jurkat with higher doses (≥40 µM) which are above the range required for ASM inhibition. BMDMs, however, were more sensitive and a reduction in cell viability was observed after 48h beginning from 5 µM **(Fig. 20B)**.

One known well-established mechanism of toxicity by nitrogen-containing bisphosphonates (N-BPs) is the inhibition of farnesyl pyrophosphate (FPP) synthase in the mevalonate pathway (Dunford et al., 2001; Luckman et al., 1998; van Beek et al., 1999a, b). Products of this pathway (particularly geranylgeranyl diphosphate) are used for an important post-translational lipid modification of proteins called prenylation. The majority of prenylated proteins are small GTPases, and this modification is important for their proper function since the lipid prenyl group serves to anchor proteins to the cellular membranes and is also important in protein:protein interactions (Rogers et al.,

2000). Thus, dysregulation of small GTPases is linked to the toxicity of N-BPs (Roelofs et al., 2006).

Whether ARC39 could potentially inhibit FPP synthase was investigated by detecting unprenylated Rap1A/RAP1A protein (Ras-related protein 1A) in L929 and HepG2, respectively after treatment with increasing doses of ARC39. Accumulation of unprenylated RAP1A servers as a surrogate marker for FPP synthase inhibition by bisphosphonates (Roelofs et al., 2006).

After 24h, higher levels of unprenylated Rap1A in L929 compared to vehicle-treated cells were detected, particularly with doses that led to toxicity at 48h **(Fig. 20C)**. Accumulation of unprenylated RAP1A was also present in HepG2 albeit to a lesser extent **(Fig. 20D)**.

This suggests that inhibition of FPP synthase could be, at least partially, a potential cause for the toxicity seen at later time points with ARC39.

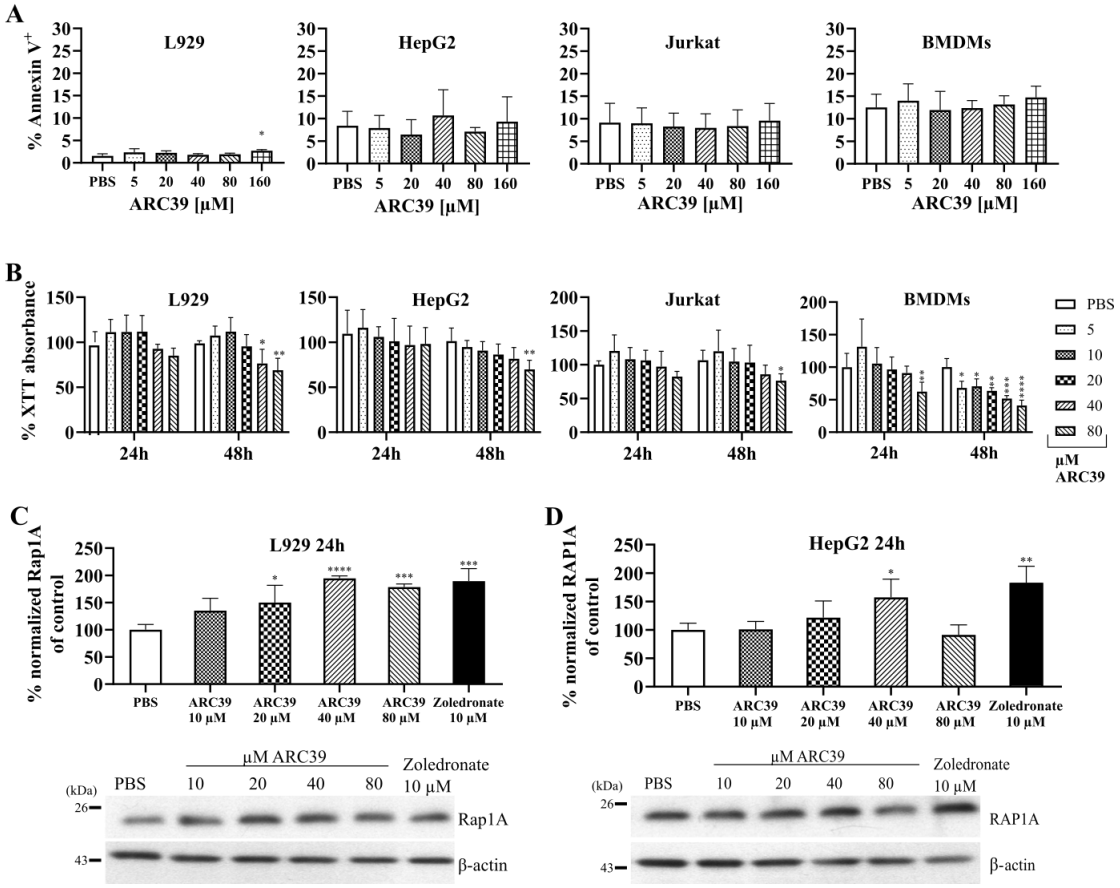

Figure 20. Toxicity of ARC39 *in vitro*. (A-D) L929, HepG2, Jurkat and BMDMs were treated with ARC39 as indicated. **(A)** After 24h treatment, cells were stained with Annexin V / PI and analyzed by flow cytometry. **(B)** After 24h and 48h treatment, cell viability was determined with XTT reduction assay. **(C, D)** Unprenylated Rap1A, RAP1A protein, respectively normalized to β-actin in L929, HepG2 cells, respectively after 24h treatment with ARC39 with representative western blots. Zoledronate served as a positive control. Control values are normalized to their mean. Data represented as mean ± SD, n=3-4 experiments. One-way ANOVA was used in (A, C, D) and two-way ANOVA in (B), both followed by Bonferroni correction. **P*<0.05 ***P*<0.01 ****P*<0.001 *****P*<0.0001.

3.10 Effect of ARC39 on the lysosomal compartment

To this end, L929 cells were treated for 2h indicative of a direct effect of the compound on the lysosomes, or for 24h indicative of an indirect effect due to accumulation of sphingomyelin and potential adaptive lysosomal responses.

First, LysoTracker Red and LysoSensor Blue were used to assess the volume of the acidic compartment and pH, respectively. The fluorescence intensity of LysoTracker is not dependent on the pH value but it fluoresces only in an acidic environment, which means that significant alkalization of the endo-lysosomal compartment could lead to a decrease in the MFI of LysoTracker as there is less volume of the acidic compartment. The LysoSensor Blue probe used is also a lysosomotropic compound but, unlike LysoTracker, its MFI is dependent on pH. LysoSensor Blue does not emit or emits minimally at neutral pH, but its MFI increases proportionally to the degree of protonation. Typically, cells are incubated with higher concentrations of the LysoSensor probe (here 10 μM) to minimize differences in uptake, so that the MFI is dependent primarily on the pH (protonation).

After 2h, ARC39 had no significant effect on the MFI of LysoTracker or LysoSensor, while amitriptyline and desipramine led to a reduction in the signal of both **(Fig. 21A-C)**. This is consistent with previous observations, since FIASMAs are weak bases and could lead to an initial alkalization of the lysosomes (Elojeimy et al., 2006; Petersen et al., 2013).

After 24h, however, ARC39 increased the signal of LysoTracker only **(Fig. 21A, B)**, which could be attributed to the accumulation of sphingomyelin and a potential adaptive lysosomal response. Amitriptyline and desipramine led after 24h to an even more pronounced increase in the signal of LysoTracker **(Fig. 21A, B)**. At the concentrations used, none of the compounds led to a change in the pH after 24h compared to the

control, suggesting that the pH is restored and the initial increase in pH due to alkalization (drop in LysoSensor signal) is compensated. Of note, NH_4Cl, the positive control used for alkalization, led after 24h to an increase in the signal of both LysoTracker and LysoSensor, suggesting a compensatory adaptive response.

These observations are in agreement with a study that addressed the influence of many lysosomotropic drugs on the lysosomal compartment in detail (Lu et al., 2017).

Next and more importantly, the effect of ARC39 on other lysosomal phospholipases and subsequent phospholipidosis was investigated. To this end, a LipidTOX phospholipidosis detection reagent was used, which consists of exogenous fluorescently labeled phospholipids and is commonly used and well-established in the detection of phospholipidosis (Klutzny et al., 2017; Lu et al., 2017; Muehlbacher et al., 2012).

There was no significant accumulation of phospholipids 24h after treatment with ARC39 compared to amiodarone, the positive control **(Fig. 21D, E)**. Of note, there was ~20% increase in LipidTOX signal with ARC39 that did not show dose dependence between 10-20 µM.

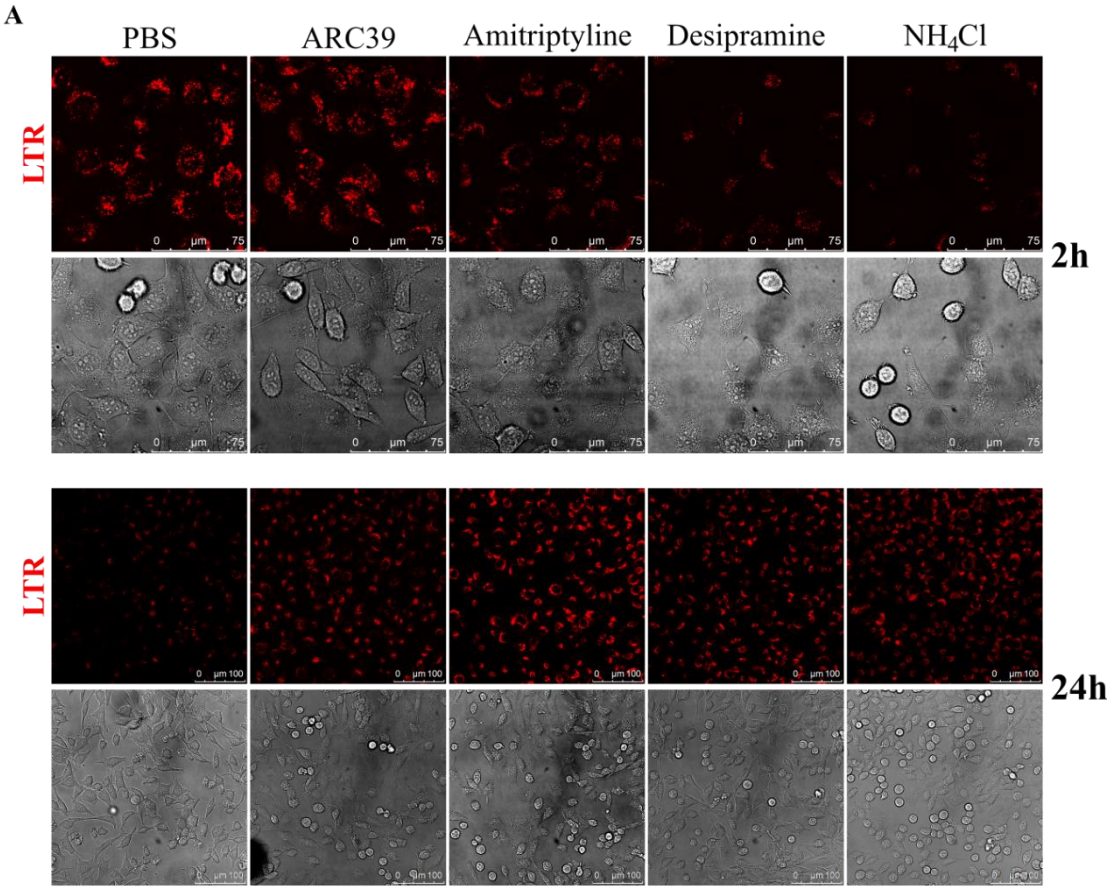

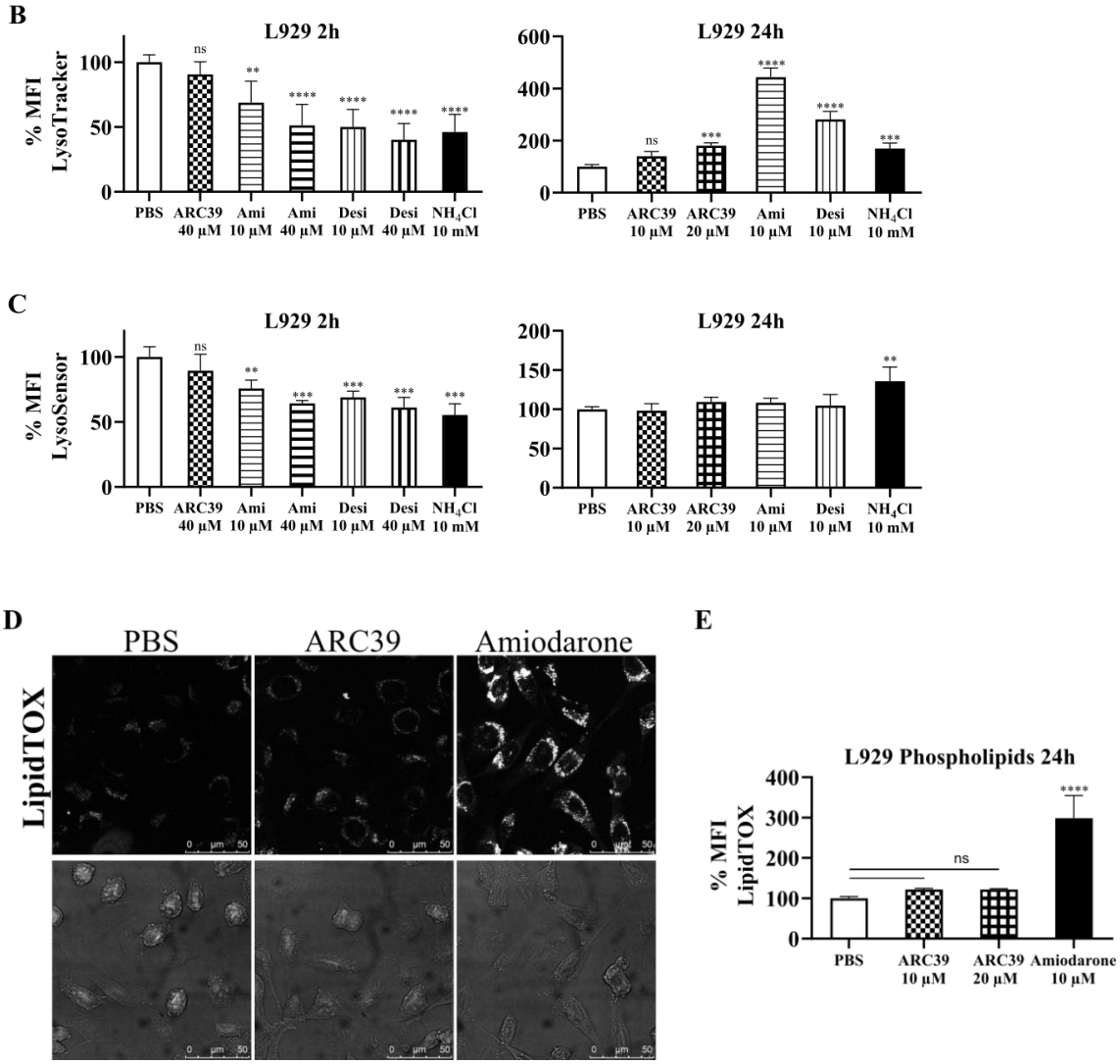

Figure 21. Effect of ARC39 on lysosomes. (A) L929 cells were treated 2h (up) or 24h (down) with PBS, 40 µM ARC39 for 2h, 20 µM ARC39 for 24h, 10 µM amitriptyline, 10 µM desipramine or 10 mM NH_4Cl as a positive control. Then, LysoTracker Red (LTR) was added to a final concentration of 25 nM for 30 min at 37°C. Fresh medium was added and the cells were analyzed by confocal microscopy. Magnification 100× (up) and 40× (down). **(B)** After treatment for 2h or 24h as indicated, MFI of LTR was determined by flow cytometry. **(C)** After treatment for 2h or 24h as indicated, LysoSensor Blue DND-167 was added to a final concentration of 10 µM for 30 min at 37°C then the MFI was determined by flow cytometry. **(D)** L929 cells were incubated for 24h with LipidTOX Green phospholipidosis detection reagent (1:1000), together with PBS, 20 µM ARC39 or 10 µM amiodarone as a positive control, and then were analyzed with confocal microscopy for phospholipid accumulation, magnification 100×. **(E)** After treatment for 24h as indicated together with 1:1000 LipidTOX Green, its MFI was determined with flow cytometry for phospholipid accumulation. Control values are normalized to their mean. Data represented as mean ± SD, n=3 experiments. One-way ANOVA was used followed by Bonferroni correction. ***P*<0.01 ****P*<0.001 *****P*<0.0001.

3.11 ARC39 *in vivo*

To test the potential effectiveness of ARC39 in the context of ASM inhibition *in vivo*, ARC39 was applied intraperitoneally in C57BL/6 wild-type mice. Importantly, at least

for clodronate, it was reported that intraperitoneal absorption in mice was nearly complete judged by the drug concentration in bone which was identical to i.v. administration (Monkkonen and Ylitalo, 1990).

3.11.1 Toxicity of ARC39 in vivo

Knowing the pharmacokinetics of bisphosphonates and their very high affinity to bone surfaces, it was assumed that high doses may be required to reach sufficient concentrations for ASM inhibition in organs. Thus, experiments were first undertaken to determine the maximal non-toxic dose both in a single-dose **(Fig. 22)** and a multiple-dose regimen as follows: every 12h for 96h, a total of 8 times **(Fig. 23)**.

The following serological markers were determined in the serum of treated mice in a matched manner at 24h and 10d after the single-dose treatment, or at 12h and 10d after the short-term multiple-dose treatment: Blood urea nitrogen (BUN), aspartate transaminase/glutamate-oxaloacetate transaminase (GOT), alanine transaminase/glutamate-pyruvate transaminase (GPT), lactate dehydrogenase (LDH), creatine phosphokinase (CPK), and amylase.

Very high doses led to toxicity, as indicated by elevated LDH, impaired renal function indicated by elevated BUN levels, liver damage indicated by elevated GOT levels, morbidity and lethality. Very high single doses led also to elevated amylase and CPK **(Fig. 22A)**. Elevated BUN and GOT were observed in the early time point after a very high single dose **(Fig. 22A)**, while only elevated GOT was observed in the early time point after a toxic dose in the short-term multiple-dose treatment **(Fig. 23A)**. Notably, acute renal toxicity *in vivo* of certain N-BPs was reported in rats (ibandronate and zoledronate) (Pfister et al., 2003) and in patients (zoledronate) (Chang et al., 2003; Markowitz et al., 2003).

The result of these experiments was determination of maximal subtoxic doses to be utilized as a beginning to investigate ASM inhibition *in vivo*. These corresponded to 0.32 mM 10 µL/g (~1.2 mg/kg) single dose and 0.16 mM 10 µL/g (~0.6 mg/kg) every 12h for 96h, corresponding to a total cumulative dose of 4.8 mg/kg. Despite the elevation in BUN and GPT on day 10 with the later dosage, it was chosen because this elevation was slight, GOT levels went back to normal, and, importantly, the clinical score of the mice was normal.

Of note, these doses are roughly 5-10-fold higher than usually reported doses for other clinically relevant bisphosphonates (Markowitz et al., 2003), and close or above doses used in rodents for renal toxicity studies (Pfister et al., 2003).

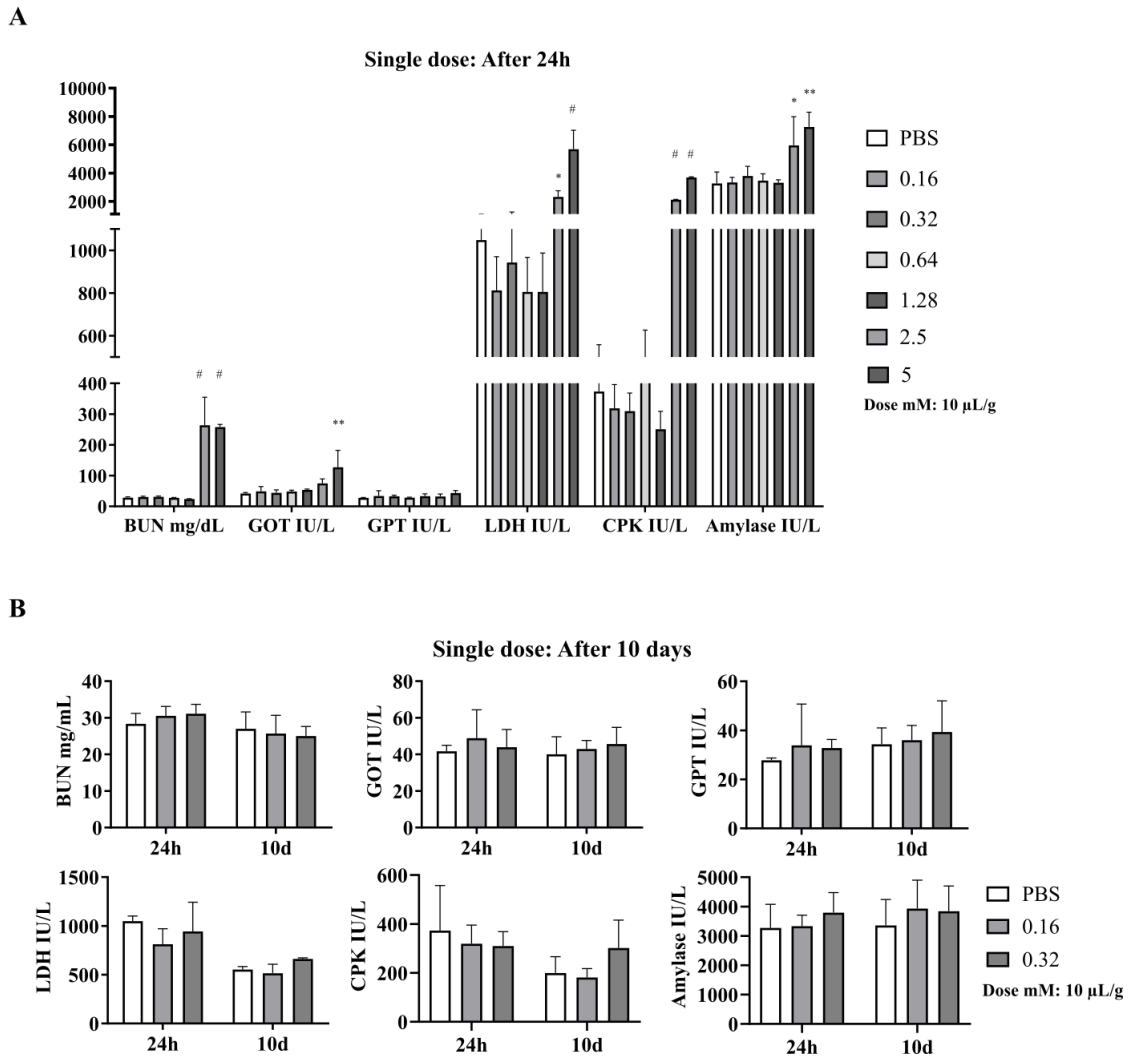

Figure 22. Toxicity of ARC39 *in vivo* in a single-dose regimen. The compound was applied i.p. for one time at the indicated doses. After 24h in **(A)** and after 10d in the same individuals in **(B)**, serum was collected and the following serological markers were assessed: Blood urea nitrogen (BUN), glutamate-oxaloacetate transaminase (GOT) / aspartate transaminase, glutamate-pyruvate transaminase (GPT) / alanine transaminase, lactate dehydrogenase (LDH), creatine phosphokinase (CPK) and amylase. On day 10, only the three groups that did not exhibit significant morbidity or lethality between 24h-10d are shown. Data represented as mean ± SD, n=3 mice per group. One-way ANOVA was used in (A) and two-way ANOVA was in (B), both followed by Bonferroni correction. **P*<0.05 ***P*<0.01 #*P*<0.0001.

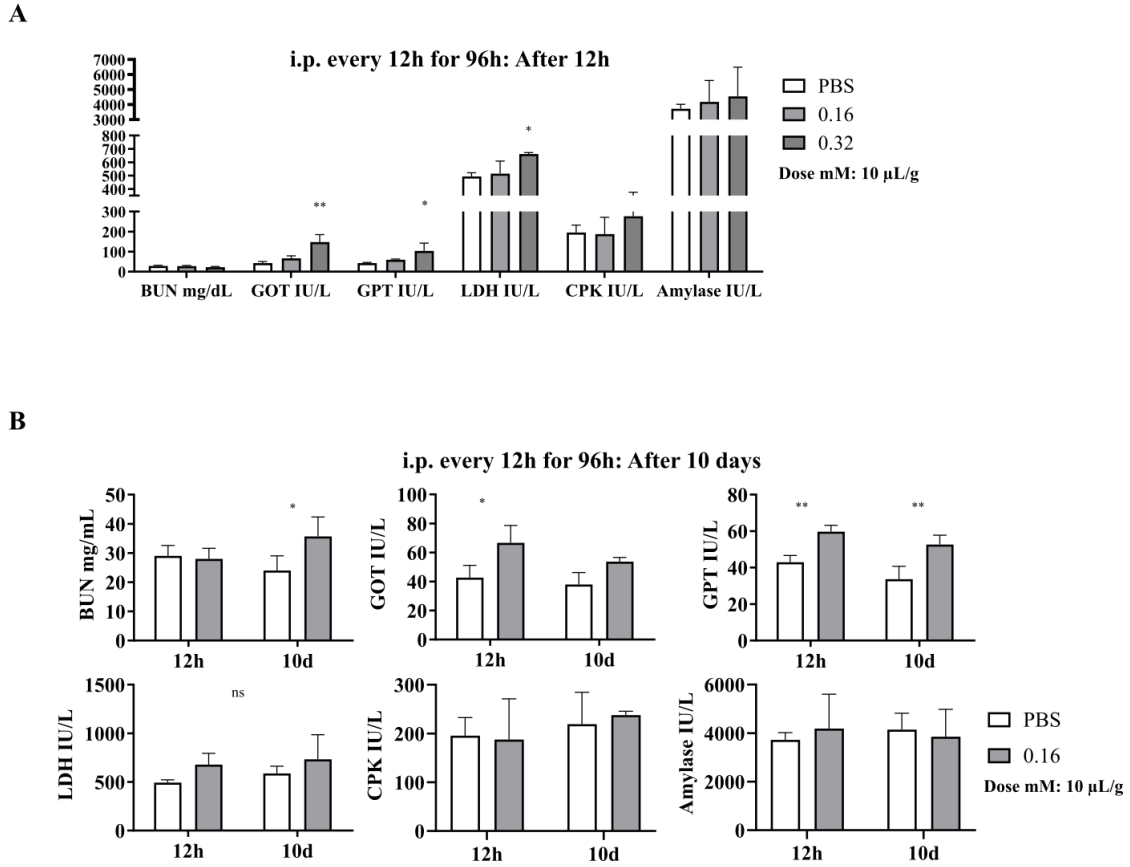

Figure 23. Toxicity of ARC39 *in vivo* in a multiple-dose regimen. The compound was applied i.p. every 12h for 96h. After 12h in **(A)** and after 10d in the same individuals in **(B)**, serum was collected and the following serological markers were assessed: Blood urea nitrogen (BUN), glutamate-oxaloacetate transaminase (GOT) / aspartate transaminase, glutamate-pyruvate transaminase (GPT) / alanine transaminase, lactate dehydrogenase (LDH), creatine phosphokinase (CPK) and amylase. On day 10, only the two groups that did not exhibit significant morbidity or lethality between 12h-10d are shown. Data represented as mean ± SD, n=3 mice per group. One-way ANOVA was used in (A) and two-way ANOVA was in (B), both followed by Bonferroni correction. **P*<0.05 ***P*<0.01.

3.11.2 ASM inhibition by ARC39 in vivo

The compound was applied i.p. as mentioned above: a single dose 1.2 mg/kg, and short-term multiple-dose treatment for a total cumulative dose of 4.8 mg/kg.

To this end, following tissues were investigated subsequently: Peritoneal lavage, serum or plasma, liver, spleen, and brain.

In a first approach, ASM activity was determined in tissue lysates with the conventional assay after a single dose as indicated **(Fig. 24A)** or 12h after the short-term multiple-dose regimen **(Fig. 24B)**. No significant reduction was detected in either case except locally in the peritoneal lavage and slightly in liver and spleen 12h after the single dose.

There was even an increase in ASM activity in the liver after the multiple-dose treatment.

However, since the conventional assay may be in this case subject to artifacts as mentioned earlier because organs are usually many-fold more diluted than cells during processing steps, sphingomyelins were quantitated by mass spectrometry in the indicated organs after the multiple-dose short-term treatment. A relevant and significant increase in total sphingomyelins was only observed locally in the peritoneal lavage **(Fig. 24C)**. Ceramides were not changed (not shown).

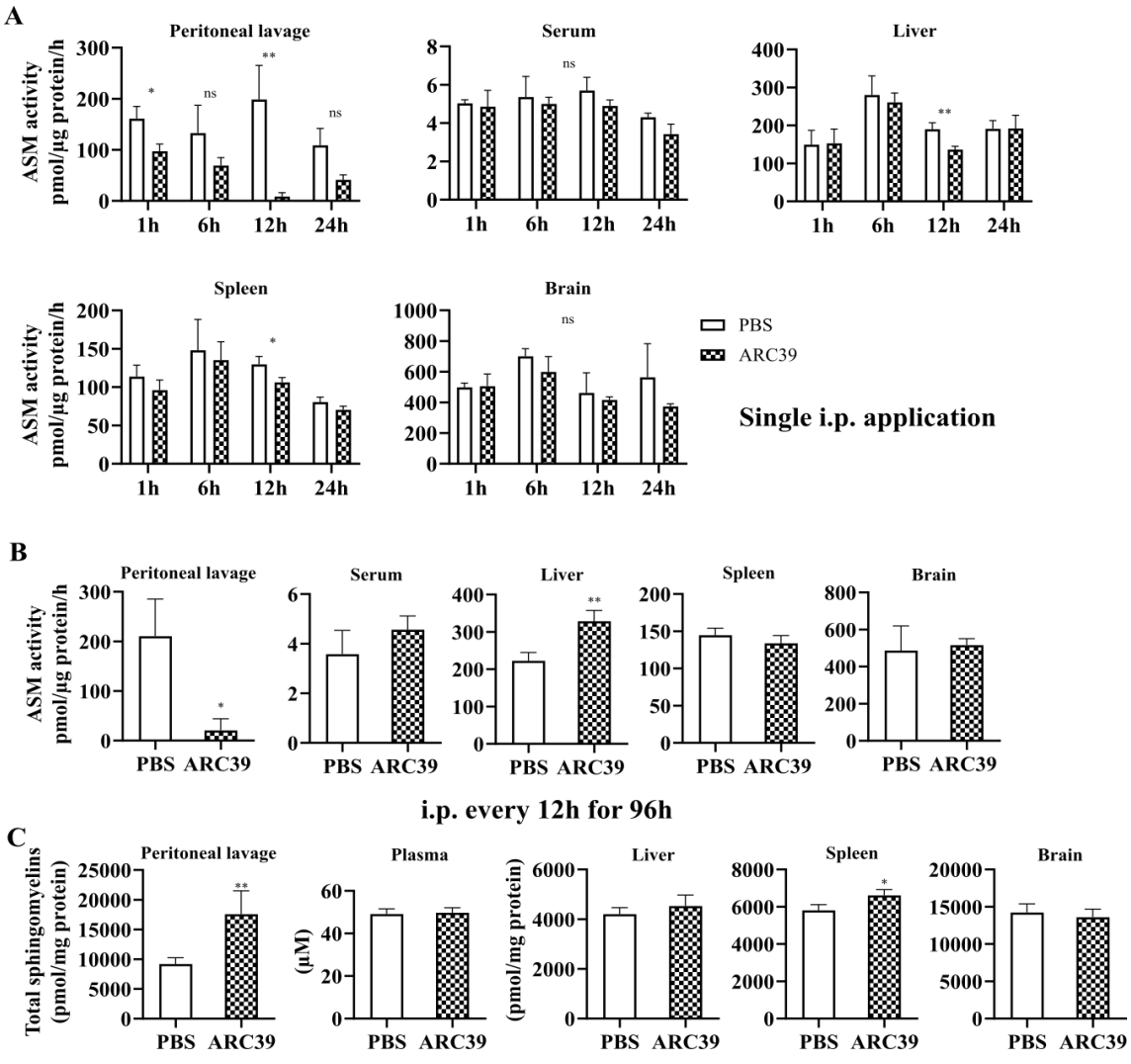

Figure 24. ASM inhibition by ARC39 *in vivo*. (A) ARC39 was applied i.p. once at a dose of 0.32 mM 10 µL/g and ASM activity was subsequently determined at the indicated time points post-injection. **(B, C)** ARC39 was applied i.p. every 12h for 96h at a dose of 0.16 mM 10 µL/g then ASM activity in **(B)** and sphingomyelin content with mass spectrometry in **(C)** was determined 12h after the last injection. Data represented as mean ± SD, n=3 mice per group in (A, B) and n=4 in (C). Unpaired Student ‘s *t*-test was used. **P*<0.05 ***P*<0.01

4 Discussion

Inhibition of acid sphingomyelinase could be utilized as an investigational tool and potentially as a therapeutic intervention in the future (Becker et al., 2010; Beckmann et al., 2019; Carpinteiro et al., 2015; Klutzny et al., 2017). FIASMAs are widely used as inhibitors of acid sphingomyelinase *in vitro* and *in vivo* and are clinically approved and generally well tolerated. However, FIASMAs act in an indirect manner and at least *in vitro* it has been shown that some of them may inhibit other enzymes involved in lipid and especially sphingolipid metabolism. *In vivo*, FIASMAs lead to a relevant reduction of ceramide related to the inhibition of the acid sphingomyelinase and have been successfully used to reproduce the phenotype observed in ASM heterozygous mice in models of cystic fibrosis and major depression (Gulbins et al., 2013; Teichgraber et al., 2008).

4.1 General characteristics of ASM inhibition by ARC39 in cell culture and in micellar assays

At least for research purposes, it is desirable to validate other more selective and potent ASM inhibitors. In this study, ARC39 was characterized, which is one of the most potent ASM inhibitors developed so far (Arenz, 2010). Data presented here show that ARC39 inhibits both L-ASM and S-ASM efficiently and selectively *in vitro* by directly blocking the catalytic activity without downregulating ASM mRNA or protein and, more importantly, works rather specifically without inhibiting acid ceramidase downstream of ASM and other acid hydrolases in the lysosomal sphingolipid catalytic pathways. Elojeimy et al. reported that desipramine inhibits acid ceramidase at 10 µM *in vitro* in a time-dependent manner (Elojeimy et al., 2006). Similar results regarding acid ceramidase activity were obtained here with both amitriptyline and desipramine in L929 cells. Upon treatment with ARC39, no significant induction of phospholipidosis was detected nor an inhibitory effect on SphK1, SphK2, NC or NSM could be measured.

4.2 The ability of ARC39 to reach the endo-lysosomal compartment and inhibit L-ASM *in vitro*

Since ARC39 is a bisphosphonate, it is highly negatively charged at physiological pH. Thus, it is unlikely that passive diffusion through membranes occurs. The compound

has been used in numerous studies to obtain outcomes related to ASM inhibition, e.g. it inhibited platelet-activating factor-induced pulmonary edema in isolated, ventilated, and perfused rat lungs (Roth et al., 2009a), cellular stress response and death receptor signaling (Chung et al., 2016; Martinez et al., 2012; Sosna et al., 2016; Voigt et al., 2014), and murine acute lung injury following transfusion of aged platelets *in vivo* when WT platelets had been stored with ARC39 (McVey et al., 2017). There was, however, no clear evidence whether the compound could effectively reach the endo-lysosomal compartment and inhibit L-ASM since the majority of these biological effects are linked to S-ASM and/or surface activity of L-ASM upon translocation onto the outer leaflet of the plasma membrane. Here, following evidence of efficient L-ASM inhibition by ARC39 *in vitro* is provided, as treatment with ARC39 led to:

1) A dose- and time-dependent decrease in ASM activity determined with a FRET probe-based *in-situ* assay in intact living cells.
2) A dose-dependent increase of sphingomyelins and sphingomyelins/ceramides ratio after 24h treatment as determined by mass spectrometry.
3) Lysosomal accumulation of exogenous BODIPY FL sphingomyelin.

It should be noted here that the MFI of BODIPY-sphingomyelin may not be an accurate indicator of ASM inhibition since 1) the BODIPY FL molecule is attached to the fatty acyl chain in ceramide and, thus, downstream products are also fluorescent and 2) differences in uptake and/or the size of the endo-lysosomal compartment may also partially account for the differences in MFI. However, the increase in BODIPY FL fluorescence after 24h treatment with ARC39 is somehow close to the increase in endogenous sphingomyelins as determined by mass spectrometry. This increase in the fluorescence intensity of BODIPY FL-sphingomyelin after ASM inhibition could be attributed to the aggregation of the dye within an acidic compartment.

The fact that ARC39 obviously acts in living cells is consistent with the early findings that bisphosphonates are able to enter the cytoplasm and other organelles (Felix et al., 1984). One particular study by Thompson et al. confirmed the cellular uptake of alendronate and zoledronate (N-BPs) by fluid-phase endocytosis in the presence of Ca^{2+} and that these compounds accumulate in the endocytic vesicles (Thompson et al., 2006). This is also consistent with kinetics of ASM inhibition by ARC39, since time had a positive effect on it, and it increased over hours analogues to the trafficking of N-BPs as

their intracellular concentrations within the endocytic pathway increase over hours until reaching saturation (Thompson et al., 2006).

Initially an IC_{50} of 20 nM was obtained (directly with the enzyme) with ARC39 (Roth et al., 2009a). This shift between the nanomolar range and micromolar range in cell culture may be explained by the following points:

- Different assays and reaction conditions: The initial value was obtained using, among others, a different substrate HMU-PC (6-hexadecanoylamino-4-methylumbelliferonephosphorylcholine) and a different detergent Triton X-100. Using BODIPY-C_{12}-sphingomyelin tends to give higher values that also shift with increasing concentrations of sphingomyelin in the assay buffer, consistent with a mechanism of a competitive inhibitor (C. Arenz unpublished observations).
- Binding to proteins and albumin in serum, which was observed with other bisphosphonates (Lin, 1996).
- A potential need for higher concentrations to promote complex formation with Ca^{+2} so that endocytic internalization takes place (Thompson et al., 2006).

4.3 Changes in endogenous sphingolipids after treatment with ARC39

In the two investigated cell lines L929 and HepG2, close results were obtained with mass spectrometric analysis that show accumulation of sphingomyelins and reduction in ceramides, sphingosine and particularly S1P downstream without having a direct inhibitory effect on sphingosine kinases 1 and 2. The fact that there are overall no significant changes in dihydrosphingosine and dihydroceramides would suggest that *de novo* synthesis is not affected.

Although these results provide quite valuable insight, it should be emphasized that the mass spectrometric analysis was to this end performed on whole-cell lysates. This may underestimate or obscure changes that take primarily place in certain cellular compartments or organelles depending on the localization of the corresponding enzymes, e.g. changes in sphingomyelins, ceramides and sphingosine within the endo-lysosomal compartment, endoplasmic reticulum or Golgi, which may in turn be of a biological significance. Thus, this analysis reflects only a rough image about the actual change without providing specific spatial information.

4.4 Functional validation of ASM inhibition by ARC39

Addressed here is also an additional functional validation for ASM inhibition by ARC39, which abrogated platelet- and ASM-promoted adhesion of B16F10 melanoma cells *in vitro*. This effect is in turn attributed to a platelet-derived zinc-dependent cell surface ASM activity and also supernatant activity (S-ASM) (Carpinteiro et al., 2015). Consistently, this effect was inhibited by adding 1 µM ARC39 only during the short 5 min incubation of cells and platelets/rhASM with no previous preincubation required. Of note, when WT platelets had been stored with ARC39, transfusion of these platelets into recipient mice abrogated acute lung injury although the platelets were thoroughly washed before transfusion (McVey et al., 2017).

4.5 Toxicity *in vitro*

In vitro, the toxicity of ARC39 is generally low relative to the efficacy of ASM inhibition. Bisphosphonates are widely used in the clinic as antiresorptive reagents to treat certain bone disorders like osteoporosis and to impede osteolytic lesions in cancer metastasis and multiple myeloma. Inhibition of FPP synthase is one major mechanism of action but also a cause of N-BP toxicity (Dunford et al., 2001; Luckman et al., 1998; van Beek et al., 1999a, b). Unlike ARC39, however, in which the -NH_2 group is located in the R^1 side chain, it is located in all other clinically relevant N-BPs in the R^2 side chain. Dunford et al. reported on the structure-activity relationship between the inhibition of FPP synthase *in vitro* and inhibition of bone resorption *in vivo* in N-BPs (Dunford et al., 2001). In fact, Brown et al. reported that replacing the hydroxyl group in the R^1 chain by an amino group abolished or markedly reduced the antiresorptive potency of osteoclasts and the ability of both olpadronate and pamidronate but not etidronate to inhibit the growth of amoeba (Brown et al., 1998). Interestingly, one similarity between ARC39 and etidronate is that they both do not originally contain an amino group or a nitrogen in their R^2 side chains, which is in contrast to olpadronate and pamidronate.

Data presented in this study suggest that ARC39 could potentially inhibit FPP synthase and lead to unprenylated RAP1A accumulation. However, the potency and the relevance of this inhibition requires further investigation. In this study, this effect was so far investigated only in L929 and HepG2 since they were mostly used, although more

pronounced toxicity was observed in BMDMs. Future studies should, however, address toxicity and FPP synthase inhibition in more detail in macrophage-related cells like retinal pigmented epithelium or osteoclasts since cells with high phagocytic capacity may 1) efficiently uptake and accumulate high levels of bisphosphonates, 2) be more sensitive to dysregulation in small GTPases.

The reason for the observation that in both L929 and HepG2 with higher doses RAP1A tend to be decreased between 40 µM and 80 µM is unknown but may be a compensatory response downregulating protein synthesis. Indeed, one report showed that unprenylated small GTPases are in the active state and may affect cellular function by sustained inappropriate activation (Dunford et al., 2006).

4.6 Effect on the lysosomal compartment

The rationale for investigating the lysosomal compartment is:

- ASM is a lysosomal enzyme. Thus, local changes in sphingolipids, particularly accumulation of sphingomyelin may affect the lysosomes.
- According to the proposed mechanism of internalization of N-BPs (Thompson et al., 2006), which is predominantly fluid-phase endocytosis, these compounds are most abundant and highly concentrated within the endocytic pathway inside the cells. Thus, they basically reach the endo-lysosomal compartment. Notably, fluorescently labeled alendronate significantly co-localized with fluorescently labeled dextran (Thompson et al., 2006).
- Lysosomotropic compounds including FIASMAs trigger significant changes in lysosomal homeostasis and function independent of ASM inhibition.

Using LysoTracker and LysoSensor staining, ARC39 affected the lysosomal compartment only minimally compared to amitriptyline and desipramine. The increase in LysoTracker intensity observed after 24h with ARC39 may be attributed to ASM inhibition, sphingomyelin accumulation and a potential lysosomal adaptive response.

The more prominent increase in lysosomal volume with amitriptyline and desipramine after 24h indicated by the LysoTracker signal is also in agreement with a previous report (Lu et al., 2017), which suggested that lysosomal dysfunction or stress caused by various lysosomotropic compounds evokes an adaptive biogenic lysosomal response in which the transcription factors TFEB, TFE3 and MITF play a role.

It should be also noted that here the increase in LysoTracker signal compared with vehicle-treated cells was somehow blunted when cells had been fed for 24h with exogenous BODIPY sphingomyelin **(Fig. 14A and 15A)**. One possible explanation is that treating with exogenous sphingomyelin alone could lead to some increase in the lysosomal volume and some degree of an adaptive lysosomal response.

More importantly, no significant accumulation of phospholipids was detected after 24h with LipidTOX reagent upon treatment with ARC39. This indicates high specificity of the compound based on the assumption that it is concentrated within the endo-lysosomal compartment due to the mechanism of the cellular uptake. These data also suggest that the inhibitor spares other phospholipases within the endo-lysosomal compartment.

Drug-induced phospholipidosis emerges through several mechanisms, one of which is functional inhibition of lysosomal phospholipases in a mechanism similar to ASM (Muehlbacher et al., 2012). Notably in this *in vitro* study by Muehlbacher et al., 51 compounds out of 262 induced phospholipidosis in H4 neuroglioma cell line, and 45 of these 51 compounds inhibited ASM. According to the criteria of the study, amitriptyline and desipramine induced phospholipidosis at 5 µM but not at 2.5 µM, while amiodarone led to significant phospholipids at 2.5 µM. Amiodarone is a potent antiarrhythmic agent that is used in the clinic to treat ventricular arrhythmias and atrial fibrillation. Generally, drug-induced phospholipidosis is an accepted side effects of many medications. In some cases, however, it is linked to clinically relevant consequences. The most frequently reported clinical complication related to drug-induced phospholipidosis is liver toxicity, in particular with amiodarone (Goldman et al., 1985; Lewis et al., 1990). There is no clear causative link between drug-induced phospholipidosis and toxicity in the lung and the central nervous system, where phospholipidosis may just be an association (Camus et al., 1989; Cartwright et al., 2009; Gonzalez-Rothi et al., 1995). Due to its potential side effects, drug-induced phospholipidosis is currently being considered particularly within the early stages of drug design (Chatman et al., 2009; Reasor et al., 2006), and drug approval and registration, even by the FDA (Kruhlak et al., 2008).

4.7 ARC39 *in vivo*

The inhibitory effect of ARC39 on ASM *in vitro* could not be confirmed *in vivo*. When applying high subtoxic doses i.p., a relevant increase in sphingomyelins was only detected in locally in the peritoneal lavage.

As a bisphosphonate, ARC39 may have high affinity to bone surfaces and could be very rapidly cleared from the plasma and soft tissues predominantly by bone and also by excretion in the kidney, with no evidence of further metabolism of N-BPs like alendronate (Lin, 1996; Lin et al., 1992; Lin et al., 1991; Weiss et al., 2008). One limitation in the current study is that so far there is no established method for quantitating ARC39 in tissues.

Bisphosphonates form three-dimensional structures that are capable of binding divalent metal ions such as Mg^{+2}, Fe^{+2}, and particularly Ca^{+2} by coordination of one oxygen from each phosphonate group with the divalent cation. The affinity for calcium can be further increased if one of the side chains (R^1) is a hydroxyl or a primary amino group (like ARC39) because this allows the formation of a tridentate conformation that is able to bind Ca^{+2} more effectively than otherwise a bidentate conformation (Jung et al., 1973). The high avidity of bisphosphonates for Ca^{+2} ions is the basis of the bone-targeting property of these compounds leading to their rapid clearance from the circulation and localization to hydroxyapatite bone mineral surfaces, particularly where bone turnover is higher, like in trabecular bone (Lin, 1996). The knowledge of their pharmacokinetics comes essentially from studies in animals with radiolabeled bisphosphonates. Among the soft non-calcified tissues, the highest concentrations of zoledronate were found in kidney followed by spleen followed by liver in rats after a short-term treatment, and in kidney and thyroid gland in dogs at 96h after a single intravenous dose (Weiss et al., 2008). These concentrations were, however, still 10-100-fold lower than those in bones.

The cause of the slight accumulation of sphingomyelin in spleen and liver (also reduction of ASM activity after a single dose) is unknown but could be related to the tissue distribution of bisphosphonates leading to relatively higher concentrations in liver and spleen. In addition, there is evidence that very high single intravenous doses of clodronate, alendronate and pamidronate (20-40 mg/kg) in mice and rats lead to

accumulation and retention in liver, spleen, lung and kidney (Lin, 1996). The mechanism is unknown but is assumed that in high intravenous doses bisphosphonates are able to form large complexes with metal ions that are phagocytosed and retained in these tissues. This could also explain liver and kidney toxicity observed here. However, such accumulation and retention was not observed after intraperitoneal application in mice (Monkkonen and Ylitalo, 1990).

On the other hand, there is currently no reliable method to determine ASM inhibition *in vivo* directly without possibly interfering with the enzyme-inhibitor interaction. Quantitating tissue sphingomyelin instead may provide useful information, although it may not always reflect ASM inhibition, particularly in a short-term treatment.

In any case, local administration of such compounds, e.g. inhalation may still be an option.

Generally, there is still a need for improved compounds suitable for systemic administration *in vivo* which can reach tissue concentrations relevant to ASM inhibition with lower doses. One promising approach to circumvent the need for high doses and the problem of bisphosphonate pharmacokinetics could be a new ARC39 prodrug which can be cleaved intracellularly into the active ARC39. This compound is currently being developed.

Nanoparticle coating for targeted tissue delivery *in vivo* could be another possible strategy (Donida et al., 2018). This last option is particularly worth considering when targeting the compound to the central nervous system since bisphosphonates do not bypass the blood brain barrier, which could be utilized as a novel therapy in a model of Farber disease, a rare lysosomal storage disorder, where a recent proof-of-concept study suggested that decreasing Asm activity is a potential therapeutic option (Beckmann et al., 2019).

4.8 Technical considerations for monitoring ASM activity *in-situ* with the FRET probe

As mentioned earlier, amitriptyline was used as an ASM inhibitor to compare the conventional ASM assay and the assay with the FRET probe due to the fact that it is an indirect inhibitor, and the inhibition determined in the assay reflects primarily the degradation of the ASM protein. The fact that a dose-response was obtainable in living

cells, led to consider the new assay primarily successful. Importantly, NSM was inactive against as similar ASM FRET probe (Pinkert et al., 2017). Additionally, due to the size (MW: 1299 g/mol) and polarity of this FRET probe, it is probably predominantly uptaken by endocytosis and thus reaches primarily the endo-lysosomal compartment with minimal contact during the incubation period to the inner leaflet of the plasma membrane where NSM resides.

The obtained residual activity values with the new assay, which are higher than those obtained with the conventional assay, probably reflect more closely the real activity because:

- Mass spectrometry data showed that after treatment 24h with ARC39, the ratio of sphingomyelins/ceramides was still increased when increasing the dose from 20 µM to 40 µM, indicating that there is still actually some residual activity at 20 µM as detected after 6h (~10%) with the FRET probe.
- It is unlikely that a pharmacological inhibition would lead to 0% residual activity. This means that the conventional assay used here has a certain threshold for sensitivity.

Importantly, regarding the inevitable ~10% residual ASM activity with the FRET probe no matter how high the dose or how long the incubation time of the inhibitor, it is currently difficult to know how accurate or in what extent this reflects the reality because of the following considerations:

- Due to technical reasons, the green fluorescence at 520 nm (corresponding to the cleavage of the substrate) may still be higher than the background fluorescence once the substrate is uptaken even if there is theoretically no cleavage at all. In this case, a positive control, e.g. 20-40 µM ARC39 + 20-40 µM amitriptyline may be used and the green fluorescence value may be considered 5% residual activity.
- Cells are briefly trypsinized after the assay in the absence of the inhibitors and before analysis with flow cytometry. Some of the activity may be recovered.
- Lastly, it should be noted that since amitriptyline affects pH of the lysosome, the fluorescence of FAM in the probe may be affected by these changes compared

to the control samples. However, at least with the doses used here, pH was restored after 24h.

4.9 The new FRET probe-based ASM assay as a platform to validate new ASM inhibitors

New high throughput screening approaches are being developed to discover new direct ASM inhibitors, in which test compounds are incubated with the recombinant ASM (to be published by Mohamed et al.) One screening included a large library of clinically relevant compounds. A prominent hit from this screening was compound X1 (please note that the real name and structure of the compound cannot be revealed here before it is published).

The compound had been first tested in L929 cells with the conventional ASM assay without the ability to detect any inhibition in ASM activity up to 160 µM inhibitor (not shown).

However, using the FRET probe-based *in-situ* ASM assay, it was possible to obtain a dose-response within 2h, and the residual activity reached ~50% at 40-80 µM **(Fig. 25)**, suggesting a moderate inhibitor.

Unlike ARC39, it was not possible to detect the effect of this inhibitor with the conventional assay, suggesting that it binds to ASM with lower affinity and/or since it is less potent, the processing and dilution steps in the assay interfere with its interaction with the enzyme. This may theoretically apply to many other test compounds as their actual effect may be underestimated or undetectable with the conventional assay.

The mother compound could now be modified to produce more potent inhibitors, and these in turn could be tested *in cellulo* with the FRET probe.

These results suggest the use of the new FRET probe-based ASM assay as a more reliable platform that is well suited for evaluating the potency of new candidates *in cellulo*, thus aiding the discovery, development and validation of new ASM inhibitors.

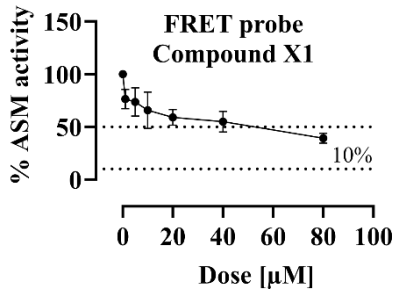

Figure 25. The FRET probe-based *in-situ* ASM assay as a platform to validate new ASM inhibitors. L929 cells were treated as indicated with compound X1 or with DMSO control (0.2% and 0.4%) for 2h then were incubated for 30 min with 1 µM FRET probe. Cells were subsequently washed, briefly trypsinized and analyzed by flow cytometry. A dose-response was obtainable, which was not possible with the conventional assay (not shown). Data represented as mean ± SD, n=3 experiments.

4.10 Outlook: A new ARC39 prodrug with potential efficacy *in vivo*

In an effort to circumvent the problem of the high bone affinity *in vivo*, a new ARC39 prodrug is currently being tested (synthesized by Z. Mohamed). In this new compound, three acetoxymethyl moieties are attached to form ester bonds with three oxygens in the 2 phosphonate groups (called 3Am-ARC39) **(Fig. 26A)**. These highly lipophilic acetoxymethyl moieties significantly reduce the charge of the molecule and are generally used to make compounds cell permeable. Once inside the cell, the ester bond is cleaved by non-specific esterases generating the active compound. The critical issue with ARC39 as a bisphosphonate is the potential high affinity to bone as mentioned earlier. This “masking” of the charged oxygen atoms would decrease the affinity to bone significantly while simultaneously increasing membrane permeability and distribution to other tissues.

The inhibition of ASM with this compound was tested in intact cells with the FRET probe **(Fig. 26B)** and is generally comparable with the original compound.

The cleavage of the 3Am-ARC39 into active ARC39 with exposed oxygen in the phosphonates is essential for ASM inhibition. The fact that the 3Am-ARC39 is active in cells suggests that is it cleaved within the endo-lysosomal compartment at least partially because if active ARC39 forms in the cytosol, it is unlikely that it passes spontaneously through the lysosomal membrane at a rate fast enough to reach relevant concentrations in the endo-lysosomes.

Future studies will be directed toward:

- Determination of the efficiency and kinetics of the cleavage of 3Am-ARC39 into active ARC39.
- Investigating whether/to which extent esterases in serum could contribute to the cleavage *ex vivo* to determine how much 3Am-ARC39 could be converted to ARC39 in the circulation. It is expected that the less cleavage and formation of active ARC39 in the circulation, the more favorable the pharmacokinetics would be.
- Investigating whether 3Am-ARC39 could be used as an efficient ASM inhibitor *in vivo*.

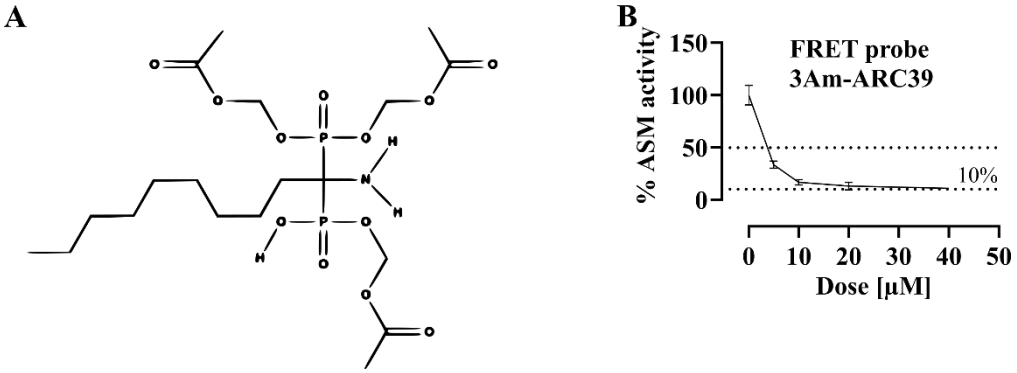

Figure 26. A new modified ARC39: 3Am-ARC39. (A) Chemical structure of the new modified ARC39 showing the three covalently linked acetoxymethyl groups. **(B)** L929 cells were treated as indicated with 3Am-ARC39 as indicated or with DMSO control (0.2% and 0.4%) for 2h then were incubated for 30 min with 1 µM FRET probe. Cells were subsequently washed, briefly trypsinized and analyzed by flow cytometry. Data represented as mean ± SD, n=2 experiments.

5 Abstract

Background: Inhibition of acid sphingomyelinase (ASM), a lysosomal enzyme that catalyzes the hydrolysis of sphingomyelin into ceramide and phosphorylcholine, may serve as an investigational tool or as a therapeutic intervention in many disease processes. Specific and direct inhibitors of ASM are to this date not sufficiently characterized.

Aim: This study aims to characterize the bisphosphonate 1-aminodecylidene bis-phosphonic acid (ARC39), a direct inhibitor of ASM, *in vitro* and *in vivo* in order to provide useful input about its potential application as a new ASM inhibitor.

Results: ARC39 is as a selective inhibitor of ASM *in vitro*, leading to specific and efficient (>90%) inhibition of both secretory and lysosomal ASM. Investigating sphingomyelin phosphodiesterase 1 (*SMPD1/Smpd1*) mRNA, ASM protein and the effect of protease inhibitors on ASM inhibition suggests that direct inhibition of the catalytic activity of ASM is the major mechanism of action of ARC39 in cultured cells, which differs from the functional inhibitors of ASM (FIASMAs). Evidence of a dose- and time-dependent inhibition of lysosomal ASM in intact living cells by ARC39 is provided. Functionally, ARC39 inhibits platelet- and ASM-promoted adhesion of melanoma cells. The toxicity of ARC39 is low at concentrations relevant for ASM inhibition *in vitro*, and it does not lead to pronounced alterations in the lysosomal compartment and does not induce phospholipidosis *in vitro*. However, when applied i.p. *in vivo*, even subtoxic high doses administered as a short-term treatment were sufficient to inhibit ASM and induce sphingomyelin accumulation only locally in the peritoneal lavage but not in serum/plasma, liver, spleen or brain.

Conclusion: ARC39 is a highly potent and specific ASM inhibitor *in vitro*. However, it is not well suited for systemic administration *in vivo*, which requires further investigation with other possible chemical modifications or alternatives.

5 Zusammenfassung

Hintergrund: Die Hemmung der sauren Sphingomyelinase (ASM), ein lysosomales Enzym, welches die Hydrolyse von Sphingomyelin in Ceramid und Phosphorylcholin beschleunigt, kann als Untersuchungsinstrument oder als therapeutische Intervention bei vielen Krankheitsvorgängen dienen. Spezifische und direkte Inhibitoren von ASM sind bis heute nicht ausreichend charakterisiert.

Zielsetzung: Diese Studie zielt darauf ab, das Bisphosphonat 1-Aminodecyliden-bis-phosphonsäure (ARC39), ein direkter Inhibitor der ASM, *in vitro* und *in vivo* zu charakterisieren, um Erkenntnisse über seine mögliche Anwendung als neuer ASM-Inhibitor zu gewinnen.

Ergebnisse: ARC39 ist ein selektiver Inhibitor von ASM *in vitro*, der zu einer spezifischen und effizienten (>90%) Hemmung sowohl der sekretorischen als auch der lysosomalen ASM führt. Die Untersuchungen der Sphingomyelinphosphodiesterase 1 (*SMPD1/Smpd1*) mRNA, des ASM-Proteins und der Wirkung von Protease-Inhibitoren auf die Hemmung der ASM legen nahe, dass eine direkte Hemmung der katalytischen Aktivität der ASM der Hauptwirkmechanismus von ARC39 in kultivierten Zellen ist, was sich von den funktionellen Inhibitoren von ASM (FIASMAs) unterscheidet. Es liegen Nachweise für eine dosis- und zeitabhängige Hemmung der lysosomalen ASM in intakten, lebenden Zellen durch ARC39 vor. In funktionellen Untersuchungen hemmt ARC39 die Blutplättchen- und ASM-induzierte Adhäsion von Melanomzellen an Fibronektin beschichteten Flächen. Die zelluläre Toxizität von ARC39 ist bei für die ASM-Hemmung *in vitro* relevanten Konzentrationen gering, es kommt nicht zu messbaren Veränderungen im lysosomalen Kompartiment oder zur Induktion von Phospholipidose. Allerdings reichten bei intraperitonealer Anwendung *in vivo* selbst subtoxische hohe Dosierungen, die als Kurzzeitbehandlung verabreicht wurden, aus, um messbar ASM zu hemmen oder eine Akkumulation von Sphingomyelin nur lokal in der Peritoneallavage aber nicht in Serum/Plasma, Leber, Milz oder Gehirn zu induzieren.

Schlussfolgerung: ARC39 ist ein hochpotenter und spezifischer ASM-Inhibitor *in vitro*. Er eignet sich jedoch nicht für die systemische Verabreichung *in vivo*, was weitere Untersuchungen mit anderen möglichen chemischen Modifikationen oder Alternativen erfordert.

6 References

1. Adams, C., Icheva, V., Deppisch, C., Lauer, J., Herrmann, G., Graepler-Mainka, U., Heyder, S., Gulbins, E., and Riethmueller, J. (2016). Long-Term Pulmonal Therapy of Cystic Fibrosis-Patients with Amitriptyline. Cell Physiol Biochem *39*, 565-572.
2. Albouz, S., Boutry, J.M., Dubois, G., Bourdon, R., Hauw, J.J., and Baumann, N. (1981). Lipid and lysosomal enzymes in human fibroblasts cultured with perhexiline maleate. Naunyn Schmiedebergs Arch Pharmacol *317*, 173-177.
3. Arenz, C. (2010). Small molecule inhibitors of acid sphingomyelinase. Cell Physiol Biochem *26*, 1-8.
4. Babalola, J.O., Wendeler, M., Breiden, B., Arenz, C., Schwarzmann, G., Locatelli-Hoops, S., and Sandhoff, K. (2007). Development of an assay for the intermembrane transfer of cholesterol by Niemann-Pick C2 protein. Biol Chem *388*, 617-626.
5. Bartelsen, O., Lansmann, S., Nettersheim, M., Lemm, T., Ferlinz, K., and Sandhoff, K. (1998). Expression of recombinant human acid sphingomyelinase in insect Sf21 cells: purification, processing and enzymatic characterization. J Biotechnol *63*, 29-40.
6. Becker, K.A., Riethmuller, J., Luth, A., Doring, G., Kleuser, B., and Gulbins, E. (2010). Acid sphingomyelinase inhibitors normalize pulmonary ceramide and inflammation in cystic fibrosis. Am J Respir Cell Mol Biol *42*, 716-724.
7. Beckmann, N., Becker, K.A., Kadow, S., Schumacher, F., Kramer, M., Kuhn, C., Schulz-Schaeffer, W.J., Edwards, M.J., Kleuser, B., Gulbins, E., and Carpinteiro, A. (2019). Acid Sphingomyelinase Deficiency Ameliorates Farber Disease. Int J Mol Sci *20*.
8. Beckmann, N., Kadow, S., Schumacher, F., Gothert, J.R., Kesper, S., Draeger, A., Schulz-Schaeffer, W.J., Wang, J., Becker, J.U., Kramer, M., Kuhn, C., Kleuser, B., Becker, K.A., Gulbins, E., and Carpinteiro, A. (2018). Pathological manifestations of Farber disease in a new mouse model. Biol Chem *399*, 1183-1202.
9. Bedia, C., Camacho, L., Abad, J.L., Fabrias, G., and Levade, T. (2010). A simple fluorogenic method for determination of acid ceramidase activity and diagnosis of Farber disease. J Lipid Res *51*, 3542-3547.
10. Brady, R.O., Kanfer, J.N., Mock, M.B., and Fredrickson, D.S. (1966). The metabolism of sphingomyelin. II. Evidence of an enzymatic deficiency in Niemann-Pick diseae. Proc Natl Acad Sci U S A *55*, 366-369.

11. Brown, R.J., van Beek, E., Watts, D.J., Lowik, C.W., and Papapoulos, S.E. (1998). Differential effects of aminosubstituted analogs of hydroxy bisphosphonates on the growth of Dictyostelium discoideum. J Bone Miner Res *13*, 253-258.
12. Callahan, J.W., Jones, C.S., Davidson, D.J., and Shankaran, P. (1983). The active site of lysosomal sphingomyelinase: evidence for the involvement of hydrophobic and ionic groups. J Neurosci Res *10*, 151-163.
13. Camus, P., Joshi, U.M., Lockard, V.G., Petrini, M.F., Lentz, D.L., and Mehendale, H.M. (1989). Effects of drug-induced pulmonary phospholipidosis on lung mechanics in rats. J Appl Physiol (1985) *66*, 2437-2445.
14. Carpinteiro, A., Becker, K.A., Japtok, L., Hessler, G., Keitsch, S., Pozgajova, M., Schmid, K.W., Adams, C., Muller, S., Kleuser, B., Edwards, M.J., Grassme, H., Helfrich, I., and Gulbins, E. (2015). Regulation of hematogenous tumor metastasis by acid sphingomyelinase. EMBO Mol Med *7*, 714-734.
15. Cartwright, M.E., Petruska, J., Arezzo, J., Frank, D., Litwak, M., Morrissey, R.E., MacDonald, J., and Davis, T.E. (2009). Phospholipidosis in neurons caused by posaconazole, without evidence for functional neurologic effects. Toxicol Pathol *37*, 902-910.
16. Chang, J.T., Green, L., and Beitz, J. (2003). Renal failure with the use of zoledronic acid. N Engl J Med *349*, 1676-1679; discussion 1676-1679.
17. Chatman, L.A., Morton, D., Johnson, T.O., and Anway, S.D. (2009). A strategy for risk management of drug-induced phospholipidosis. Toxicol Pathol *37*, 997-1005.
18. Chung, H.Y., Hupe, D.C., Otto, G.P., Sprenger, M., Bunck, A.C., Dorer, M.J., Bockmeyer, C.L., Deigner, H.P., Graler, M.H., and Claus, R.A. (2016). Acid Sphingomyelinase Promotes Endothelial Stress Response in Systemic Inflammation and Sepsis. Mol Med *22*, 412-423.
19. Donida, B., Tauffner, B., Raabe, M., Immich, M.F., de Farias, M.A., de Sa Coutinho, D., Machado, A.Z., Kessler, R.G., Portugal, R.V., Bernardi, A., Frozza, R., Moura, D.J., Poletto, F., and Vargas, C.R. (2018). Monoolein-based nanoparticles for drug delivery to the central nervous system: A platform for lysosomal storage disorder treatment. Eur J Pharm Biopharm *133*, 96-103.
20. Dunford, J.E., Rogers, M.J., Ebetino, F.H., Phipps, R.J., and Coxon, F.P. (2006). Inhibition of protein prenylation by bisphosphonates causes sustained activation of Rac, Cdc42, and Rho GTPases. J Bone Miner Res *21*, 684-694.
21. Dunford, J.E., Thompson, K., Coxon, F.P., Luckman, S.P., Hahn, F.M., Poulter, C.D., Ebetino, F.H., and Rogers, M.J. (2001). Structure-activity relationships for inhibition of

farnesyl diphosphate synthase in vitro and inhibition of bone resorption in vivo by nitrogen-containing bisphosphonates. J Pharmacol Exp Ther *296*, 235-242.

22. Elojeimy, S., Holman, D.H., Liu, X., El-Zawahry, A., Villani, M., Cheng, J.C., Mahdy, A., Zeidan, Y., Bielwaska, A., Hannun, Y.A., and Norris, J.S. (2006). New insights on the use of desipramine as an inhibitor for acid ceramidase. FEBS Lett *580*, 4751-4756.
23. Felix, R., Guenther, H.L., and Fleisch, H. (1984). The subcellular distribution of [14C]dichloromethylenebisphosphonate and [14C]1-hydroxyethylidene-1,1-bisphosphonate in cultured calvaria cells. Calcif Tissue Int *36*, 108-113.
24. Ferlinz, K., Hurwitz, R., Vielhaber, G., Suzuki, K., and Sandhoff, K. (1994). Occurrence of two molecular forms of human acid sphingomyelinase. Biochem J *301 (Pt 3)*, 855-862.
25. Goggel, R., Winoto-Morbach, S., Vielhaber, G., Imai, Y., Lindner, K., Brade, L., Brade, H., Ehlers, S., Slutsky, A.S., Schutze, S., Gulbins, E., and Uhlig, S. (2004). PAF-mediated pulmonary edema: a new role for acid sphingomyelinase and ceramide. Nat Med *10*, 155-160.
26. Goldman, I.S., Winkler, M.L., Raper, S.E., Barker, M.E., Keung, E., Goldberg, H.I., and Boyer, T.D. (1985). Increased hepatic density and phospholipidosis due to amiodarone. AJR Am J Roentgenol *144*, 541-546.
27. Gonzalez-Rothi, R.J., Zander, D.S., and Ros, P.R. (1995). Fluoxetine hydrochloride (Prozac)-induced pulmonary disease. Chest *107*, 1763-1765.
28. Gorelik, A., Illes, K., Heinz, L.X., Superti-Furga, G., and Nagar, B. (2016). Crystal structure of mammalian acid sphingomyelinase. Nat Commun *7*, 12196.
29. Grassme, H., Henry, B., Ziobro, R., Becker, K.A., Riethmuller, J., Gardner, A., Seitz, A.P., Steinmann, J., Lang, S., Ward, C., Schuchman, E.H., Caldwell, C.C., Kamler, M., Edwards, M.J., Brodlie, M., and Gulbins, E. (2017). beta1-Integrin Accumulates in Cystic Fibrosis Luminal Airway Epithelial Membranes and Decreases Sphingosine, Promoting Bacterial Infections. Cell Host Microbe *21*, 707-718 e708.
30. Grassme, H., Riethmuller, J., and Gulbins, E. (2007). Biological aspects of ceramide-enriched membrane domains. Prog Lipid Res *46*, 161-170.
31. Gulbins, A., Schumacher, F., Becker, K.A., Wilker, B., Soddemann, M., Boldrin, F., Muller, C.P., Edwards, M.J., Goodman, M., Caldwell, C.C., Kleuser, B., Kornhuber, J., Szabo, I., and Gulbins, E. (2018). Antidepressants act by inducing autophagy controlled by sphingomyelin-ceramide. Mol Psychiatry *23*, 2324-2346.
32. Gulbins, E., and Li, P.L. (2006). Physiological and pathophysiological aspects of ceramide. Am J Physiol Regul Integr Comp Physiol *290*, R11-26.

33. Gulbins, E., Palmada, M., Reichel, M., Luth, A., Bohmer, C., Amato, D., Muller, C.P., Tischbirek, C.H., Groemer, T.W., Tabatabai, G., Becker, K.A., Tripal, P., Staedtler, S., Ackermann, T.F., van Brederode, J., Alzheimer, C., Weller, M., Lang, U.E., Kleuser, B., Grassme, H., and Kornhuber, J. (2013). Acid sphingomyelinase-ceramide system mediates effects of antidepressant drugs. Nat Med *19*, 934-938.
34. Hasilik, A., Waheed, A., and von Figura, K. (1981). Enzymatic phosphorylation of lysosomal enzymes in the presence of UDP-N-acetylglucosamine. Absence of the activity in I-cell fibroblasts. Biochem Biophys Res Commun *98*, 761-767.
35. He, X., Miranda, S.R., Xiong, X., Dagan, A., Gatt, S., and Schuchman, E.H. (1999). Characterization of human acid sphingomyelinase purified from the media of overexpressing Chinese hamster ovary cells. Biochim Biophys Acta *1432*, 251-264.
36. Hurwitz, R., Ferlinz, K., and Sandhoff, K. (1994a). The tricyclic antidepressant desipramine causes proteolytic degradation of lysosomal sphingomyelinase in human fibroblasts. Biol Chem Hoppe Seyler *375*, 447-450.
37. Hurwitz, R., Ferlinz, K., Vielhaber, G., Moczall, H., and Sandhoff, K. (1994b). Processing of human acid sphingomyelinase in normal and I-cell fibroblasts. J Biol Chem *269*, 5440-5445.
38. Jenkins, R.W., Canals, D., Idkowiak-Baldys, J., Simbari, F., Roddy, P., Perry, D.M., Kitatani, K., Luberto, C., and Hannun, Y.A. (2010). Regulated secretion of acid sphingomyelinase: implications for selectivity of ceramide formation. J Biol Chem *285*, 35706-35718.
39. Jenkins, R.W., Idkowiak-Baldys, J., Simbari, F., Canals, D., Roddy, P., Riner, C.D., Clarke, C.J., and Hannun, Y.A. (2011). A novel mechanism of lysosomal acid sphingomyelinase maturation: requirement for carboxyl-terminal proteolytic processing. J Biol Chem *286*, 3777-3788.
40. Jung, A., Bisaz, S., and Fleisch, H. (1973). The binding of pyrophosphate and two diphosphonates by hydroxyapatite crystals. Calcified Tissue Research *11*, 269-280.
41. Kappe, C., Mohamed, Z.H., Naser, E., Carpinteiro, A., and Arenz, C. (2020). A Novel Visible Range FRET Probe for Monitoring Acid Sphingomyelinase Activity in Living Cells. Chemistry *26*, 5780-5783.
42. Klutzny, S., Lesche, R., Keck, M., Kaulfuss, S., Schlicker, A., Christian, S., Sperl, C., Neuhaus, R., Mowat, J., Steckel, M., Riefke, B., Prechtl, S., Parczyk, K., and Steigemann, P. (2017). Functional inhibition of acid sphingomyelinase by Fluphenazine triggers hypoxia-specific tumor cell death. Cell Death Dis *8*, e2709.

43. Kolter, T., and Sandhoff, K. (2005). Principles of lysosomal membrane digestion: stimulation of sphingolipid degradation by sphingolipid activator proteins and anionic lysosomal lipids. Annu Rev Cell Dev Biol *21*, 81-103.
44. Kolzer, M., Arenz, C., Ferlinz, K., Werth, N., Schulze, H., Klingenstein, R., and Sandhoff, K. (2003). Phosphatidylinositol-3,5-Bisphosphate is a potent and selective inhibitor of acid sphingomyelinase. Biol Chem *384*, 1293-1298.
45. Kolzer, M., Ferlinz, K., Bartelsen, O., Hoops, S.L., Lang, F., and Sandhoff, K. (2004a). Functional characterization of the postulated intramolecular sphingolipid activator protein domain of human acid sphingomyelinase. Biol Chem *385*, 1193-1195.
46. Kolzer, M., Werth, N., and Sandhoff, K. (2004b). Interactions of acid sphingomyelinase and lipid bilayers in the presence of the tricyclic antidepressant desipramine. FEBS Lett *559*, 96-98.
47. Kornhuber, J., Medlin, A., Bleich, S., Jendrossek, V., Henkel, A.W., Wiltfang, J., and Gulbins, E. (2005). High activity of acid sphingomyelinase in major depression. J Neural Transm (Vienna) *112*, 1583-1590.
48. Kornhuber, J., Muehlbacher, M., Trapp, S., Pechmann, S., Friedl, A., Reichel, M., Muhle, C., Terfloth, L., Groemer, T.W., Spitzer, G.M., Liedl, K.R., Gulbins, E., and Tripal, P. (2011). Identification of novel functional inhibitors of acid sphingomyelinase. PLoS One *6*, e23852.
49. Kornhuber, J., Rhein, C., Muller, C.P., and Muhle, C. (2015). Secretory sphingomyelinase in health and disease. Biol Chem *396*, 707-736.
50. Kornhuber, J., Tripal, P., Reichel, M., Muhle, C., Rhein, C., Muehlbacher, M., Groemer, T.W., and Gulbins, E. (2010). Functional Inhibitors of Acid Sphingomyelinase (FIASMAs): a novel pharmacological group of drugs with broad clinical applications. Cell Physiol Biochem *26*, 9-20.
51. Kornhuber, J., Tripal, P., Reichel, M., Terfloth, L., Bleich, S., Wiltfang, J., and Gulbins, E. (2008). Identification of new functional inhibitors of acid sphingomyelinase using a structure-property-activity relation model. J Med Chem *51*, 219-237.
52. Kruhlak, N.L., Choi, S.S., Contrera, J.F., Weaver, J.L., Willard, J.M., Hastings, K.L., and Sancilio, L.F. (2008). Development of a phospholipidosis database and predictive quantitative structure-activity relationship (QSAR) models. Toxicol Mech Methods *18*, 217-227.
53. Lang, P.A., Schenck, M., Nicolay, J.P., Becker, J.U., Kempe, D.S., Lupescu, A., Koka, S., Eisele, K., Klarl, B.A., Rubben, H., Schmid, K.W., Mann, K., Hildenbrand, S., Hefter, H., Huber, S.M., Wieder, T., Erhardt, A., Haussinger, D., Gulbins, E., and Lang,

F. (2007). Liver cell death and anemia in Wilson disease involve acid sphingomyelinase and ceramide. Nat Med *13*, 164-170.

54. Le Stunff, H., Giussani, P., Maceyka, M., Lepine, S., Milstien, S., and Spiegel, S. (2007). Recycling of sphingosine is regulated by the concerted actions of sphingosine-1-phosphate phosphohydrolase 1 and sphingosine kinase 2. J Biol Chem *282*, 34372-34380.
55. Lewis, J.H., Mullick, F., Ishak, K.G., Ranard, R.C., Ragsdale, B., Perse, R.M., Rusnock, E.J., Wolke, A., Benjamin, S.B., Seeff, L.B., and et al. (1990). Histopathologic analysis of suspected amiodarone hepatotoxicity. Hum Pathol *21*, 59-67.
56. Lima, S., Milstien, S., and Spiegel, S. (2014). A real-time high-throughput fluorescence assay for sphingosine kinases. J Lipid Res *55*, 1525-1530.
57. Lin, J.H. (1996). Bisphosphonates: a review of their pharmacokinetic properties. Bone *18*, 75-85.
58. Lin, J.H., Chen, I.W., and Duggan, D.E. (1992). Effects of dose, sex, and age on the disposition of alendronate, a potent antiosteolytic bisphosphonate, in rats. Drug Metab Dispos *20*, 473-478.
59. Lin, J.H., Duggan, D.E., Chen, I.W., and Ellsworth, R.L. (1991). Physiological disposition of alendronate, a potent anti-osteolytic bisphosphonate, in laboratory animals. Drug Metab Dispos *19*, 926-932.
60. Linke, T., Wilkening, G., Lansmann, S., Moczall, H., Bartelsen, O., Weisgerber, J., and Sandhoff, K. (2001). Stimulation of acid sphingomyelinase activity by lysosomal lipids and sphingolipid activator proteins. Biol Chem *382*, 283-290.
61. Lu, S., Sung, T., Lin, N., Abraham, R.T., and Jessen, B.A. (2017). Lysosomal adaptation: How cells respond to lysosomotropic compounds. PLoS One *12*, e0173771.
62. Luckman, S.P., Hughes, D.E., Coxon, F.P., Graham, R., Russell, G., and Rogers, M.J. (1998). Nitrogen-containing bisphosphonates inhibit the mevalonate pathway and prevent post-translational prenylation of GTP-binding proteins, including Ras. J Bone Miner Res *13*, 581-589.
63. Maceyka, M., Harikumar, K.B., Milstien, S., and Spiegel, S. (2012). Sphingosine-1-phosphate signaling and its role in disease. Trends Cell Biol *22*, 50-60.
64. Maor, I., Mandel, H., and Aviram, M. (1995). Macrophage uptake of oxidized LDL inhibits lysosomal sphingomyelinase, thus causing the accumulation of unesterified cholesterol-sphingomyelin-rich particles in the lysosomes. A possible role for 7-Ketocholesterol. Arterioscler Thromb Vasc Biol *15*, 1378-1387.

65. Marathe, S., Schissel, S.L., Yellin, M.J., Beatini, N., Mintzer, R., Williams, K.J., and Tabas, I. (1998). Human vascular endothelial cells are a rich and regulatable source of secretory sphingomyelinase. Implications for early atherogenesis and ceramide-mediated cell signaling. J Biol Chem *273*, 4081-4088.
66. Markowitz, G.S., Fine, P.L., Stack, J.I., Kunis, C.L., Radhakrishnan, J., Palecki, W., Park, J., Nasr, S.H., Hoh, S., Siegel, D.S., and D'Agati, V.D. (2003). Toxic acute tubular necrosis following treatment with zoledronate (Zometa). Kidney Int *64*, 281-289.
67. Martinez, T.N., Chen, X., Bandyopadhyay, S., Merrill, A.H., and Tansey, M.G. (2012). Ceramide sphingolipid signaling mediates Tumor Necrosis Factor (TNF)-dependent toxicity via caspase signaling in dopaminergic neurons. Mol Neurodegener *7*, 45.
68. Matsuzawa, Y., and Hostetler, K.Y. (1980). Inhibition of lysosomal phospholipase A and phospholipase C by chloroquine and 4,4'-bis(diethylaminoethoxy) alpha, beta-diethyldiphenylethane. J Biol Chem *255*, 5190-5194.
69. McGovern, M.M., Wasserstein, M.P., Giugliani, R., Bembi, B., Vanier, M.T., Mengel, E., Brodie, S.E., Mendelson, D., Skloot, G., Desnick, R.J., Kuriyama, N., and Cox, G.F. (2008). A prospective, cross-sectional survey study of the natural history of Niemann-Pick disease type B. Pediatrics *122*, e341-349.
70. McVey, M.J., Kim, M., Tabuchi, A., Srbely, V., Japtok, L., Arenz, C., Rotstein, O., Kleuser, B., Semple, J.W., and Kuebler, W.M. (2017). Acid sphingomyelinase mediates murine acute lung injury following transfusion of aged platelets. Am J Physiol Lung Cell Mol Physiol *312*, L625-L637.
71. Mendis, S. (1989). Magnesium, zinc, and manganese in atherosclerosis of the aorta. Biol Trace Elem Res *22*, 251-256.
72. Milanino, R., Moretti, U., Concari, E., Marrella, M., and Velo, G.P. (1988). Copper and zinc status in adjuvant-arthritic rat: studies on blood, liver, kidneys, spleen and inflamed paws. Agents Actions *24*, 365-376.
73. Monkkonen, J., and Ylitalo, P. (1990). The tissue distribution of clodronate (dichloromethylene bisphosphonate) in mice. The effects of vehicle and the route of administration. Eur J Drug Metab Pharmacokinet *15*, 239-243.
74. Muehlbacher, M., Tripal, P., Roas, F., and Kornhuber, J. (2012). Identification of drugs inducing phospholipidosis by novel in vitro data. ChemMedChem *7*, 1925-1934.
75. Muhle, C., and Kornhuber, J. (2017). Assay to measure sphingomyelinase and ceramidase activities efficiently and safely. J Chromatogr A *1481*, 137-144.

76. Nahrlich, L., Mainz, J.G., Adams, C., Engel, C., Herrmann, G., Icheva, V., Lauer, J., Deppisch, C., Wirth, A., Unger, K., Graepler-Mainka, U., Hector, A., Heyder, S., Stern, M., Doring, G., Gulbins, E., and Riethmuller, J. (2013). Therapy of CF-patients with amitriptyline and placebo--a randomised, double-blind, placebo-controlled phase IIb multicenter, cohort-study. Cell Physiol Biochem *31*, 505-512.
77. Newrzella, D., and Stoffel, W. (1992). Molecular cloning of the acid sphingomyelinase of the mouse and the organization and complete nucleotide sequence of the gene. Biol Chem Hoppe Seyler *373*, 1233-1238.
78. Newrzella, D., and Stoffel, W. (1996). Functional analysis of the glycosylation of murine acid sphingomyelinase. J Biol Chem *271*, 32089-32095.
79. Petersen, N.H., Olsen, O.D., Groth-Pedersen, L., Ellegaard, A.M., Bilgin, M., Redmer, S., Ostenfeld, M.S., Ulanet, D., Dovmark, T.H., Lonborg, A., Vindelov, S.D., Hanahan, D., Arenz, C., Ejsing, C.S., Kirkegaard, T., Rohde, M., Nylandsted, J., and Jaattela, M. (2013). Transformation-associated changes in sphingolipid metabolism sensitize cells to lysosomal cell death induced by inhibitors of acid sphingomyelinase. Cancer Cell *24*, 379-393.
80. Pfister, T., Atzpodien, E., and Bauss, F. (2003). The renal effects of minimally nephrotoxic doses of ibandronate and zoledronate following single and intermittent intravenous administration in rats. Toxicology *191*, 159-167.
81. Pinkert, T., Furkert, D., Korte, T., Herrmann, A., and Arenz, C. (2017). Amplification of a FRET Probe by Lipid-Water Partition for the Detection of Acid Sphingomyelinase in Live Cells. Angew Chem Int Ed Engl *56*, 2790-2794.
82. Qiu, H., Edmunds, T., Baker-Malcolm, J., Karey, K.P., Estes, S., Schwarz, C., Hughes, H., and Van Patten, S.M. (2003). Activation of human acid sphingomyelinase through modification or deletion of C-terminal cysteine. J Biol Chem *278*, 32744-32752.
83. Quintern, L.E., Schuchman, E.H., Levran, O., Suchi, M., Ferlinz, K., Reinke, H., Sandhoff, K., and Desnick, R.J. (1989). Isolation of cDNA clones encoding human acid sphingomyelinase: occurrence of alternatively processed transcripts. EMBO J *8*, 2469-2473.
84. Quintern, L.E., Weitz, G., Nehrkorn, H., Tager, J.M., Schram, A.W., and Sandhoff, K. (1987). Acid sphingomyelinase from human urine: purification and characterization. Biochim Biophys Acta *922*, 323-336.
85. Reagan, J.W., Jr., Hubbert, M.L., and Shelness, G.S. (2000). Posttranslational regulation of acid sphingomyelinase in niemann-pick type C1 fibroblasts and free cholesterol-enriched chinese hamster ovary cells. J Biol Chem *275*, 38104-38110.

86. Reasor, M.J., Hastings, K.L., and Ulrich, R.G. (2006). Drug-induced phospholipidosis: issues and future directions. Expert Opin Drug Saf *5*, 567-583.
87. Roelofs, A.J., Thompson, K., Gordon, S., and Rogers, M.J. (2006). Molecular mechanisms of action of bisphosphonates: current status. Clin Cancer Res *12*, 6222s-6230s.
88. Rogers, M.J., Gordon, S., Benford, H.L., Coxon, F.P., Luckman, S.P., Monkkonen, J., and Frith, J.C. (2000). Cellular and molecular mechanisms of action of bisphosphonates. Cancer *88*, 2961-2978.
89. Roth, A.G., Drescher, D., Yang, Y., Redmer, S., Uhlig, S., and Arenz, C. (2009a). Potent and selective inhibition of acid sphingomyelinase by bisphosphonates. Angew Chem Int Ed Engl *48*, 7560-7563.
90. Roth, A.G., Redmer, S., and Arenz, C. (2009b). Potent inhibition of acid sphingomyelinase by phosphoinositide analogues. Chembiochem *10*, 2367-2374.
91. Roth, A.G., Redmer, S., and Arenz, C. (2010). Development of carbohydrate-derived inhibitors of acid sphingomyelinase. Bioorg Med Chem *18*, 939-944.
92. Ruiz-Arguello, M.B., Veiga, M.P., Arrondo, J.L., Goni, F.M., and Alonso, A. (2002). Sphingomyelinase cleavage of sphingomyelin in pure and mixed lipid membranes. Influence of the physical state of the sphingolipid. Chem Phys Lipids *114*, 11-20.
93. Schissel, S.L., Jiang, X., Tweedie-Hardman, J., Jeong, T., Camejo, E.H., Najib, J., Rapp, J.H., Williams, K.J., and Tabas, I. (1998a). Secretory sphingomyelinase, a product of the acid sphingomyelinase gene, can hydrolyze atherogenic lipoproteins at neutral pH. Implications for atherosclerotic lesion development. J Biol Chem *273*, 2738-2746.
94. Schissel, S.L., Keesler, G.A., Schuchman, E.H., Williams, K.J., and Tabas, I. (1998b). The cellular trafficking and zinc dependence of secretory and lysosomal sphingomyelinase, two products of the acid sphingomyelinase gene. J Biol Chem *273*, 18250-18259.
95. Schissel, S.L., Schuchman, E.H., Williams, K.J., and Tabas, I. (1996). Zn2+-stimulated sphingomyelinase is secreted by many cell types and is a product of the acid sphingomyelinase gene. J Biol Chem *271*, 18431-18436.
96. Schneider, P.B., and Kennedy, E.P. (1967). Sphingomyelinase in normal human spleens and in spleens from subjects with Niemann-Pick disease. J Lipid Res *8*, 202-209.
97. Schuchman, E.H., and Desnick, R.J. (2017). Types A and B Niemann-Pick disease. Mol Genet Metab *120*, 27-33.

98. Schuchman, E.H., Suchi, M., Takahashi, T., Sandhoff, K., and Desnick, R.J. (1991). Human acid sphingomyelinase. Isolation, nucleotide sequence and expression of the full-length and alternatively spliced cDNAs. J Biol Chem *266*, 8531-8539.

99. Sosna, J., Philipp, S., Fuchslocher Chico, J., Saggau, C., Fritsch, J., Foll, A., Plenge, J., Arenz, C., Pinkert, T., Kalthoff, H., Trauzold, A., Schmitz, I., Schutze, S., and Adam, D. (2016). Differences and Similarities in TRAIL- and Tumor Necrosis Factor-Mediated Necroptotic Signaling in Cancer Cells. Mol Cell Biol *36*, 2626-2644.

100. Takahashi, I., Takahashi, T., Mikami, T., Komatsu, M., Ohura, T., Schuchman, E.H., and Takada, G. (2005). Acid sphingomyelinase: relation of 93lysine residue on the ratio of intracellular to secreted enzyme activity. Tohoku J Exp Med *206*, 333-340.

101. Teichgraber, V., Ulrich, M., Endlich, N., Riethmuller, J., Wilker, B., De Oliveira-Munding, C.C., van Heeckeren, A.M., Barr, M.L., von Kurthy, G., Schmid, K.W., Weller, M., Tummler, B., Lang, F., Grassme, H., Doring, G., and Gulbins, E. (2008). Ceramide accumulation mediates inflammation, cell death and infection susceptibility in cystic fibrosis. Nat Med *14*, 382-391.

102. Testai, F.D., Landek, M.A., Goswami, R., Ahmed, M., and Dawson, G. (2004). Acid sphingomyelinase and inhibition by phosphate ion: role of inhibition by phosphatidyl-myo-inositol 3,4,5-triphosphate in oligodendrocyte cell signaling. J Neurochem *89*, 636-644.

103. Thompson, K., Rogers, M.J., Coxon, F.P., and Crockett, J.C. (2006). Cytosolic entry of bisphosphonate drugs requires acidification of vesicles after fluid-phase endocytosis. Mol Pharmacol *69*, 1624-1632.

104. van Beek, E., Pieterman, E., Cohen, L., Lowik, C., and Papapoulos, S. (1999a). Farnesyl pyrophosphate synthase is the molecular target of nitrogen-containing bisphosphonates. Biochem Biophys Res Commun *264*, 108-111.

105. van Beek, E., Pieterman, E., Cohen, L., Lowik, C., and Papapoulos, S. (1999b). Nitrogen-containing bisphosphonates inhibit isopentenyl pyrophosphate isomerase/farnesyl pyrophosphate synthase activity with relative potencies corresponding to their antiresorptive potencies in vitro and in vivo. Biochem Biophys Res Commun *255*, 491-494.

106. Voigt, S., Philipp, S., Davarnia, P., Winoto-Morbach, S., Roder, C., Arenz, C., Trauzold, A., Kabelitz, D., Schutze, S., Kalthoff, H., and Adam, D. (2014). TRAIL-induced programmed necrosis as a novel approach to eliminate tumor cells. BMC Cancer *14*, 74.

107. Wasserstein, M.P., Desnick, R.J., Schuchman, E.H., Hossain, S., Wallenstein, S., Lamm, C., and McGovern, M.M. (2004). The natural history of type B Niemann-Pick disease: results from a 10-year longitudinal study. Pediatrics *114*, e672-677.

108. Wasserstein, M.P., and Schuchman, E.H. (1993). Acid Sphingomyelinase Deficiency. In GeneReviews((R)), M.P. Adam, H.H. Ardinger, R.A. Pagon, S.E. Wallace, L.J.H. Bean, K. Stephens, and A. Amemiya, eds. (Seattle (WA)).

109. Weiss, H.M., Pfaar, U., Schweitzer, A., Wiegand, H., Skerjanec, A., and Schran, H. (2008). Biodistribution and plasma protein binding of zoledronic acid. Drug Metab Dispos *36*, 2043-2049.

110. Xiong, Z.J., Huang, J., Poda, G., Pomes, R., and Prive, G.G. (2016). Structure of Human Acid Sphingomyelinase Reveals the Role of the Saposin Domain in Activating Substrate Hydrolysis. J Mol Biol *428*, 3026-3042.

111. Xu, M., Xia, M., Li, X.X., Han, W.Q., Boini, K.M., Zhang, F., Zhang, Y., Ritter, J.K., and Li, P.L. (2012). Requirement of translocated lysosomal V1 H(+)-ATPase for activation of membrane acid sphingomyelinase and raft clustering in coronary endothelial cells. Mol Biol Cell *23*, 1546-1557.

112. Zeidan, Y.H., Pettus, B.J., Elojeimy, S., Taha, T., Obeid, L.M., Kawamori, T., Norris, J.S., and Hannun, Y.A. (2006). Acid ceramidase but not acid sphingomyelinase is required for tumor necrosis factor-{alpha}-induced PGE2 production. J Biol Chem *281*, 24695-24703.

113. Zhang, Y., Li, X., Becker, K.A., and Gulbins, E. (2009). Ceramide-enriched membrane domains--structure and function. Biochim Biophys Acta *1788*, 178-183.

114. Zhang, Y., Li, X., Carpinteiro, A., and Gulbins, E. (2008). Acid sphingomyelinase amplifies redox signaling in Pseudomonas aeruginosa-induced macrophage apoptosis. J Immunol *181*, 4247-4254.

115. Zhou, Y.F., Metcalf, M.C., Garman, S.C., Edmunds, T., Qiu, H., and Wei, R.R. (2016). Human acid sphingomyelinase structures provide insight to molecular basis of Niemann-Pick disease. Nat Commun *7*, 13082.

7 Appendix

7.1 List of tables

7.2 List of figures

Appendix: List of figures

7.3 Abbreviations

AC	Acid ceramidase (human AC, murine Ac)
ADME	Absorption, Distribution, Metabolism and Excretion
Ami	Amitriptyline
AP	Alkaline phosphatase
ASM	Acid sphingomyelinase (human ASM, murine Asm)
BMP	Bis(monoacylglycero)phosphate
bNPP	bis(*p*-nitrophenyl)phosphate
BSA	Bovine serum albumin
BUN	Blood urea nitrogen
C1P	Ceramide-1-phosphate
Cer	Ceramide
CF	Cystic fibrosis
CFTR	Cystic fibrosis transmembrane conductance regulator
CHO	Chinese hamster ovary
CPK	Creatine phosphokinase
DAG	Diacylglycerol
Desi	Desipramine
dhSph	Dihydrosphingosine
FCS	Fetal calf serum
FEV1	Forced expiratory volume in 1 sec
FIASMA	Functional inhibitor of acid sphingomyelinase
FPP	Farnesyl pyrophosphate
FRET	Förster resonance energy transfer
GOT	Glutamate-oxaloacetate transaminase/aspartate transaminase
GPT	Glutamate-pyruvate transaminase/alanine transaminase
HMU-PC	6-hexadecanoylamino-4-methylumbelliferonephosphorylcholine
HPLC	High performance liquid chromatography
HPRT1	Hypoxanthine phosphoribosyltransferase 1 (human *HPRT1*, murine *Hprt1*)
HRP	Horseradish peroxidase
HS	HEPES-buffered saline
i.p.	Intraperitoneal
i.v.	Intravenous
L-ASM	Lysosomal ASM
LDH	Lactate dehydrogenase
L-sup	L929-derived supernatant medium
LTR	LysoTracker Red
MEM	Minimum essential medium
MFI	Mean fluorescence intensity
mRNA	Messenger ribonucleic acid
MS	Mass spectrometry
N-BP	Nitrogen-containing bisphosphonate
NC	Neutral ceramidase (human NC, murine Nc)
NPC	Niemann Pick type C
NPD	Niemann Pick disease
NSM	Neutral sphingomyelinase (human NSM, murine Nsm)

PAGE	Polyacrylamide gel electrophoresis
PBS	Phosphate-buffered saline
PFA	Paraformaldehyde
PI	Phosphatidylinositol
PL	Proline-rich linker
Plt	Platelet
RAP1A	Ras-related protein 1A (human RAP1A, murine Rap1A)
rhASM	Recombinant human acid sphingomyelinase
rhSphK1	Recombinant human sphingosine kinase 1
rhSphK2	Recombinant human sphingosine kinase 2
RT	Room temperature
RT-PCR	Real-time polymerase chain reaction
S1P	Sphingosine-1-phosphate
S-ASM	Secretory ASM
SDS	Sodium dodecyl sulfate
SM	Sphingomyelin
SMPD1	Sphingomyelin phosphodiesterase 1 (human *SMPD1*, murine *Smpd1*)
SP	Signal peptide
Sph	Sphingosine
SphK1	Sphingosine kinase 1
SphK2	Sphingosine kinase 2
TBS-T	Tris-buffered saline-TWEEN
TLC	Thin layer chromatography

Acknowledgements

First, I would like to thank Prof. Dr. Erich Gulbins for giving me this opportunity and Dr. Alexander Carpinteiro for his excellent scientific guidance, his patience, encouragement and kindness, and for teaching me lots of things.

I am very grateful for the great academic and practical support and kindness of Dr. Stephanie Kadow who also taught me a lot.

I would like to thank Prof. Katrin Anne-Becker for her excellent academic and practical support.

I also would like to thank Gabriele Hessler and Barbara Pollmeier for their great work and technical help in the experiments and for their kindness.

I would like to thank Our collaboration partners: Dr. Fabian Schumacher at the Department of Toxicology, Institute of Nutritional Science in Potsdam for his remarkable contribution in this work and his thorough valuable remarks. Prof. Dr. Christoph Arenz and Zainelabdeen Ahmed at the Institute of Chemistry, Humboldt Universität zu Berlin for their remarkable technical support, valuable feedback and thought-provoking discussions.

I would like to thank the members of the thesis committee for taking effort and time to evaluate my Dr. med thesis.

I owe all my present and past colleagues at the Institute of Molecular Biology a huge thank for being humane, positive, cooperative, and for sharing their interesting thoughts with me:

Dr. Yuqing Wu, Ashraf Swaidan, Fahime Heshemi Arani, Claudine Kühn, Melanie Kramer, Simone Keitsch, Hannelore Disselhoff, Matthias Soddeman, Kristin Schimank, Bettina Peter, Andrea Riehle, Dr. Heike Gulbins, Dr. Rabea Verhaegh, Carolin Sehl, Barbara Wilker, Salina Begum, Karen Hung, Anne Koch, Helga Pätsch.

Biggest thank to my parents Maha and Nooredden for being supportive without limits, understanding, aware and ahead of their time: Without you nothing would have been. A big yet never enough thank is to my dearest friends Naya, Youssuf, Ali, Muzaffar, Salma, and Mais: Without you breathing is insignificant.

Der Lebenslauf ist in der Online-Version aus Gründen des Datenschutzes nicht enthalten.

Der Lebenslauf ist in der Online-Version aus Gründen des Datenschutzes nicht enthalten.